Title
Physical Human-Robot Interaction in Spherical Tensegrity Robots

Author
Barkan, Andrew Robert

Publication Date
2021

Peer reviewed|Thesis/dissertation

Physical Human-Robot Interaction in Spherical Tensegrity Robots

by

Andrew Robert Barkan

A dissertation submitted in partial satisfaction of the

requirements for the degree of

Doctor of Philosophy

in

Engineering - Mechanical Engineering

in the

Graduate Division

of the

University of California, Berkeley

Committee in charge:

Professor Alice M. Agogino, Chair
Assistant Professor Hannah Stuart
Associate Professor Anca Dragan

Fall 2021

Physical Human-Robot Interaction in Spherical Tensegrity Robots

Abstract

Physical Human-Robot Interaction in Spherical Tensegrity Robots

by

Andrew Robert Barkan

Doctor of Philosophy in Engineering - Mechanical Engineering

University of California, Berkeley

Professor Alice M. Agogino, Chair

As intelligent robots become more pervasive in the facilitation and execution of historically human-centric tasks, we, as roboticists, must continue to improve upon our methodologies for intuitive and efficient human-robot interaction (HRI). This is especially relevant to robotic systems that are intended to operate in close proximity to humans where physical contact is either intentional or inevitable. The vast majority of research in physical human-robot interaction (pHRI) has focused on exclusively anthropomorphic realizations of interactions that involve complex and rigid traditional serial robotic systems, which rely on sophisticated sensing and control implementations to accommodate physical contact. Furthermore, the breadth of the pHRI research domain has remained limited by the largely anthropocentric perspective of prioritizing human-like interactions as well as the overwhelming emphasis placed on contact avoidance as an essential feature in autonomous and mobile robotic systems. In contrast, the somewhat recent proliferation of soft robotic systems, like tensegrity robots, built with an intrinsic tolerance for physical contact have shown tremendous promise as platforms for enabling pHRI.

Tensegrity robots are a class of soft robotic systems whose structures consist of a set of rigid bodies suspended in isolation via a network of cable elements. The advantages of a tensegrity robot include low density, configurable compliance, and structural resilience at the cost of greater complexity in modeling and control. These unique mechanical characteristics make tensegrity robots well-suited to applications that demand robustness to physical contact. In this dissertation, we examine the design and implementation of a force-sensing tensegrity as a robotic platform for enabling novel physical interactions and for exploring new avenues for pHRI with compliant robotic systems. First, we explore the potential for a new language of pHRI that leverages non-anthropomorphic, compliant, and mobile robotic systems. We then present the *Class-1* spherical six-bar tensegrity topology as a scaffolding for implementing the detection of physical human-robot interactions. Several force-sensing tensegrity prototypes are designed, constructed, and tested to explore the capacity for reliable contact detection.

To demonstrate the ability of the force-sensing tensegrity to distinguish between physical interactions, we propose a methodology for inferring intent from physical interactions using a supervised learning framework that features contemporary classification algorithms including deep neural networks. Additionally, we conduct a series of human subject experiments to examine the intuitiveness of physical interaction with the tensegrity as well as the robustness and generalizability of the aforementioned supervised learning framework.

There are broad implications from these results on the future of pHRI research leveraging similar robotic implementations, which could be capable of offering completely new functionalities for physical interaction. The methodologies and frameworks presented here can be extended to various tensegrity topologies, fully actuated tensegrity platforms, and even compliant robotic systems outside the domain of tensegrities. As a result, we hope that pHRI researchers will be inspired to utilize compliant systems like our force-sensing tensegrity as viable platforms for investigating physical interaction. In summation, the problems addressed here constitute an exciting and potentially paradigm-shifting investigation of the utility of tensegrity robots as platforms for a new language and embodiment of pHRI with compliant robotic systems.

To my parents, Cindy and Anthony Barkan

Throughout my life and academic career, you've shown me nothing but unconditional love and support. By always believing in me and my dreams, I've been inspired to achieve more than I ever thought possible. You've instilled in me a lifetime of hard-learned lessons and taught me what it means to be a caring and thoughtful person. I dedicate this dissertation to you with all of my love.

Contents

List of Figures

List of Tables

Acknowledgments

In the pursuit of my research, I've been supported by so many individuals who have offered their valuable time and resources in order to make my work possible. I'd like to acknowledge their meaningful contributions to the research presented here in this dissertation and to thank them sincerely. I truly stand on the shoulders of giants.

First, I'd like to thank my academic advisor and mentor, Professor Alice M. Agogino, who has helped me to fluorish in my career as a student and as a researcher. I first came to the BEST Lab part way through my curriculum as a doctoral student from another lab, and Alice graciously and generously helped me to feel welcomed within her research group. I was incredibly humbled by Alice's commitment to serving her students and the academic and scientific community in general. Alice continuously supported me by providing me with the freedom and agency to pursue my interests and passion in research. Through her mentorship, I've grown into a more thoughtful person, and her lessons continue to inspire me to push the boundaries of what is possible in all facets of my career.

In addition to my advisor, I've been fortunate to have the support of the other two members of my dissertation committee. Professor Hannah Stuart and Professor Anca Dragan have provided their wisdom and expertise at all stages of my doctoral journey, and I have benefitted immensely from their guidance.

The Berkeley Emergent Space Tensegrities Lab has been a second home to me in my time at Berkeley, and I have the members of the BEST Lab and the team at Squishy Robotics to thank for that. There are so many fond memories and shared stories that I will continue to cherish as I move on to the next chapter of my career. I'd like to thank Andrew Sabelhaus, Douglas Hutchings, Brian Cera, Alan Zhang, Deniz Dogruer, George Moore, Elena Duran Lopez, and all past and present BEST students who have also helped along the way.

I'd also like to highlight the undergraduate and master's students who have worked directly with me toward the completion of various projects related to my research. I've had the great privilege of mentoring and collaborating with a number of truly gifted students, and this dissertation would not have been feasible without their contributions. Thank you Akhil Padmanabha, Sala Tiemann, Albert Lee, Matthew Kanter, and Yash Agarwal for all of your hard work.

Finally, I'd like to conclude by acknowledging my loved ones. To my friends Justin Hunt, Varun Nalam, and Zahi Kakish: You've been the best colleagues and co-founders a person could ask for. Beyond being supportive friends, you've inspired me to finish this Ph.D. out of spite for completing yours before me. To my partner Zoe Plaxco: I cannot fully express the extent to which you have positively impacted my life during my time as a doctoral student. I am forever grateful for your love and support. To my parents, Anthony and Cindy, and my brother, Ben: I wouldn't be where I am today if you hadn't believed in me through it all. Every one of my accomplishments are also yours. Thank you.

Chapter 1

Introduction

The focus of this dissertation is the exploration of how the unique properties of tensegrity robots can be leveraged toward investigating and implementing novel mechanisms for physical human-robot interaction (pHRI). Tensegrity describes a class of structures that consists of a set of rigid bodies suspended in static equilibrium via a network of interconnected cable elements, which are often elastic. The term itself is a portmanteau of tensile (or tension) and integrity, alluding to how structural integrity is achieved by securing the rigid members of the structure in place via the tension of the cable elements. Tensegrity structures are lightweight, compliant, resilient, and configurable, which makes them highly attractive for a variety of applications in the design of dynamic robotic systems. Realizations of tensegrity concepts in robotics are frequently directed toward applications that exceed the mechanical capabilities of traditional rigid robotic architectures, such as applications that involve extreme environments and demanding operating conditions. The Berkeley Emergent Space Tensegrities Lab (BEST Lab)[1] at UC, Berkeley partnered alongside NASA Ames Intelligent Robotics Group (IRG) demonstrated the advantages of tensegrity in the development of *SUPERball* [55], which is a spherical tensegrity module intended for use in space exploration. In industry, tensegrity robots have emerged as a prominent solution to the challenge of mission-critical data acquisition in disaster response scenarios. *Squishy Robotics, Inc.*—a close industry collaborator with the BEST Lab—develops sensing solutions that feature incredible structural robustness and impact resistance through the use of tensegrity design principles. Built with the capacity to be deployed from extreme heights without sustaining critical damage, these tensegrity sensors are perfectly suited to applications in emergency response and offer first responders the ability to gather essential information on the ground in areas that would otherwise be completely inaccessible to either humans or alternative robotic solutions.

As tensegrity robots are introduced into potentially dangerous and uncertain conditions with human operators, we must consider how to best facilitate efficient and intuitive human-robot interfaces for the operation of this emergent technology. It is vital for the end users of these systems to have reliable interfaces to communicate effectively with their devices. Dis-

[1] Website: https://best.berkeley.edu/

aster response scenarios, for example, introduce a number of challenges to the use of common human-robot interfaces due to the expectation of severely limiting environmental factors such as overwhelming noise, visual obstruction, time sensitivity, and more. As a result, the typical modalities of human-robot interaction run substantial risk of failure. Furthermore, tensegrity robots represent a class of robots that neither resemble conventional robotic systems in form nor operate using recognizable mechanisms. This class of non-anthropomorphic, compliant, and dynamic robotic systems offers roboticists the opportunity to reimagine the standard approaches to human-robot interaction so as to capitalize on the unique characteristics of these devices.

Specifically, tensegrity robots offer radically new possibilities for the field of pHRI due to their inherent robustness to physical contact and their configurable form factor. Instead of relying on complex sensing and control schemes in rigid architectures to mimic tolerance to physical contact, we can utilize compliant systems that are expressly designed with the intent to be handled and impacted. In doing so, we open new avenues for communication and cooperation through physical manipulation. Previously, there could be no imagining of a device that could withstand being picked up and tossed across a room without being destroyed. With a tensegrity robot like the products being developed at *Squishy Robotics, Inc.*[2], this interaction can take the form of a valid and expressive input to facilitate the system's operation in real scenarios. In this dissertation, we will attempt to make a compelling case for the utility of such pHRI modalities and demonstrate how tensegrity robots can serve as a vessel for exploring the exciting new possibilities for this innovative class of compliant robotic systems.

1.1 Research Objectives

In order to communicate the focal points of this dissertation to the reader, we will present the main research objectives here. The research objectives outlined in this section represent the key research questions addressed by our work in pHRI with tensegrity systems.

1. **Design of a Force-Sensing Tensegrity Robot** : The six-bar spherical tensegrity configuration has been demonstrated to be an excellent structural platform for the development of rapidly deployable and robust sensor robots. Using this particular topology of tensegrity robots, we seek to augment it with the ability to detect external forces imparted to its structure. By taking advantage of the properties of tensegrity structures, it will be possible to achieve tremendous bandwidth in terms of force-sensing with the use of only a limited amount of embedded sensing. We can then employ this prototype in investigating the extent to which force-sensing can be used to construct novel human-robot interaction mechanisms.

2. **Development of Strategies for pHRI with Compliant Robotic Systems** : Once we have developed a force-sensing tensegrity capable of detecting different forms

[2]Website: https://squishy-robotics.com/

of physical contact, it can be used as a platform for exploring innovative physical interaction mechanisms. While there have been numerous studies into the development of physical interaction methodologies with conventional anthropomorphic robotic systems, tensegrity robots like the six-bar spherical tensegrity introduce new avenues for research into types of physical interactions that had previously been impossible. We must therefore begin to develop strategies that capitalize on the properties of this new class of compliant robotic systems so as to maximize their utility in real-life human-robot cooperative scenarios.

3. **Performance of Force-Sensing Tensegrity Robots in pHRI** : In the process of developing this new embodiment of pHRI with compliant robotic systems like the six-bar spherical tensegrity, we will assess the performance of these mechanisms from both quantitative and qualitative perspectives in an HRI context. In order to be useful in a given application, it is desirable for the interface between human and robot to have certain characteristics such as intuitiveness, robustness, and simplicity. We will attempt to investigate these characteristics as they pertain to our newly developed pHRI strategies using a combination of human subjects experiments and simulated interactions.

1.2 Dissertation Outline

The following section outlines the structure of the dissertation in terms of its chapters in their order of appearance:

- **Chapter 2** : Relates topics that are relevant to the background and motivation of this dissertation starting with a discussion of historic pHRI strategies and and the existing gaps in research pertaining to pHRI with compliant robotic systems. We introduce tensegrity robotics along with previous examples of force-sensing in tensegrities.

- **Chapter 3** : Provides an overview of traditional tensegrity modeling techniques in order to introduce the subject of our research objectives in the six-bar spherical tensegrity robot. This representation will then be used to guide a discussion into the theory of tensegrity statics and dynamics which are relevant to the design of a force-sensing tensegrity prototype.

- **Chapter 4** : Presents the iterative design process behind the development of two force-sensing tensegrity prototypes which will be used as platforms for investigating pHRI with compliant robotic systems.

- **Chapter 5** : Introduces our proposed strategies for establishing a new language of pHRI with compliant robotic systems through supervised learning frameworks. This chapter will also include an analysis on the potential performance of these strategies as well as the feasibility of its deployment in real-life applications.

- **Chapter 6** : Presents a series of human subjects experiments used to assess the performance of our new pHRI strategies in representative contexts. We also extend our supervised learning framework to more realistic scenarios involving sequences of interactions. Additionally, we will discuss qualitative observations from these studies that will shed light on the advantages and disadvantages of the proposed methodologies.
- **Chapter 7** : Concludes with a summarization of the research involved in this dissertation along with the implications of our results on future work in pHRI with compliant robotic systems.

Chapter 2

Background and Motivation

2.1 Trends in Physical Human-Robot Interaction

When desiging a robotic system for a particular application, a roboticist or engineer considers all facets of the application and its conditions in order to extract critical design requirements. A manipulator intended to function as an assembler of sensitive electronics must have precise actuation to enable pick-and-place operations. Autonomous vehicles should have robust visual perception in order to facilitate navigation through complex and dynamic environments. An animatronic system that replicates the motion of a human character will naturally inherit anthropomorphic characteristics. These three example applications involve robotic systems that are expressly designed to operate in human environments and are some of the most familiar and representative categories of robotic systems in the world today. It then makes intuitive sense that the majority of research in human-robot interaction (HRI) has featured systems that are, at the very least, reminiscent of one of the aforementioned architectures. However, earlier versions of these systems were not originally designed with human-robot interaction as a priority. As a result, researchers in the field of HRI would develop methogolodies and strategies primarily for adapting conventional robotic systems to HRI applications. While these kinds of approaches are certainly valuable in terms of taking advantage of the most widely available technology, it circumvents the need to optimize the design of robotic systems to be more suited to HRI in the first place.

As the demand for automation in new sectors continues to increase, robots have begun to assume a greater number of human roles as well as occupy a larger presence in human environments. To meet the unique requirements of these human-centered applications, considerable advancements in sensing and actuation have led to the development of sophisticated robotic architectures that feature desirable HRI properties. Perhaps the most prominent indicator of this trend is the creation of *cobots*, or collaborative robots. A cobot describes a type of robot that is specifically designed to support HRI and to work in close proximity with humans. The arrival of cobots marked a pivotal shift in the focus of HRI research because it emphasized the idea that physical contact between human and robot was not only tolerable,

Figure 2.1: Two modern collaborative robots, or *cobots*, designed for human-robot interaction. On the left is *KUKA*'s LBR iiwa and on the right is the *Universal Robots*' UR16e. Each manipulator is instrumented with integrated force-sensing to detect forces in operation.

but it could be leveraged toward more effective and safe automation in human contexts. As humans, we naturally we appreciate the importance of physical contact as a modality for interacting with the world, but it was only recently that we began to pursue the idea that we could equip robots with the same capability. To illustrate the importance of this shift in thinking, we can consider how cobots have influenced the landscape of both industrial automation and HRI research.

Since the introduction of cobots by Peshkin and Colgate in the early 2000s [51], leaders in industrial automation like *KUKA*, *FANUC*, and *Yaskawa* along with newer players in the space like *Universal Robots* have developed cobot products aimed at enabling close-proximity human-robot collaboration in areas such as manufacturing. Typically, these robots resemble the traditional serial manipulator; however, they have the distinct advantage of integrated force sensing. This force sensing allows a cobot to quickly respond to physical stimulus, which helps ensure human worker safety around such high-power and high-intertia automation equipment. Suddenly, manufacturers are afforded the option to have humans and robots coexist in the same space, dramatically improving the density and efficiency of certain manufacturing operations that require both precise automation and human intervention.

The phrase physical human-robot interaction (pHRI) is generally used to describe scenarios in which physical contact between a human and robot is utilized to collaborate, cooperate, or communicate toward separate or common goals. In response to the increased interest in the development of platforms like collaborative robots, research specifically in the field of physical human-robot interaction has gained tremendous momentum [17, 26, 46]. Equipped with commercially available cobots like *KUKA*'s LBR iiwa and *Universal Robots*' UR16e

shown in Figure 2.1, researchers in physical human-robot interaction demonstrated numerous advantages of force feedback in the safe and effective operation of these devices and, by extension, the value of intentional design for physical contact.

In terms of hardware innovation, the primary focus has been to develop systems with force sensing either preemptively in the design of its actuation mechanism as seen in series elastic actuators [11, 69] or retroactively by instrumenting the end effector or other interfacing components [37]. These instances represent pHRI studies that are mostly concerned with force-sensing as it pertains to the proprioception of the robotic system as it comes into contact during its operation. This modality of sensing can provide critical information about dynamics, as in the case of shared manipulation tasks [3, 49], or operator intent, as it can be used to condition inference models that attempt to model a robot's understanding of a human's latent objectives within a pHRI context [47]. Distinct from this category of proprioceptive force-sensing implementations are those that seek to replicate some degree of tactile, or touch, sensing to extract subtle information from surface contact [7, 16]. Novel tactile force-sensor modules can enable robots with the ability to detect extremely fine details in surface geometry [30, 50]. For each of these categories, the majority of the associated studies have still relied on either instrumentation that augments original functionality or arguably extrinsic realizations of force-sensing and robustness to physical contact.

Recognizing the limitations of rigid robotic architectures in the face of increasingly contact-oriented applications, roboticists have pivoted to a new class of robotic systems that features inherent structural compliance at the cost of reduced control fidelity. Soft robotics is a field of robotics that encompasses robotic systems designed with mechanically flexible properties [36]. By taking advantage of the compliance of elastic materials, soft robotic systems offer intrinsically safe operation [1] as well as impressive impact resilience [9]. Immediately, researchers recognized that these advantages translated to impactful applications in pHRI [52]. Commonly, these systems are driven using pneumatically actuated mechanisms [66], which can be instrumented with force sensing by clever use of geometry and pressure detection. Still, the accompanying uncertainty of elastic materials coupled with imprecise actuation reveals the need for more structurally deterministic operation in these compliant systems. This leads us to our discussion of a new class of compliant robotic systems—tensegrity robots—in which compliant and rigid aspects work in concert to offer compelling advantages to pHRI applications.

2.2 Tensegrity Robots and Applications

The term *tensegrity* was first coined in the 1960's by the original inventor of the concept, Buckminster Fuller, and describes structures that consist of rigid elements held in compression via a tension network of cable elements. With dramatic forms and unlimited configurations, they quickly captured the imagination of artists like Kenneth Snelson who created striking tensegrity sculptures like those pictured in Figure 2.2. Each individual rigid element of a tensegrity structure is isolated but is allowed to displace based on the deformation of the

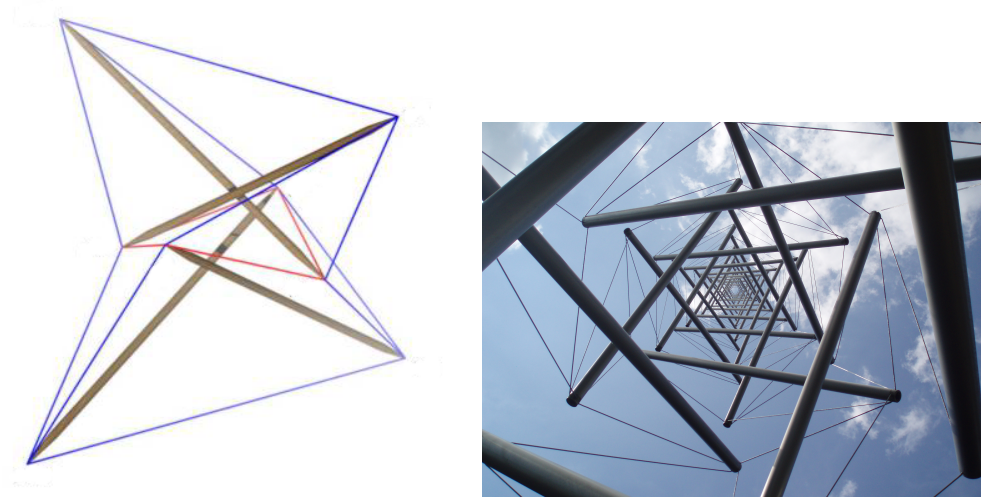

Figure 2.2: Examples of tensegrity structures in some of their earliest forms by American contemporary sculptor Kenneth Snelson. On the left is the Tensegrity X-Module Tetrahedron sculpture (1959) and on the right is Needle Tower II (1969).

attached cable elements. Because the rigid elements of a tensegrity structure only experience compressive loads as a result of the interconnected network of cable elements, the structure is devoid of signficant moments (or torques), which greatly reduces the occurrence of stress concentrations. The result is a structure that exhibits surprising structural integrity and resilience while still being flexible enough to dynamically adapt to physical perturbations.

The unique mechanical properties of tensegrity structures attracted the attention of civil engineers and architects who applied these concepts to load-bearing structures [24] and grand architectural feats such as the Kurilpa Bridge in Brisbane. Tensegrity principles have also been featured by biologists as a way to model a variety of naturally occurring biological structures [31, 32]. Eventually, roboticists also recognized the potential of tensegrity concepts and began applying them to the development of innovative robotic systems.

One of the main themes in robotic implementations of tensegrity concepts is leveraging the natural compliance and configurability of tensegrity structures toward creating robots that are tailored to extreme conditions of operation. It's certainly possible that there is no application or environment more extreme or demanding than space exploration. In 2012, NASA began exploring the development of a tensegrity-based planetary surface lander that could compactly store in a launch vehicle, deploy to an expanded state from low orbit, and withstand the impact of an unassisted descent. Dubbed *SUPERball*, this six-bar spherical tensegrity robot lander was highly influential in the space of compliant robotic systems [55]. Other examples of innovative tensegrity robots include a duct-exploring robot [22], a quadrupedal robot with tensegrity spine [53], and bio-inspired tensegrity manipulators [40]. There have even been recent examples of tensegrities that have been configured with quadro-

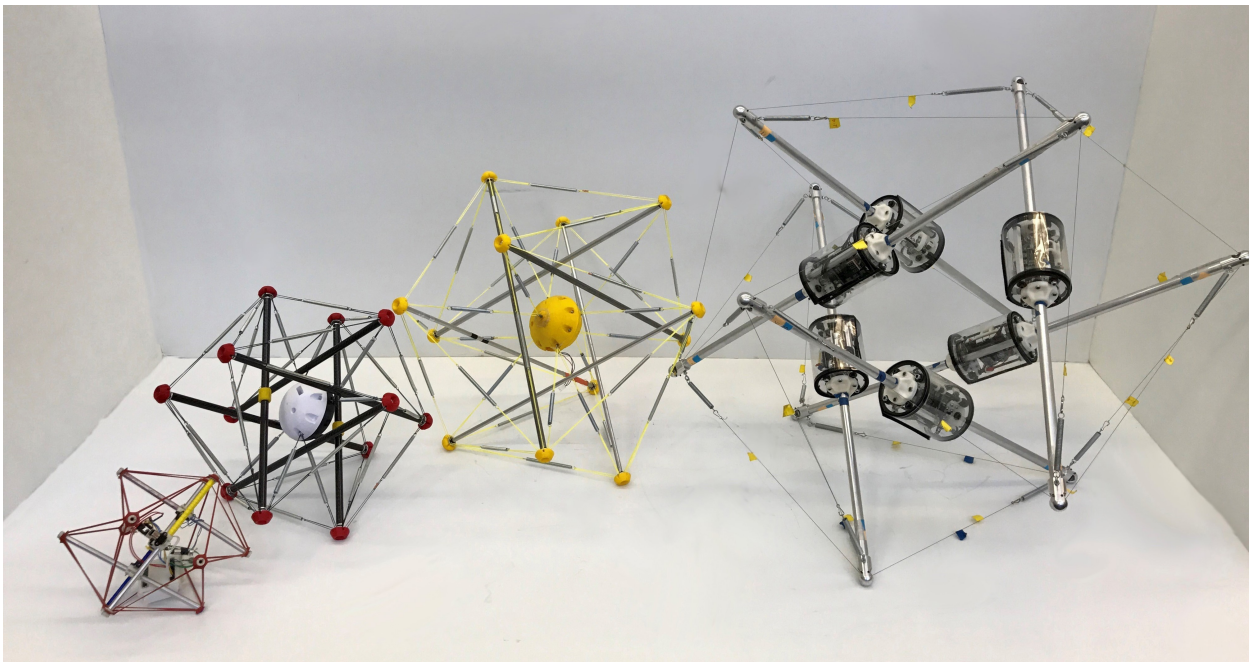

Figure 2.3: Four examples of six-bar spherical tensegrity robots developed by researchers at the BEST Lab at UC, Berkeley and *Squishy Robotics, Inc.*. On the left are three examples of passive spherical tensegrity systems and the rightmost device is a cable-actuated version.

tors to create physically robust flying vehicles [1]. The Berkeley Emergent Space Tensegrities Lab (BEST Lab) at the University of California, Berkeley has specialized in iterating on the classic six-bar spherical tensegrity robot toward practical use cases. Figure 2.3 shows a few different scales of BEST Lab's six-bar spherical tensegrity robots. BEST Lab researchers have even demonstrated robust and efficient locomotion via cable actuation in the elastic members of the six-bar spherical tensegrity topology [12, 13]. Drawing upon the knowledge gained from these projects, BEST Lab researchers founded *Squishy Robotics, Inc.* to begin the commercial development of tensegrity-inspired robotic sensing solutions for applications such as disaster response.

The structure of a tensegrity lends itself naturally to the dispersal of forces through its connected members. Researchers have exploited this property toward the design of tensegrity devices that have the ability to detect forces as they are distributed through the structure in response to external stimulus. In fact, [62] demonstrates a simulated tensegrity force sensor that is capable of accurately measuring forces and torques imparted to the external structure through instrumentation of the elastic members. Recently, researchers at Yale presented a six-bar spherical tensegrity with robotic skin and external force sensors at the nodes, or connecting vertices, of the tensegrity structure that allows complete state estima-

[1] Website: tensodrone.io

tion [10]. Beyond the use of force sensing as an augmentation to structural diagnostics or state estimation, we see the inherent sensitivity of tensegrity structures to physical stimulus as a pathway to rich interactions through contact with a human operator. This can be useful in cases where robotic systems are attached to human operators as in the case of a tensegrity-inspired exosuit [41]. Since tensegrity concepts are often used to model biological structures, it also makes intuitive sense to design tensegrity mechanisms that seek to mimick the physical compliance of human biomechanisms, such as shoulders [43]. Another demonstration of the potential for leveraging physical interaction in tensegrities was shown in an evaluation of an actuated shape-changing tensegrity device [67]. The aforementioned system was developed to adapt its control policy in the presence of external constraints enforced by physical interactions during self-initiated changes in tensegrity shape. While these examples are compelling and positive indications of the suitability of using tensegrities for pHRI, we see a need for studies that focus more directly on the problem of creating a pHRI framework that is capable of facilitating the exchange of information through force sensing in a tensegrity. To our knowledge, no study has yet investigated the use of force sensing in tensegrity robots as a sensing modality for enabling physical human-robot interaction.

2.3 A New Language and Embodiment of pHRI

With soft robots and, more specifically, compliant robotic platforms like tensegrity robots becoming commonplace in human-centered applications both in research and in industry, there is an associated need for the investigation of methodologies that promote intuitive physical human-robot interaction with these devices. As mentioned previously in our coverage of the contemporary pHRI research landscape, pHRI studies have been disproportionately directed at applications featuring one of the few standard robotic architectures. Being humans ourselves, roboticists and engineers have a natural tendency to ascribe anthropic qualities to our creations, and research in pHRI is conditioned by these projections as a result [19]. The appearance of decidedly non-anthropomorphic and unfamiliar robotic systems like tensegrity robots that exhibit unprecedented robustness to physical contact upend our previous notions of how physical interactions might take place between a human operator and a robotic agent. We can start to see evidence of a reevaluation of accepted norms in HRI topics as new investigations into human perception of unique systems like soft robots begin to arise [33]. In particular, untethered and amorphous spherical tensegrity robots occupy a new space of compliant mobile robots, which offer radically new possibilities for rich physical interactions.

Previously, unmmanned aerial vehicles (UAVs) and autonomous ground delivery vehicles spanned the entire space of potential mobile robotic devices. In such systems, physical human-robot interaction is the enemy, and contact with humans is avoided at all cost in order to protect both the humans and the devices themselves. The rigid construction of modern robotic architectures is prone to being damaged when caught in collision, and the high inertia of these systems poses a threat to the safety of humans who exist in close proximity. As a result, we must use sophisticated planning methodologies to guarantee safety during

the execution of trajectories so that we can avoid obstacles [28]. Otherwise, researchers have resorted to creating custom enclosures to protect the sensitive components of these systems from damage [45]. Consider instead a device with similar locomotion capabilities (e.g., ground or air mobility) that actively welcomes and adapts to physical contact without risking harm to humans. A human operator or bystander might grab the device, deform it, impact it, or even toss it if they so choose. Unlike a standard UAV or other conventional mobile robot, a six-bar spherical tensegrity robot, like the products being developed by *Squishy Robotics, Inc.*, has the ability to withstand all of these physical interactions without sustaining critical damage. Recent work through collaboration with the HiPeR Lab[2] at Berkeley has even shown that the properties of six-bar spherical tensegrity structures can support tensegrity quadrotor robots that are contact tolerant, creating UAVs that offer greater flexibility to collisions in flight [71]. But why stop at only tolerating this contact in operation? If possible, we should also seek to exploit the capacity for physical interaction toward more expressive and intuitive cooperation between robot and human.

Because our current methodologies surrounding pHRI are ill-suited to exploring this novel space of physical interactions, we highlight the need for developing investigative technology and accompanying strategies that will help us characterize the advantages of pHRI with such compliant robotic systems. Thus, our goal is to design a tensegrity device that will serve as a useful platform for investigating this new embodiment of pHRI. Our hope is that resulting studies with this device will lend insight into the development of methodologies that can leverage the unique mechanical properties of similar devices in real human-centered applications. As a backdrop for this first-of-its-kind study into pHRI with compliant robots, we present the application of tensegrity robots in disaster response as an illustrative set of scenarios that can benefit greatly from leveraging the physical modality of interaction.

2.4 Applications in Disaster Response

One of the most exciting and impactful fields in robotics that has been gaining traction in recent decades is the development of robots for disaster response applications. A tremendous amount of funding from government agencies like NSF and DARPA has been poured into research projects aimed at the development of robotic systems that are intended to support first responders. These robotic devices can provide teams of first responders with improved task efficiency and situational awareness, all while limiting the risk to human safety in potentially dangerous disaster scenarios. This is typically accomplished through the design of specialized platforms that feature robust locomotion to navigate harsh and hazardous terrain and sophisticated sensing to enable real-time data acquisition [34, 58]. Teams of robotic agents can explore and map the space of a disaster scene while powerful software architectures fuse sensor information into mission-critical diagnostics and prognostics [5, 23, 70]. Even with the introduction of this game-changing technology, it is still absolutely necessary for humans to remain in the loop throughout the deployment and operation of

[2]Website: https://hiperlab.berkeley.edu/

these robotic devices. Due to the dynamic and unpredictable nature of these missions, human-level decision making and dexterity will continue to assume dominant roles in the execution of nearly all disaster response tasks. Furthermore, experts point to issues of ease of use, robustness, and data accessibility as primary barriers to adoption for the latest robotic disaster response technology [18].

In an effort to address some of these issues, the team at *Squishy Robotics, Inc.* is developing rapidly deployable sensor robots inspired by tensegrity design principles. Droppable from a height of $1000m$ and featuring a range of configurable sensor payloads, their stationary six-bar spherical tensegrity robot can provide first responders with essential and perhaps even life-saving intel in disaster response scenarios with unparalleled reliability. Currently, technology is being developed to equip these robots with robust locomotion both on land, using novel cable-driven mechanisms, and in the air as a quadrotored drone. This system is an excellent demonstration of how tensegrity concepts in robotics can provide impactful solutions to real-life problems such as those encountered in disaster response. Even so, the introduction of this relatively unfamiliar platform and the hope for its eventual adoption in industry begs the question of how we can address issues of HRI and ease-of-use for first responders.

Imagine a hypothetical disaster response scenario at a building collapse in a chemical manufacturing plant. Besides the obstructions from debris and the heat of the spreading fire, there are many additional distractions and mitigating factors that complicate the successful completion of any task at hand. General visibility is low due to the presence of airborne particulate from fires. Unexpectedly rough terrain prevents conventional ground mobility. The presence of chemical hazards necessitates the use of bulky HazMat suits that have the disadvantage of limiting the vision, manual dexterity, and verbal communication of the first responders wearing them. First responders are expected to overcome these obstacles and distractions under extreme pressure and time constraints in order to complete their tasks. On top of all of this, first responder must devote considerable cognititive load toward handling robotic devices. Moreoever, first responder are typically not roboticists or experts on the operation of these robotic systems and are not equipped to diagnose the ambiguous and often esoteric technical issues that might arise.

Figure 2.4 illustrates the example disaster response scenario as well as a team of first responders utilizing a set of tensegrity robot agents to gather situational data. Suppose that in this hypothetical scenario the first responders are equipped with hybrid-mobility tensegrity robots that feature multiple interaction modalities including force-sensing and wireless communication. First responders might arrive on scene, don their HazMat equipment, and begin unpacking their tensegrity devices, which have been collapsed into untensioned forms to allow for efficient storage. The tensegrity detects that it is being unpacked by way of its force-sensing and tensions itself into a deployable state in response. Depending on the needs of the situation, the first responder may decide to employ one form of mobility or another—either ground mobility or air mobility. Instead of grappling with a clunky graphical user interface, the first responder can physically manipulate the structure of the tensegrity in a prescribed fashion to cycle through the operational modes. Upon detecting a certain type

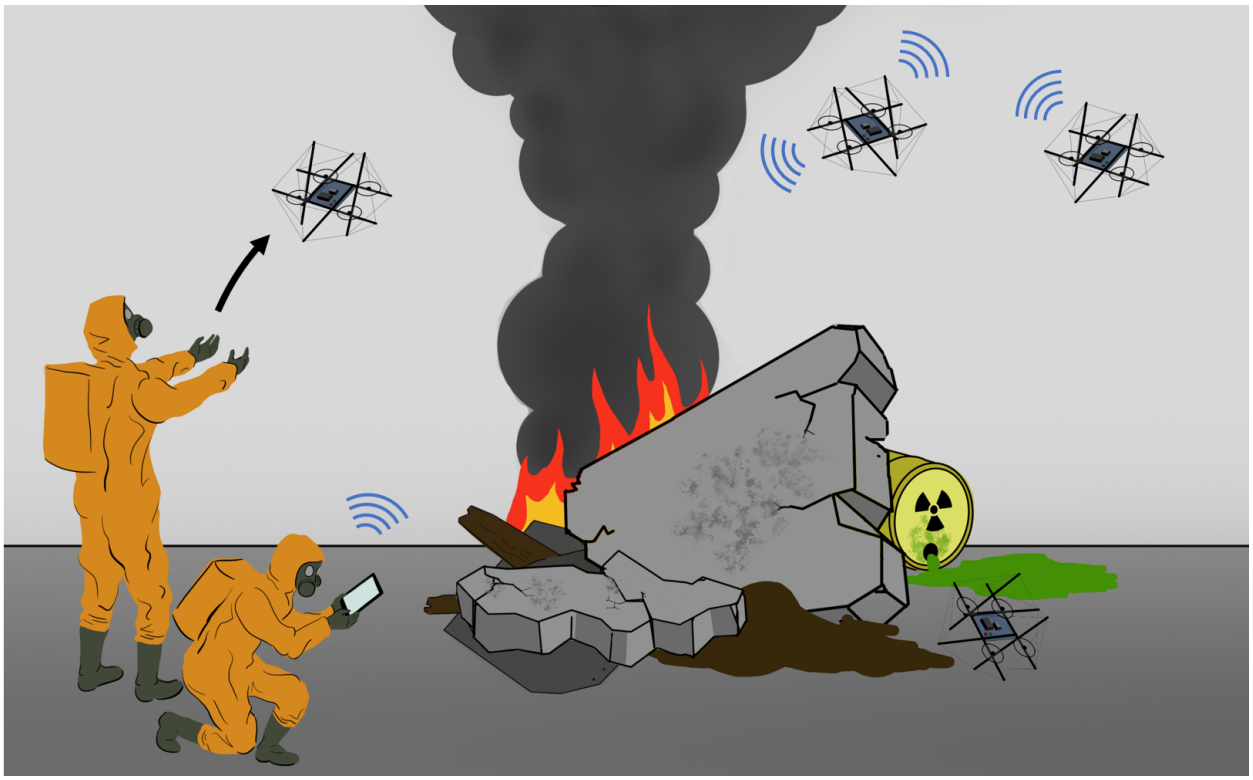

Figure 2.4: Illustration of a representative application of physical human-robot interaction with force-sensing tensegrity robotic devices being employed in a disaster response scenario. In this example, tensegrity robots are being deployed and operated using multiple interaction modalities depending on the needs of the scenario.

of physical interaction, the device spins its rotors to indicate to the human operator that it is primed for flight, and the first responder tosses the tensegrity robot into the air to allow it to begin it's autonomous tasks.

The scenario described is just one example of how physical interaction might simplify the operation of robotic systems and facilitate the execution of human-robot paired tasks in disaster response. There are many other potential applications for the proposed technology that can leverage the intuitiveness of physical contact as a way to communicate and cooperate toward an objective. In this dissertation, we will make the argument that the force-sensing six-bar spherical tensegrity represents a valuable resource for investigating this new modality of physical interaction with compliant robotic systems.

Chapter 3

Tensegrity Modeling and Analysis

3.1 Introduction

Tensegrity structures come in a variety of shapes and sizes depending on the requirements of the application. The subject of the research presented in this dissertation will be a specific class and topology of tensegrity structures called a class-1 six-bar spherical tensegrity. *Class-1* describes a category of tensegrity structures in which all rigid members of the structure are isolated—not directly connected to each other. The six-bar spherical tensegrity is a specific topology of tensegrity structure that approximates the shape of an icosahedron. This particular topology of tensegrity is a popular choice for analysis of unanchored tensegrities because its symmetry in structure is conducive to energy absorption from arbitrarily directed external forces and it's spherical shape makes it suited to rolling locomotion.

In order to support our discussion of force sensing in the context of this tensegrity structure, an important first step is to present our chosen modeling approach. The theoretical modeling of the tensegrity structure in both the static and dynamic case will provide insights into how we can design suitable force sensing instrumentation to enable our studies on physical interaction. It will also give us a chance to review the unique characteristics of tensegrity structures that contribute to its favorable mechanical properties.

Before reviewing the specifics of historic and recent work in the modeling of tensegrity structures, it will be useful to present some common tensegrity terminology to aid in our discussion. As covered previously, a tensegrity structure is a branching network of two kinds of interconnected structural members: rigid elements (colloquially referred to here as bars or rods) and cable elements (cables). The connections between these elements are referred to as the nodes of the structure. In general, *class-k* tensegrities are tensegrity structures that consist of nodes that are connected to at most k rigid elements. Hence, in the case of class-1 tensegrities (like the one being considered in this study), each node is only connected to one rigid element. The remaining details for describing a tensegrity representation will be left to the following sections of this chapter.

3.2 Prior Work

In this section, we will discuss relevant prior work on the modeling of tensegrity structures and devices. Since the first instances of tensegrity design principles appearing in real-life applications, there have been many advancements toward the complete and accurate modeling of their behavior in both static and dynamic cases. Despite efforts to standardize these approaches, researchers have yet to arrive at a unified representation for tensegrity systems due to discrepancies in areas of complexity and numerical performance.

Some of the earliest tensegrity modeling methodologies for static structures were originally presented in work by Sultan et. al. [61], which covers general prestressability conditions of stable tensegrity structures. At the same time, Skelton et. al. [60] presented an analytical modeling of the nonlinear dynamics of tensegrities. Later, this work was formalized by Skelton and de Oliveira in *Tensegrity Systems* [59], which attempts to create a set of tools for the design and analysis of tensegrity structures as well as the control of actuated tensegrity devices. Importantly, the authors introduce the *connectivity matrix* as a fundamental concept for representing tensegrity configurations in terms of the connections between members. It is argued and demonstrated that by using sparse numerical representations of tensegrity configurations, it is possible to make strong conclusions about the static and dynamic characteristics of the structure without dealing with complex trigonometric terms that arise in a more classical modeling approach. Our work in the static analysis of forces in the six-bar spherical tensegrity will draw heavily from the aforementioned configuration-based representation of tensegrities demonstrated in [59].

While [59] presents an elegant minimal representation of tensegrity dynamics by leveraging a configuration-based representation, researchers have recently suggested alternative formulations that rely on traditional methods in Euclidean space [12, 29]. Although these methods introduce numerical sensitivity in simulation, they facilitate the more natural application of classical control theory techniques to actuated tensegrity robots. To address numerical stability issues, [12] uses a simplified point mass dynamics formulation to reduce the occurrence of singularities and the rigidity of inherently stiff contact constraints. The result is a powerful tensegrity dynamics simulator that can reliably model tensegrity structures and their interactions with simulated environments. We will employ this dynamics simulator in the analysis of forces in the six-bar spherical tensegrity as it responds to external perturbations in a few nominal cases.

3.3 Contributions of this Chapter

The purpose of this chapter is to utilize contemporary tensegrity modeling techniques in the modeling of the six-bar spherical tensegrity device that is featured in our work on pHRI with compliant robotic systems. This representation will be used to analyze the six-bar spherical tensegrity's suitability for force-sensor instrumentation and for detecting physical interactions. Specifically, we will use a static analysis of the forces in the tensegrity structure

through the force density method (FDM) to illustrate that we can reliably distinguish between various physical interactions that impart forces on the external structure of the device. Secondly, we will use a well-established dynamics model and simulator to forecast expected force measurements on the different components of the structure in order to support the design of force-sensor integration, which will be covered in the subsequent chapter.

3.4 Representation of the Six-Bar Spherical Tensegrity Topology

This section will focus on creating a tangible representation of our six-bar spherical tensegrity to aid in our analysis of this topology's mechanical properties. To do this, we will adopt a classical approach to representing tensegrity configurations that centers around the connectivity of a given tensegrity structure. By connectivity, we are referring to the specific way that the individual members of the structure are connected to one another resulting in a network of rigid elements and cable elements.

First, we will describe the number and arrangement of the six-bar spherical tensegrity's rigid and cable elements that contribute to its resulting form. Throughout this discussion, it will be helpful to refer to Figure 3.1 as an illustration of this topology's composition. As the name suggests, there are a total of six bars or rods ($n_r = 6$ where r stands for rod) in the structure of the six-bar spherical tensegrity. Ideally, the rods are arranged so that they belong to pairs with each pair lying in one of the three orthogonal planes of a standard three-dimensional Euclidean space. Furthermore, each pair of rods is orthogonal to the other pairs within its respective plane. The ends of each rod in a pair are aligned, and the resulting node positions form the twelve vertices that outline an icosahedron shape. Before discussing the cable connections, it should also be noted that there exists a single node located at the center of the structure that is not connected to any of the rods of the structure. This thirteenth node will represent what we will introduce later on as the *payload* of the tensegrity device.

The exact positions of the nodes in three-dimensional space in an ideal case (i.e. when there are no external loads and members are massless) can be determined from the vertices of a properly scaled regular icosahedron. We start with the nominal length of a rod, l_r, which is then used to determine the desired edge length, l_e, of the icosahedron using the following equation:

$$l_e = \frac{l_r * \sqrt{\frac{3}{2}}}{2} \tag{3.1}$$

We can then use l_e to compute the coordinates of the vertices of a regular icosahedron. Interestingly, the positions of the vertices of a regular icosahedron are directly related to the golden ratio, ϕ:

$$\phi = \frac{1 + \sqrt{5}}{2} \tag{3.2}$$

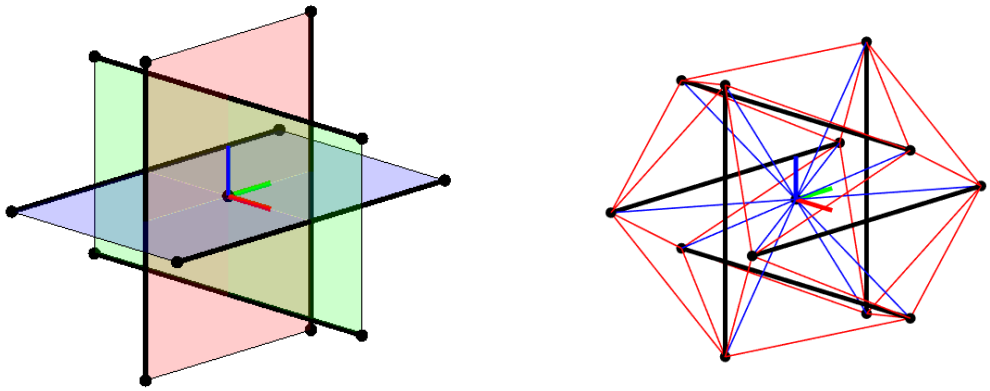

Figure 3.1: Diagrams of our six-bar spherical tensegrity topology showing rod arrangement and cable network. The left image shows the orthogonality of the rod arrangement, and the right image shows cable connections including the central payload node.

The exact positions of the vertices, and thus the nodes of the structure, are then found via the full set of permutations of the following coordinates:

$$\begin{array}{rrrr} (& 0, & \pm\frac{l_e}{2*\phi}, & \pm\frac{l_e}{2} \quad), \\ (& \pm\frac{l_e}{2*\phi}, & \pm\frac{l_e}{2}, & 0 \quad), \\ (& \pm\frac{l_e}{2}, & 0, & \pm\frac{l_e}{2*\phi} \quad), \end{array} \tag{3.3}$$

There are a total of thirty-six cable elements ($n_c = 36$ where c stands for cable) that connect between the thirteen nodes ($n = 13$) of the tensegrity structure, resulting in forty-two total structural members ($m = 42$). As shown by the red lines in Figure 3.1, the twenty-four outer cables (those that exclusively connect between the twelve end points of the rods and not the central payload node) coincide with the edges of an icosahedron shape, creating a series of triangular faces on the external surface of the structure. However, we do not add cables on the six edges that would connect rods that are lying in the same plane. The twelve remaining cables connect the central payload node to the twelve rod nodes and are shown as blue lines in Figure 3.1.

Having discussed the rod, cable, and node arrangements, we can introduce the *connectivity matrix* for this six-bar spherical tensegrity. A connectivity matrix is a sparse matrix of ones and minus ones that encodes rod and cable connections to simplify computations in the analysis of tensegrity structures, such as the determination of static equilibrium [59] or of stable node positions given a rod and cable arrangement, which is referred to as tensegrity

form-finding [64, 65]. Each row of the connectivity matrix corresponds to either a rod or cable member within the tensegrity structure, and each column entry of a row represents a potential node connection. It can be helpful to think of this representation as a graph structure where rows are edges and columns are nodes. Explicitly, we define the connectivity matrix, $\mathbf{C} \in \mathbb{R}^{(n_r+n_c)\times n}$, where structural member i connects nodes j and k for $j < k$, as the following:

$$\mathbf{C}(a,b) = \begin{cases} 1 & \text{if} \quad a = i, b = j \\ -1 & \text{if} \quad a = j, b = i \\ 0 & \text{else} \end{cases} \tag{3.4}$$

Notice that as a result of the way $\mathbf{C}$ is constructed, all rows must sum to zero. Using 3.4 and the desired topology, we can construct $\mathbf{C}$ to represents the connectivity of the six-bar spherical tensegrity. For the sake of readability, we will section $\mathbf{C}$ into blocks $\mathbf{C}_c \in \mathbb{R}^{n_c\times n}$ and $\mathbf{C}_r \in \mathbb{R}^{n_r\times n}$ representing the cable connectivity and cable rod respectively.

$$\mathbf{C} = \begin{bmatrix} \mathbf{C}_c \\ \mathbf{C}_r \end{bmatrix} \tag{3.5}$$

The full connectivity matrix for our chosen six-bar spherical tensegrity is as follows:

$$\mathbf{C} = \begin{bmatrix}
1 & 0 & 0 & 0 & -1 & 0 & 0 & 0 & 0 & 0 & 0 & 0 & 0 \\
1 & 0 & 0 & 0 & 0 & -1 & 0 & 0 & 0 & 0 & 0 & 0 & 0 \\
1 & 0 & 0 & 0 & 0 & 0 & 0 & 0 & -1 & 0 & 0 & 0 & 0 \\
1 & 0 & 0 & 0 & 0 & 0 & 0 & 0 & 0 & 0 & -1 & 0 & 0 \\
0 & 1 & 0 & 0 & 0 & 0 & -1 & 0 & 0 & 0 & 0 & 0 & 0 \\
0 & 1 & 0 & 0 & 0 & 0 & 0 & -1 & 0 & 0 & 0 & 0 & 0 \\
0 & 1 & 0 & 0 & 0 & 0 & 0 & 0 & -1 & 0 & 0 & 0 & 0 \\
0 & 1 & 0 & 0 & 0 & 0 & 0 & 0 & 0 & 0 & -1 & 0 & 0 \\
0 & 0 & 1 & 0 & -1 & 0 & 0 & 0 & 0 & 0 & 0 & 0 & 0 \\
0 & 0 & 1 & 0 & 0 & -1 & 0 & 0 & 0 & 0 & 0 & 0 & 0 \\
0 & 0 & 1 & 0 & 0 & 0 & 0 & 0 & 0 & -1 & 0 & 0 & 0 \\
0 & 0 & 1 & 0 & 0 & 0 & 0 & 0 & 0 & 0 & 0 & -1 & 0 \\
0 & 0 & 0 & 1 & 0 & 0 & -1 & 0 & 0 & 0 & 0 & 0 & 0 \\
0 & 0 & 0 & 1 & 0 & 0 & 0 & -1 & 0 & 0 & 0 & 0 & 0 \\
0 & 0 & 0 & 1 & 0 & 0 & 0 & 0 & 0 & -1 & 0 & 0 & 0 \\
0 & 0 & 0 & 1 & 0 & 0 & 0 & 0 & 0 & 0 & 0 & -1 & 0 \\
0 & 0 & 0 & 0 & 1 & 0 & 0 & 0 & -1 & 0 & 0 & 0 & 0 \\
0 & 0 & 0 & 0 & 1 & 0 & 0 & 0 & 0 & -1 & 0 & 0 & 0 \\
0 & 0 & 0 & 0 & 0 & 1 & 0 & 0 & 0 & 0 & -1 & 0 & 0 \\
0 & 0 & 0 & 0 & 0 & 1 & 0 & 0 & 0 & 0 & 0 & -1 & 0 \\
0 & 0 & 0 & 0 & 0 & 0 & 1 & 0 & -1 & 0 & 0 & 0 & 0 \\
0 & 0 & 0 & 0 & 0 & 0 & 1 & 0 & 0 & -1 & 0 & 0 & 0 \\
0 & 0 & 0 & 0 & 0 & 0 & 0 & 1 & 0 & 0 & -1 & 0 & 0 \\
0 & 0 & 0 & 0 & 0 & 0 & 0 & 1 & 0 & 0 & 0 & -1 & 0 \\
1 & 0 & 0 & 0 & 0 & 0 & 0 & 0 & 0 & 0 & 0 & 0 & -1 \\
0 & 1 & 0 & 0 & 0 & 0 & 0 & 0 & 0 & 0 & 0 & 0 & -1 \\
\vdots & & & & & & \ddots & & & & & & \vdots \\
0 & 0 & 0 & 0 & 0 & 0 & 0 & 0 & 0 & 0 & 1 & 0 & -1 \\
0 & 0 & 0 & 0 & 0 & 0 & 0 & 0 & 0 & 0 & 0 & 1 & -1 \\
1 & 0 & -1 & 0 & 0 & 0 & 0 & 0 & 0 & 0 & 0 & 0 & 0 \\
0 & 1 & 0 & -1 & 0 & 0 & 0 & 0 & 0 & 0 & 0 & 0 & 0 \\
0 & 0 & 0 & 0 & 1 & 0 & -1 & 0 & 0 & 0 & 0 & 0 & 0 \\
0 & 0 & 0 & 0 & 0 & 1 & 0 & -1 & 0 & 0 & 0 & 0 & 0 \\
0 & 0 & 0 & 0 & 0 & 0 & 0 & 0 & 1 & 0 & -1 & 0 & 0 \\
0 & 0 & 0 & 0 & 0 & 0 & 0 & 0 & 0 & 1 & 0 & -1 & 0
\end{bmatrix} \in \mathbb{R}^{42\times 13} \tag{3.6}$$

We will refer back to the connectivity matrix often in our analysis of the six-bar spherical tensegrity structure. As an example of its utility, we can use $\mathbf{C}$ and the coordinates from

3.3 to calculate the some useful quantities. If the coordinates of the nodes are stacked in a matrix, $\mathbf{N} \in \mathbb{R}^{3\times n}$, computing a matrix of vectors, $\mathbf{V} \in \mathbb{R}^{3\times n}$, that represent the members of the structure becomes a simple matrix multiplication:

$$\mathbf{V} = \mathbf{CN} \tag{3.7}$$

In the next sections, we will use this representation to analyze the suitability of the structure for force-sensing and to help us make design decisions regarding the development of a force-sensing tensegrity prototype using the six-bar spherical tensegrity topology as a scaffold.

3.5 Static Analysis of Forces in Tensegrity Structures

Now that we have established the basic representation and characteristics of the class-1 six-bar spherical tensegrity, we can begin to discuss several theoretical results that will be relevant to our design process for the first iterations of the force-sensing tensegrity prototype. We will show that our chosen six-bar spherical topology of tensegrity will have the necessary properties to allow minimal sensor integration to achieve sufficient bandwidth in force-sensing.

The static analysis of forces in a tensegrity structure is a topic of obvious relevance to the determination of stable structures for the various applications in which tensegrity concepts can be found. As such, researchers have developed a popular methodology for conducting this analysis in a systematic way. The *force density method* (FDM) is an approach that is commonly used to determine member force conditions for assuring static equilibrium in a tensegrity network given desired node positions and external forces [56, 65]. FDM has also been used in the structuring of form-finding algorithms as well as control methods that rely on optimization-based frameworks [22, 54]. We will present the method here in an abreviated form for our purposes.

There are several important assumptions that are made about the mechanical properties of the structure in an FDM analysis. We will list them here for clarity:

- All nodes of the structure are ball joints and impart no moments on the members.
- External forces applied to the structure only occur at the nodes.
- All members are thin, massless, and do not experience deformation.

We represent each node, j, in three-dimensional Cartesian coordinate system, $\{x_j, y_j, z_j\}$, and coordinates for all nodes are accumulated into vectors for each dimension, $\mathbf{x}, \mathbf{y}, \mathbf{z} \in \mathbb{R}^n$. The external forces imparted on each node, j, of the structure, $\{p_{x,j}, p_{y,j}, p_{z,j}\}$, are defined in a similar fashion: $\mathbf{p}_x, \mathbf{p}_y, \mathbf{p}_z \in \mathbb{R}^n$. The force vectors for each axis are concatenated into a full external force vector, $\mathbf{p}$:

$$\mathbf{p} = \begin{bmatrix} \mathbf{p}_x \\ \mathbf{p}_y \\ \mathbf{p}_z \end{bmatrix} \in \mathbb{R}^{3n} \tag{3.8}$$

The *force density*, q_i, in a structural member, i, of a tensegrity network is defined as a function of the force along the member, F_i, and its length, l_i. The force densities for all structural members are concatenated into a force density vector.

$$q_i = \frac{F_i}{l_i} \tag{3.9}$$

$$\mathbf{q} = \begin{bmatrix} q_i \\ \vdots \\ q_m \end{bmatrix} \in \mathbb{R}^m \tag{3.10}$$

We can then write out the force balance equations in terms of the previously defined terms and the connectivity matrix for the tensegrity structure, $\mathbf{C}$.

$$\begin{aligned} \mathbf{C}^\top \text{diag}(\mathbf{q})\mathbf{C}\mathbf{x} &= \mathbf{p}_x \\ \mathbf{C}^\top \text{diag}(\mathbf{q})\mathbf{C}\mathbf{y} &= \mathbf{p}_y \\ \mathbf{C}^\top \text{diag}(\mathbf{q})\mathbf{C}\mathbf{z} &= \mathbf{p}_z \end{aligned} \tag{3.11}$$

Equation 3.11 can be rearranged into a linear system of equations that takes the following matrix form:

$$\mathbf{A}\mathbf{q} = \mathbf{p}, \tag{3.12}$$

where

$$\mathbf{A} = \begin{bmatrix} \mathbf{C}^\top \text{diag}(\mathbf{C}\mathbf{x}) \\ \mathbf{C}^\top \text{diag}(\mathbf{C}\mathbf{y}) \\ \mathbf{C}^\top \text{diag}(\mathbf{C}\mathbf{z}) \end{bmatrix} \in \mathbb{R}^{3n \times m} \tag{3.13}$$

Using a connectivity matrix, a set of node coordinates, and external forces acting on those nodes, we can utilize this matrix, $\mathbf{A}$, in equation 3.12 to solve for a set of valid force densities in the members of the structure. Note, however, that there is no guarantee of a solution to this system of linear equations for a given tensegrity form and accompanying external forces. Even so, this formulation provides a convenient linear relation between external physical stimulus and the internal forces experienced by the structural members. We can use this relation to better understand the potential of this structure for force sensing instrumentation.

As noted in [64, 72], the force-density method for tensegrity structures will always result in a rank deficient and noninvertible force-density matrix, $\mathbf{C}^\top\mathbf{C}$. Additionally, 3.13 will

also often be either rank deficient or non-square. Commonly, approaches utilizing FDM will employ the Moore-Penrose pseudoinverse for noninvertible matrices to solve the linear system of equations. The resulting pseudoinverse may be rank deficient as well. A consequence of this rank deficiency in the context of FDM is that the mapping between external forces and internal force densities is not unique.

Consider the function, $f_{A^+} : \mathbb{R}^{3n} \rightarrow \mathbb{R}^m$, mapping from the set of all external force vectors, $\mathbf{p} \in \mathbb{R}^{3n}$, to the set of force density vectors, $\mathbf{q} \in \mathbb{R}^m$.

$$f_{A^+}(\mathbf{p}) : \mathbf{A}^+\mathbf{p} \tag{3.14}$$

We will assume that valid node positions and connectivity matrix are given to construct $\mathbf{A}$ such that 3.12 is solveable for some non-empty set of force density vectors. Because $\mathbf{A}^+$ is potentially rank deficient, it is not necessarily true that for two distinct external force vectors, $\mathbf{p}_1$ and $\mathbf{p}_2$ where $\mathbf{p}_1 \neq \mathbf{p}_2$, $f_{A^+}(\mathbf{p}_1) \neq f_{A^+}(\mathbf{p}_2)$. This has important implications for force-sensing instrumentation of a tensegrity structure, so we will pause briefly to discuss them.

In designing a force-sensing tensegrity, our goal is to enable a tensegrity structure with the ability to not only detect when physical interactions occur with the structure but also map these interactions distinctly to, e.g., inferred intents. If we assume that all physical interactions with a tensegrity will result in some external force being applied to the nodes of the structure, then we would hope that these interactions could be distinguished by some instrumentation of the components of the tensegrity. From our discussion above, it is clear, at least in the static case, that the inherent properties of the tensegrity structure will not necessarily yield a full set of distinct force densities from distinct external forces. The question then becomes whether there exists a subset of force densities that are guaranteed to be distinct when two unique sets of external forces are applied to the structure.

Here, we present a methodology for determining a subset of force density quantities that will allow for visibility of physical interactions with the structure of the tensegrity by decomposing the original FDM relation into distinct subsystems using the block matrix pseudoinverse [8]. The resulting force density quantities will reveal suitable candidates, in terms of structural members, for force-sensor instrumentation. Consider a column-wise partitioning of the original $\mathbf{A}$ matrix:

$$\mathbf{A} = \begin{bmatrix} \mathbf{A}_a & \mathbf{A}_b \end{bmatrix}, \mathbf{A}_a \in \mathbb{R}^{3m\times(m-k)}, \mathbf{A}_b \in \mathbb{R}^{3m\times k} \tag{3.15}$$

The FDM balance equation will then become the following:

$$\begin{bmatrix} \mathbf{A}_a & \mathbf{A}_b \end{bmatrix} \begin{bmatrix} \mathbf{q}_a \\ \mathbf{q}_b \end{bmatrix} = \mathbf{p}, \tag{3.16}$$

where $\mathbf{q}_a \in \mathbb{R}^{(m-k)}$ and $\mathbf{q}_b \in \mathbb{R}^k$. For this, we can initially choose some arbitrary number of force densities, k, to partition our system.

Next, we compute the orthogonal projection matrices for each block of our column-wise partioned $\mathbf{A}$ matrix.

$$\begin{aligned} \mathbf{P}^{\perp}_{\mathbf{A}_a} &= \mathbf{I}_{3n} - \mathbf{A}_a(\mathbf{A}_a^{\top}\mathbf{A}_a)^{-1}\mathbf{A}_a^{\top} \\ \mathbf{P}^{\perp}_{\mathbf{A}_b} &= \mathbf{I}_{3n} - \mathbf{A}_b(\mathbf{A}_b^{\top}\mathbf{A}_b)^{-1}\mathbf{A}_b^{\top} \end{aligned} \tag{3.17}$$

It should be noted that the above equations are not necessarily valid for rank deficient $\mathbf{A}$. In order for this method to be valid, we must ensure that the column-wise partitioned matrices, $\mathbf{A}_a$ and $\mathbf{A}_b$, satisfy the following condition per [8]:

$$\mathcal{R}(\mathbf{A}_1) \cap \mathcal{R}(\mathbf{A}_2) = \{\mathbf{0}\} \tag{3.18}$$

This is a slightly less restrictive assumption than $\mathbf{A}$ being full column rank. With the orthogonal projection matrices, $\mathbf{P}^{\perp}_{\mathbf{A}_1}$ and $\mathbf{P}^{\perp}_{\mathbf{A}_2}$, we can reformulate the original FDM condition as two separate equations that describe the contributions of two subsets of the force density vector:

$$\begin{aligned} \mathbf{q}_a &= (\mathbf{P}^{\perp}_{\mathbf{A}_b}\mathbf{A}_a)^{+}\mathbf{p} \\ \mathbf{q}_b &= (\mathbf{P}^{\perp}_{\mathbf{A}_a}\mathbf{A}_b)^{+}\mathbf{p} \end{aligned} \tag{3.19}$$

We can then perform rank tests on each matrix quantity, $(\mathbf{P}^{\perp}_{\mathbf{A}_b}\mathbf{A}_a)^{+}$ and $(\mathbf{P}^{\perp}_{\mathbf{A}_a}\mathbf{A}_b)^{+}$. In most cases, we will find that these mappings will be short, wide matrices due to the scaling of external forces with the number of force densitities ($(\mathbf{P}^{\perp}_{\mathbf{A}_a}\mathbf{A}_b)^{+} \in \mathbb{R}^{k\times 3n}$, where $k < 3n$). As such, the most we can hope to demonstrate in this case is a fully acccessible codomain of force density values, i.e. *surjectivity*. This limitation, however, is a direct consequence of the fact that we are attempting to map *all* external forces applied to *all* nodes to a small subset of force density values. In reality, this is an ambitious prospect for any sensing implementation and would require instrumentation on the same order as the number of desired measurements. Therefore, we reduce the problem again by considering only a subset, k, of the external forces, $\mathbf{p}_b$, by partioning one of the systems in 3.19 once more to create the following:

$$\mathbf{q}_b = \mathbf{Z}_b\mathbf{p}_b, \tag{3.20}$$

where

$$\mathbf{Z}_b = (\mathbf{P}^{\perp}_{\mathbf{A}_a}\mathbf{A}_b)^{+}\mathbf{S} \tag{3.21}$$

and $\mathbf{S} \in \mathbb{R}^{k\times 3n}$ is a selection matrix with rows of ones corresponding to the columns of interest in the matrix $(\mathbf{P}^{\perp}_{\mathbf{A}_a}\mathbf{A}_b)^{+}$. If $\mathbf{Z}_b \in \mathbb{R}^{k\times k}$ matrix is full rank, then the associated mapping from $\mathbf{q}_b$ to $\mathbf{p}_b$ is *bijective*. If we assume that (1) we have instrumented structural members associated with $\mathbf{q}_b$ with force-sensing and (2) solutions exist to 3.12, $\mathbf{q}_{b,1}$ and $\mathbf{q}_{b,2}$, for two distinct subsets of external forces, $\mathbf{p}_{b,1}$ and $\mathbf{p}_{b,2}$ respectively, then the measured forces will also be distinct.

$$\text{rk}(\mathbf{Z}_b) = k, \mathbf{p}_{b,1} \neq \mathbf{p}_{b,2} \rightarrow \mathbf{q}_{b,1} \neq \mathbf{q}_{b,2} \tag{3.22}$$

By computing this decomposition, repeatedly selecting components of $(\mathbf{P}^{\perp}_{\mathbf{A}_a}\mathbf{A}_b)^{+}$, and performing the aforementioned rank check, one can arrive at a suitable subset of force density quantities that will provide reliably distinct force sensor measurements under the assumptions and conditions given. One disadvantage of this methodology is evidenced by the fact that it does not provide any guarantees about the existence of solutions to 3.12 or its partitioned counterpart. Indeed, we can expect that for many cases in which 3.22 is satisfied, the mapping is not surjective. Furthermore, the results outlined here are only applicable in a purely static case for tensegrity structures in equilibrium. We see this approach being particularly useful for the design of force-sensing implementations for large, complex tensegrity structures where there is a need for efficient sensor placement.

This result applies nicely to our unique scenario involving the six-bar spherical tensegrity. We consider the original six-bar spherical tensegrity topology without the added central payload. Instrumenting a total of 30 structural elements (24 cables and 6 bars) would require a prohibitive amount of sensor integration. Instead, we apply the technique outlined above to investigate if it would be possible to extract distinct sensor measurements by instrumenting only the 6 bars. There are other design-related considerations involved in this choice, which we will discuss in a later chapter. We calculate the $\mathbf{A}$ matrix as in 3.13 and partition it according to 3.16 with $\mathbf{A}_b$ corresponding to the bar members ($k = 6$). Note that since $\mathbf{A}$ is constructed via $\mathbf{C}$, the rows of which can be specifically ordered based on member type, $\mathbf{A}$ can be column-wise partioned to segregate cables from bars. It can be shown that this partioning will satisfy condition 3.18. We then select the external forces applied to two arbitrary nodes (for a total of six quantities) and apply a corresponding selection matrix $\mathbf{S}$. The resulting square matrix $\mathbf{Z}_b \in \mathbb{R}^{k\times k}$ is full rank, which means that the mapping is bijective.

From this analysis, we can be confident that instrumenting the six bars of the structure with force sensors will produce measurements that will be reliably distinct for different physical interactions that occur with the structure of the device. This is an important prerequisite to our later discussion about classification feasibility based on the amount of information contained in features derived from force sensor data, which will be used in the development of our supervised learning framework. For now, we will move on to modeling the dynamics of the proposed system to examine the simulated response of the structure to physical interactions in a few representative scenarios. Specifically, we can focus our attention on our anticipated measurements, which will be the compressive loads on the bars of the structure.

3.6 Dynamic Analysis of Forces Using Simplified Point Mass Dynamics

Now that we have established a theoretical basis for pursuing a specific configuration of force-sensing integration in our spherical six-bar tensegrity by using a static approach, we can begin to examine the characteristics of the proposed force measurements using the explicit dynamics of the system. Simulating the dynamics of the system with an approximate physical model will provide us with key data points for the design of force-sensor instrumentation. It will also be useful to make qualitative comparisons between data simulated in different physical interactions to further justify our selection of structural members for sensor integration.

Despite the simplicity of their constituent members, tensegrity structures are challenging to model accurately due to the connectivity of the structure and the interaction of members within the structure. This results in highly complex coupled nonlinear dynamics that can be quite sensitive to numerical instability in simulation. There have been a variety of approaches to simulating tensegrity dynamics robustly. It's common for many of these approaches to adopt a Lagrangian methodology while simultaneously making a number of simplifying assumptions. In this work, we take advantage of previous research from the BEST Lab on tensegrity dynamics simulation that uses a simplified point mass dynamics formulation, which performs well in terms of numerical stability and computational efficiency [12]. We will briefly introduce the formulation here to aid in our discussion of the physical interaction scenarios used to generate simulated measurement data.

As the name suggests, the primary assumption used in the derivation of this dynamics formulation is the use of point masses instead of distributed mass in the members of the structure. This will end up being an appropriate assumption—especially in our case—due to the way the prototype system will be constructed. Additional assumptions used in this formulation are common to many similar tensegrity dynamics simulation approaches. All nodes of the structure are ball joints and impart no moments on the structure. External forces are only applied at the nodes of the structure, and physical contact between members is neglected. Cables have an inherent elasticity, and the forces arising from cable deformation are computed based on a Hookean model with added damping. Constraints on relative node position due to rigid bars are enforced using the principle of virtual work. General forces acting on the structure (including ground contact, friction, etc.) are applied using soft approximations that are numerically stable. For more information on the details of this formulation, please refer to [12].

The states of the system are defined based on the nodes of the structure and consist of the x, y, z positions and velocities in vectors $\mathbf{p}, \dot{\mathbf{p}} \in \mathbb{R}^{3n}$.

$$\mathbf{p} = \begin{bmatrix} x_1 \\ y_1 \\ z_1 \\ \vdots \\ x_n \\ y_n \\ z_n \end{bmatrix} \quad \dot{\mathbf{p}} = \begin{bmatrix} \dot{x}_1 \\ \dot{y}_1 \\ \dot{z}_1 \\ \vdots \\ \dot{x}_n \\ \dot{y}_n \\ \dot{z}_n \end{bmatrix} \tag{3.23}$$

The equations of motion governing the dynamics are derived using a first principles approach where the sum of legal forces (i.e. forces that do not violate constraints) from each contributing source (e.g. ground contacts, system constraints, cable forces) are collected into terms for each axis. The resulting dynamics can then be written as follows:

$$\begin{aligned} \ddot{\mathbf{p}} &= \mathbf{W} \cdot \mathbf{F}_{\text{legal}} \\ \ddot{\mathbf{p}} &= \mathbf{W} \cdot \Big(-\mathbf{J}^\top (\mathbf{J}\mathbf{W}\mathbf{J}^\top)^{-1} (\dot{\mathbf{J}}\dot{\mathbf{p}} - k_s \mathbf{G} - k_d \dot{\mathbf{G}}) + \\ &\qquad (\mathbf{I}_{3n} - \mathbf{J}^\top (\mathbf{J}\mathbf{W}\mathbf{J}^\top)^{-1} \mathbf{J}\mathbf{W}) (\sum_j \gamma_j + \mathbf{F}_{\text{ext}}) \Big) \end{aligned} \tag{3.24}$$

where $\mathbf{W}$ is a matrix that represents the inverse of the point masses, $\mathbf{J}$, $\mathbf{G}$ are implicit constraint terms, γ_j are forces arising from cables, and $\mathbf{F}_{\text{ext}}$ represents external forces. Note that the terms k_s and k_d are gains that control the stiffness and damping of the implicit constraints and are used to tune the constraining forces on the system.

For the purposes of examining a simulated response to physical interaction with a system that has been instrumented with force-sensing, we must be able to extract sensor measurements. In the previous section, we described a particular configuration of sensors that would be advantageous to our goal of detecting physical interactions efficiently by instrumenting the six bars of the system. We can simulate what these measurements would look like by computing the internal forces in the bars of the structure.

We start with the earlier assumptions that the structure experiences no moments due to the connectivity of its members and that forces are only applied through the nodes. This reduces the problem down to identifying the axial loading on the bars, which, if we assume that the tensegrity is well-tensioned, will be almost exclusively compressive. Figure 3.2 shows a single bar in Cartesian space held in compression by two opposing force vectors that represent the total force applied at the nodes, $\mathbf{F}_{\text{total},a}, \mathbf{F}_{\text{total},b} \in \mathbb{R}^3$.

We project these force vectors along the bar's positional vector from both node directions. An important note is that the bar could be accelerating in any given direction due to the fact that the forces acting on the nodes are not equal. As a result, we consider the projected force from each node, $\mathbf{F}_{ab}$ and $\mathbf{F}_{ba}$, as distinct measurements.

$$\begin{aligned} \mathbf{F}_{ab} &= \frac{\mathbf{F}_{\text{total},a} \cdot \mathbf{v}_{ab}}{||\mathbf{v}_{ab}||} \mathbf{v}_{ab} \\ \mathbf{F}_{ba} &= \frac{\mathbf{F}_{\text{total},b} \cdot \mathbf{v}_{ba}}{||\mathbf{v}_{ba}||} \mathbf{v}_{ba} \end{aligned} \tag{3.25}$$

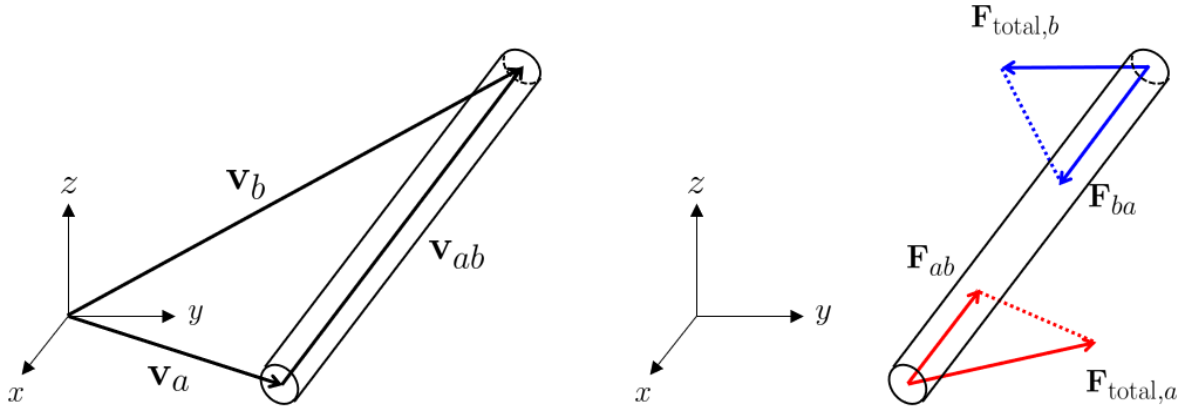

Figure 3.2: Diagram of total forces acting on a single bar held in compression. We project the total forces acting on each node along the bar in order to determine the compressive force experienced in either direction.

where $\mathbf{v}_{ab} = -\mathbf{v}_{ba}$ is a vector representing the position and orientation of the bar in space.

With this understanding of the expected force measurements, we will now present a few representative simulation scenarios of physical interactions with the system. We will then be able to analyze the measured signals in response to these perturbations in order to help us make decisions about our plans for sensor integration in the subsequent chapter. Specifically, we hope to get a sense of the expected range of forces to be measured, frequency of potential oscillations, and disparities between measured forces in given scenarios.

We define the six-bar spherical tensegrity as the subject model of our dynamics simulation largely as described earlier in this chapter with the exception of removing the central payload. Some additional configuration-specific parameters for the simulation include the effective stiffness of cable elements, cable pretension, and cable damping, which are presented in Table 3.1 below.

Effective cable stiffness	Cable pretension	Cable damping
$260N/m$	$9.75N$	$5Ns/m$

Table 3.1: Cable parameters used in dynamics simulation.

The first simulation scenario that we consider is a drop and impact with the ground from a height of approximately one meter, which simulates a human operator dropping or deploying the device. We will be dropping the tensegrity in an orientation that places one of

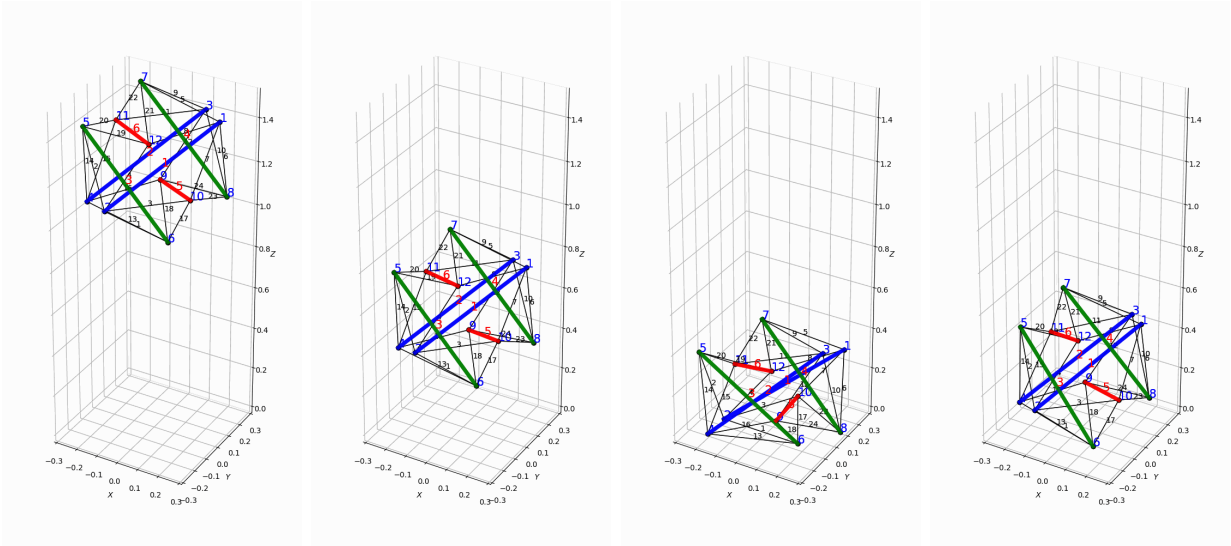

Figure 3.3: Four captured frames from the dynamics simulation scenario of dropping the tensegrity from a height of one meter, highlighting its impact with the ground. The simulation time proceeds from left to right.

the faces of its icosahedron shape aligned parallel with the ground plane, resulting in three nodes from three distinct bars impacting simultaneously. The timescale of the simulation is one millisecond. Figure 3.3 shows several captured frames from the simulation illustrating the progression of the state of the structure through its impact with the ground. We record the measured forces experienced by the bars from the direction of each node. The results are plotted in Figure 3.4.

We can see from Figure 3.4 that we are able to capture many features of the impact through the force readings on the nodes of the bar elements. To highlight a few details in the plot, the forces are initially constant due to the pretension of the structure and then immediately spike as a result of the impact. The forces then continue to oscillate as the force of the impact propagates through the structure, and the tensegrity bounces several times before settling. These data points demonstrate that force sensing through the rods of the structure will be useful in reconstructing physical interactions that involve impacts. We will now examine a different kind of physical interaction in simulation.

Because the structure of a tensegrity is often comprised of elastic elements (i.e. in the cable elements), they have an inherent degree of compliance. As a result, one can squeeze or pull on the structure, and it will deform in response. We can classify this category of contact between human and robot as another physical interaction worth investigating. We simulate a squeeze interaction by instantiating the model with it lying stationary on the ground and then applying a prescribed force to a set of nodes at the top of the structure. This will result in compression between the top nodes and the nodes that are in contact with the ground.

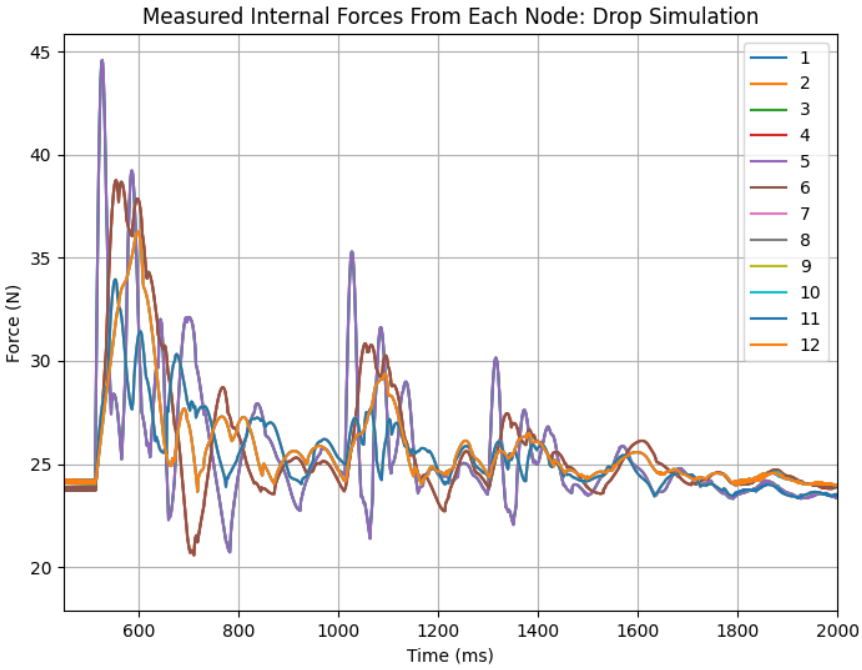

Figure 3.4: Plot of internal forces in the bars of the tensegrity during simulated scenario in which the tensegrity is being dropped from a one meter height.

To simulate the force applied by a human, we use a first-order system response to impart a smooth squeezing force to the top nodes. Specifically, nodes 3, 7, and 11 form a closed face on the top side of the structure, and we apply the following force in the z-direction to each node over a period of 3 seconds.

$$\mathbf{F}_{\text{squeeze}} = \begin{cases} -M(1-\exp^{\frac{at}{1.5}}) & if \quad 0s \leq t < 1.5s \\ -M(1-\exp^{\frac{a(3-t)}{1.5}}) & if \quad 1.5s \leq t < 3s \end{cases} \tag{3.26}$$

where M is the maximum force applied at the peak of the force trajectory and a controls the rate at which the force increases and decreases according to a first-order response model.

Figure 3.5 shows the tensegrity first in a stationary position on the ground and then being compressed to a flattened state due to the forces acting on the upper nodes. Figure 3.6 displays the internal forces throughout the simulated squeeze interaction. Again, we can extract all of the relevant features from the measured forces, which resemble the input force trajectory. What is particularly pronounced in this case is the difference between internal forces across certain members, which we hypothesize to be a result of a combination of initial orientation of the structure as well as the location of applied forces from the squeeze

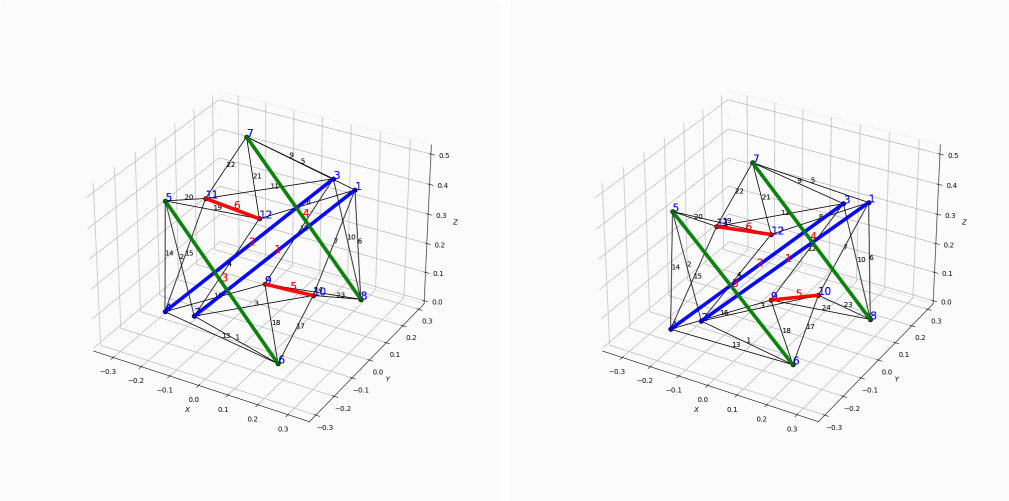

Figure 3.5: Two captured frames from the dynamics simulation scenario of squeezing the tensegrity by applying equal force downward on nodes 3, 7, and 11. The simulation time proceeds from left to right.

interaction.

From these simulated physical interaction scenarios, we can see that the chosen sensor instrumentation should be effective at capturing the necessary features of a physical interaction for the purpose of distinguishing between different types of events. In the next chapter, we will outline the process for implementing this sensing capability in the design of two force-sensing tensegrity prototypes.

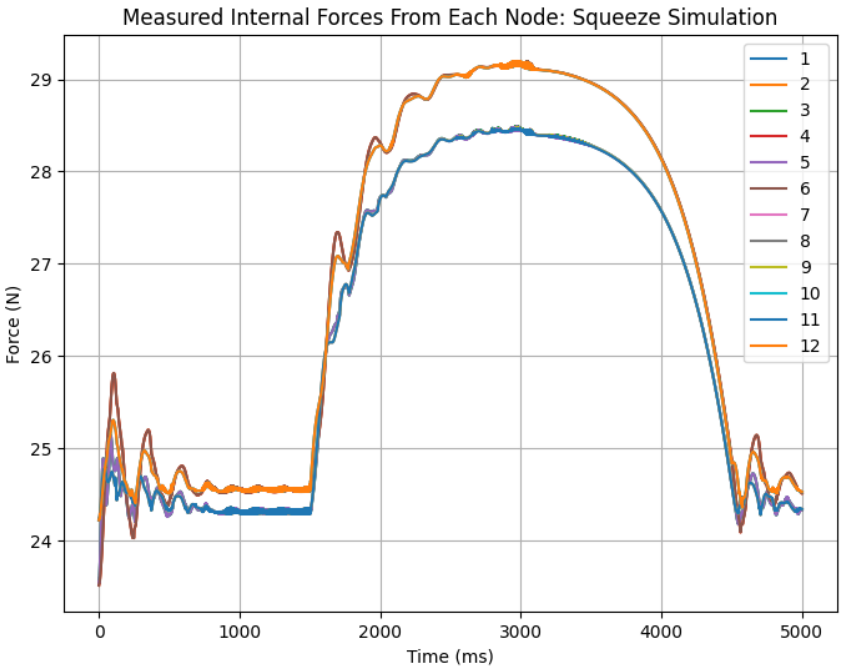

Figure 3.6: Plot of internal forces in the bars of the tensegrity during simulated scenario in which the tensegrity is being squeezed vertically on nodes 3, 7, and 11.

Chapter 4

Design of a Force-Sensing Tensegrity

4.1 Introduction

This chapter is dedicated to the design of two separate iterations of the force-sensing tensegrity, which will be used to demonstrate the feasibility of the previously discussed novel modalities of physical human-robot interaction with compliant robotic systems. The primary goal of the design process is to develop a tensegrity platform that is capable of measuring internal forces as they arise due to the manipulation of the device or reaction of the external structure to contact. We demonstrated in the previous chapter that the specific tensegrity configuration we are using has the right properties to enable minimal sensor placement while still allowing for full visibility and distinction of external forces. We will rely on these properties when making design choices with respect to the type, placement, and circuitry of sensing solution. Furthermore, the accommodation of the additional sensing capability in the structure of the device will require the construction of specially designed enclosures that do not compromise the integrity of the original structure. Finally, we will cover the implementation of the necessary embedded electronics to allow for sample acquisition, data processing, and wireless communication. Inherent to this design process will also be the consideration of usability in the context of pHRI and the facilitation of future human subject experiments to be discussed later in this work.

In our first prototype of the force-sensing tensegrity, we introduce a novel force sensor integration that extends the effective range of force-sensing at the cost of introducing an additional source of compliance to the structure. Preliminary experiments are used to demonstrate that the configuration of sensors can be used to distinguish between physical interactions in controlled conditions. The second iteration prototype improves on force sensor integration, quality of force-sensor data, and operator usability through a modular sensor packaging. We also improve on payload integration and embedded electronics to allow for additional functionality in experimental scenarios.

4.2 Prior Work

As discussed in the background and literature section of this dissertation, the incorporation of various sensing modalities in tensegrity structures in robotic applications is an inevitability. Many tensegrity robots rely on the unique features of the structure to enable novel actuation, such as in the case of cable-driven spherical tensegrity robots [12, 55]. Researchers have even proposed methods for determining appropriate sensor placement for the control of these tensegrity devices [42]. In these cases, the goal is typically to measure the properties of the structure that directly relate to controlled states for the purpose of more complete state estimation (e.g. cable lengths), which continues to be an open problem in the design of actuated tensegrity systems. There have been advances toward more robust state estimation of tensegrity structures that make use of novel sensing mechanisms, such as smart skins [10].

In contrast, there have been some examples of tensegrity structures that are themselves, in fact, sensors. These tensegrity sensors combine a multitude of smaller sensors that are integrated into the structure of the device, which are then fused together [62]. Researchers have suggested that tensegrity structures can serve dual purposes as structural members and as embedded sensor arrays [20]. Other instances of sensor placement methodologies that are similar to the theoretical framework proposed in the previous section of this dissertation can create sensor configurations for applications in monitoring of structural identification and damage detection in tensegrity structures [6].

4.3 Contributions of this Chapter

In the first part of this chapter, we discuss the necessary design considerations for instrumenting the six-bar spherical tensegrity structure with embedded force-sensing resistors (FSRs). We then describe the components used in the construction and assembly of the tensegrity structure. In the first prototype design, a novel force-sensor packaging is used to extend the effective sensing range of the FSRs. We use controlled experiments to collect preliminary measured force data to show the performance of the prototype. After discussing the advantages and disadvantages of the first prototype, we commence design of the second iteration to improve on force sensing and usability. We also describe the latest iteration of the embedded system used to collect sensor data in experimental scenarios and transmit it wirelessly to streamline human subject experiments.

4.4 First-Iteration Force-Sensing Tensegrity

There are many possible options to choose from when searching for modern force-sensing solutions. Like in any design process, it is critical to first understand the necessary requirements for the sensor before making a selection. As we discovered in the previous chapter, the chosen tensegrity structure is well-suited for instrumentation aimed at sensing forces. Because of the connectivity of the structure resulting in the propagation of external forces

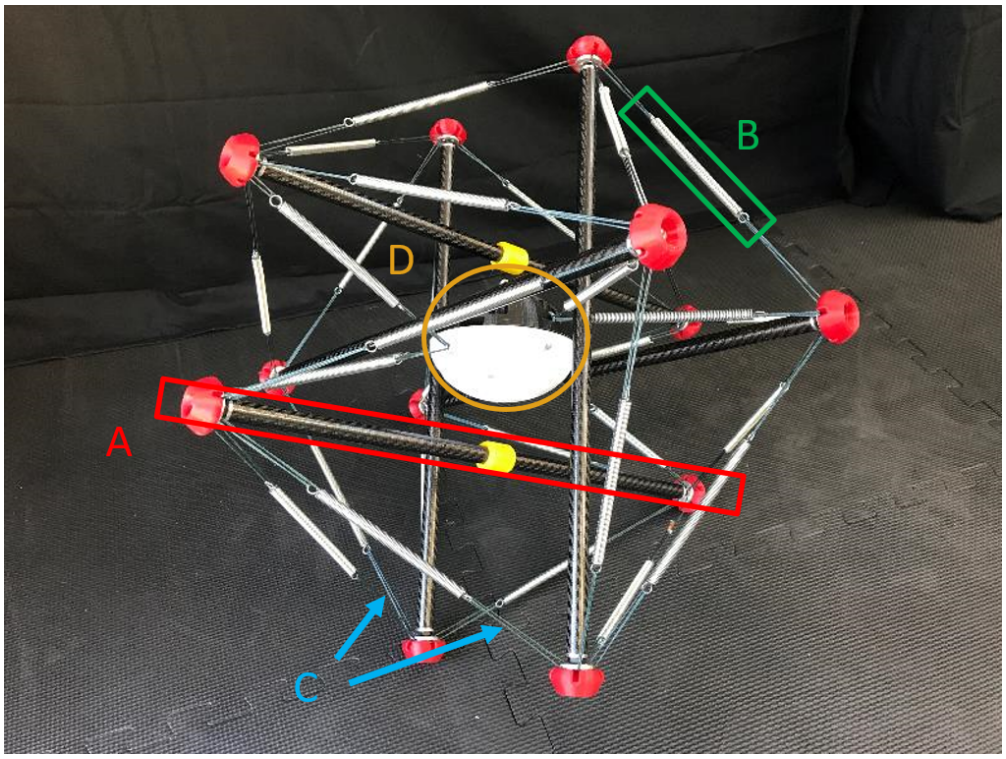

Figure 4.1: Picture of the base model of stationary six-bar spherical tensegrity used as the foundation for the force-sensing spherical tensegrity prototypes highlighting the main components.

through the rigid members, we can immediately reduce the problem of detecting external forces by a large degree to only instrumenting the bars of the structure. Furthermore, we have tangible data points for fine-tuning the sensing range of our system from the simulated physical interaction scenarios. Instead of requiring cumbersome multi-axis high-resolution force sensors at all points of the structure, we can instead rely on simpler single-axis force sensors in a limited number of locations. The problem now becomes one of desiging the system so that it can accomodate the additional sensing components. Fortunately, we were afforded the luxury of learning from the BEST lab and *Squishy Robotics Inc.*'s previous work on desiging spherical six-bar tensegrity robots. As such, we start with a discussion of the design aspects of a standard stationary (i.e. non-actuated) spherical six-bar spherical tensegrity, which will be used as the foundation of our force-sensing tensegrity prototype.

Throughout the remainder of this chapter, we will rely on the representation used in the previous chapter to describe the spherical six-bar tensegrity. The tensegrity structure comprises a total of 6 bars, 36 cables, and 12 nodes. The connectivity matrix describing the assembly of the structure is identical to 3.6. Figure 4.1 shows a fully assembled stationary spherical six-bar tensegrity.

The bars of the structure are made from carbon-fiber tubing (A in Figure 4.1), which has excellent rigidity without compromising on weight. Cable elements are constructed from nylon strings (C) in series with metal extension springs (B), creating elastic connections between members that gives the structure a controllable amount of compliance. Proprietary methods are used to design these cable assemblies with specific pretension to result in a stable tensegrity structure once fully assembled. For the purposes of our design discussion, we will treat them as standard springs with an effective spring stiffness. Finally, we have a 3D-printed central payload (D) that houses any necessary embedded electronics for sensing and communication. The payload is printed from thermoplastic polyurethane (TPU) material, which gives it the capacity to absorb moderate impacts without damage to internal components. TPU is also used to 3D-print bumpers on all 12 nodes to reduce wear on the connecting fixtures of the device.

When fully assembled, the tensegrity occupies a volume approximately equal to a sphere with a diameter of one half meter and has a weight of approximately 1 kg. Clearly, the base tensegrity scaffolding is extremeley lightweight, reasonably sized, and safely handleable by humans without risk of damage to itself or the human operator. One challenge for our design process will be to retain these properties once the system has been instrumented with additional sensing components. We will attempt to leverage as much of the original structure as possible. We can now begin to discuss strategies for designing integrated force-sensing within the bars of the spherical six-bar tensegrity.

The most common choice for detecting forces in rigid structural members is the strain gauge sensor. When integrated into a structural member with known material properties, strain gauges can provide a low-profile, accurate, and configurable way to extract internal forces in a variety of applications. They can be purchased individually to be added to components with custom geometry or they can be acquired as packaged multi-axis sensors that can be fastened into place as part of the structure itself. Unfortunately, neither case constitutes an effective solution for particular design requirements. The bars we are seeking to instrument are made from carbon fiber, which are difficult to quantify universally in terms of mechanical material properties due to the composite nature of the material and its resulting anisotropy. Since we are attempting to keep the overall weight of the system low, this also precludes the use of packaged strain gauge products due to the added weight from metal components and the typically oversized form factors.

Instead of strain gauges, we investigate the possibility of using force-sensing resistors (FSRs) for our design. As the name suggests, FSRs are sensors that can detect changes in force due to changes in resistance of a conductive polymer in response to deformation. Commonly, these kinds of force sensors are used for touch interfaces as they are well-suited for measuring compressive forces. In order to integrate this type of compressive sensor into our system, we require a location in the structure to place these FSRs that will coincide with the transmission of compressive loads from the nodes of the tensegrity to the bars. Fortunately, this requirement aligns perfectly with our previously discussed design requirement, which is to measure entirely compressive loads originating at each node of the tensegrity allowing for the desired degree of sensitivity to physical interactions. Additionally, we will see that

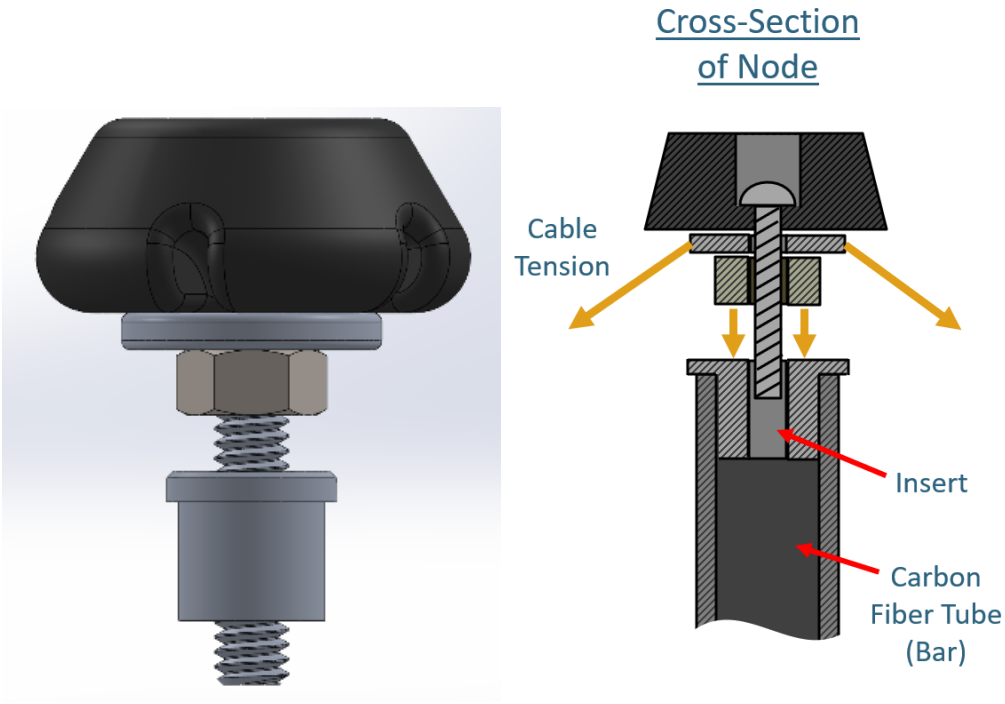

Figure 4.2: Models of the base tensegrity node to be instrumented with force sensing. The left image shows a CAD model of the upper node assembly. Right shows an approximate cross-section of the full assembly including bar, which illustrates how the upper assembly is floating with respect to the bar.

our chosen FSRs will integrate seamlessly with the node assemblies of the original tensegrity structure.

Figure 4.2 shows two renderings of the node assembly for the original tensegrity structure. On the right is an illustration of how the upper node assembly fits into the lower bar assembly. The arrangement of this part of the structure takes advantage of the unique properties of tensegrity structures by relying on the compression of bar members by the tension from cable members. The upper node assembly is floating in the longitudinal direction with respect to the lower bar assembly and motion is restricted laterally by the plunging bolt in the center being contained by the bar's insert. The insert on the lower bar assembly is not threaded, so the bolt can slide freely in the longitudinal direction within this cavity. Since the bars are necessarily held in compression by the cables to create a stable tensegrity configuration, the upper node assembly is held firmly in place against the lower bar assembly resulting in a compressive load (as illustrated by the arrows in Figure 4.2). This has the benefits of facilitating the initial assembly of the structure because of the lack of fasteners in addition to making the system easy to repair. Incidentally, the interface between the upper node assembly and the lower bar assembly constitutes an ideal location for placing a compressive

FSR-404 Specs	
Minimum force	∼0.2N
Force sensitivity range	∼0.2 - 20N
Force repeatability	±2%
Hysteresis	±10%

Table 4.1: Performance specifications for *Interlink Electronics* FSR-404.

force sensor. The translational degree of freedom created by the plunging bolt of the upper node assembly already has the desired effect of rectifying arbitrarily directed forces from the node to linear compressive forces imparted to the bar. Were we to place an FSR between the upper node assembly and the lower bar assembly, it would be possible to detect changes in compressive force resulting from any physical interaction with the external structure. This could include interactions with the nodes, cables, or bars depending on the type of physical interaction taking place.

The next step in the design process is finding an FSR model that is right for the application. As mentioned previously, most FSRs are manufactured in thin form factors that are intended for use as compressive contact interfaces. Ideally, we would want to create a bespoke fixture that enables direct surface-to-surface contact forces, which we would expect to measure. The presence of the bolt in the center of the upper node assembly, however, complicates the placement of an FSR due to the fact that there is no uninterrupted flat surface. After some searching, we were fortunate enough to find a solution that would work perfectly with the geometry of our current design. *Interlink Electronics* offers a convenient FSR form factor that features a through-hole in the center. Relevant specifications from the FSR-400 series products are shown in Table 4.1.

Immediately, we discovered a challenge to overcome with the chosen FSR's specifications in regard to the intended application. Based on the force measurements from our simulated physical interaction scenarios, the upper limit of the FSR-404's force sensitivity range will be too low for certain interaction conditions such as impacts from drops. Indeed, many of the similar FSR models operate in the same force sensitivity range. To address this potential issue, we devised a novel sensor packaging that extends the effective force sensitivity range without dramatically altering the existing geometry.

Inspired by the concept of a voltage divider, we introduce a parallel arrangement of compression springs into the sensor packaging that acts as a "force divider". Figure 4.3 shows a diagram of the proposed "force divider" configuration. By placing two springs in parallel between common surfaces, the total compressive force is distributed between the two springs, effectively reducing the force experienced by either spring by a controllable degree. The FSR can be placed in such a way that it is only measuring the compressive force from one of the two springs. We can use the following simple equation, which is analagous to the

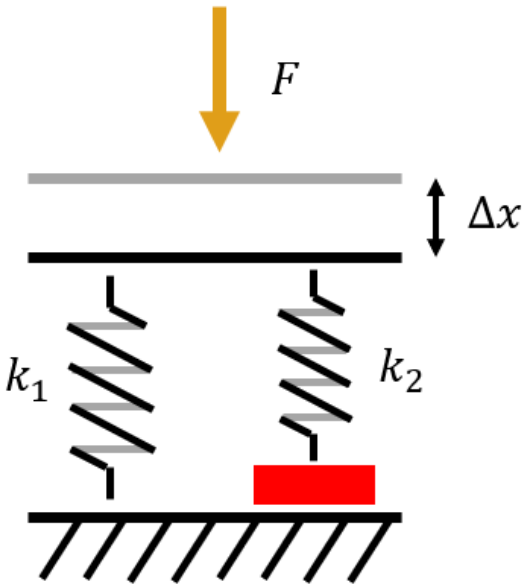

Figure 4.3: Diagram of "force divider" concept being used in the FSR sensor packaging for the first-iteration force-sensing tensegrity. The force is distributed across the two springs according to their stiffness, which can be configured to change the effective force sensitivity range in the FSR.

voltage divider equation, to convert the force signal from the FSR, F_2, to the actual internal force experienced by the structure, F.

$$F = \frac{k_1 + k_2}{k_2} F_2 \tag{4.1}$$

The fully constructed node assembly with integrated FSR as well as a cross-section of the model are shown in Figure 4.4. To achieve the desired "force divider" effect, two compression springs of different stiffnesses are aligned concentrically around the plunging bolt in the center of the upper node assembly. Special care is taken to select springs with appropriate specifications (spring stiffness, rest length, minimum length) to yield desired force sensitivity range and stroke length. The flange of the bar insert is extended to contain the springs on the bottom side while a 3D-printed washer is included above to contain the top side of the springs. Because the upper node assembly will now be traveling linearly with respect to the bar insert as a result of the added compliance, we reduce the hole size of the bar insert and turn the bolt threads down to a smooth surface to reduce friction between the bolt and insert. The FSR itself is placed on top of the bar insert so that the inner spring (k_2) compresses it without being affected by the outer spring (k_1).

One disadvantage of this sensor packaging is that it creates an additional source of compli-

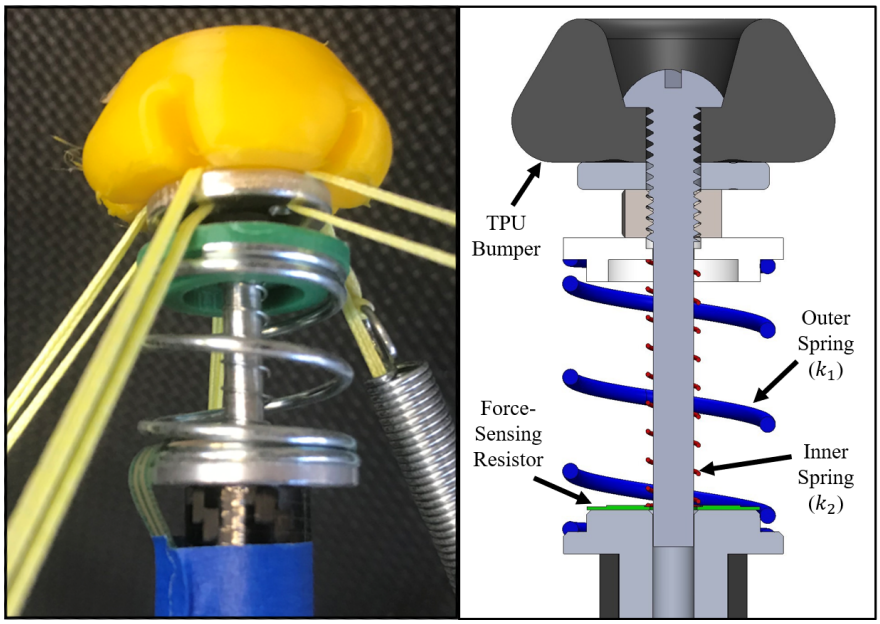

Figure 4.4: FSR integration in node of structure (first iteration). The left image shows the fully constructed node assembly with integrated FSR. On the right is a cross-section view of the node assembly CAD model showing the force divider mechanism.

ance in the structure that might influence either the stability of the tensegrity configuration or its overall stiffness to physical perturbations. To address these concerns, we recalculate cable lengths based on an extended bar length, taking into account pre-compressed extension springs, after the addition of the new sensor packaging.

To allow for the remote operation of these sensors, we needed to design a custom embedded electronics system that could support a range of functionalities including FSR data collection and wireless communication. For the FSRs, we use a voltage divider circuit to condition the raw FSR signal, which is acquired using analog inputs on a *PJRC* Teensy 3.5 microcontroller. Wireless communication is achieved using *XBee* modules to communicate to the operator's laptop to provide real time diagnostic information as well as experiment control flags for testing the force sensor array in experimental scenarios. We also include a BNO055 inertial measurement unit board to provide acceleration and orientation data to provide contextual state information in case it provides useful features to future interaction schema. The remainder of the system is devoted to power management for the various subsystems, which is powered by a 2-cell 7.4-volt lithium-ion battery. The fully assembled embedded electronics system including custom PCB is shown in Figure 4.5.

Cable pairs are routed from each of the twelve FSRs down the length of the bars toward the center of the structure where the central payload is suspended. The TPU 3D-printed central payload casing in the first-iteration prototype is refashioned from a stock central

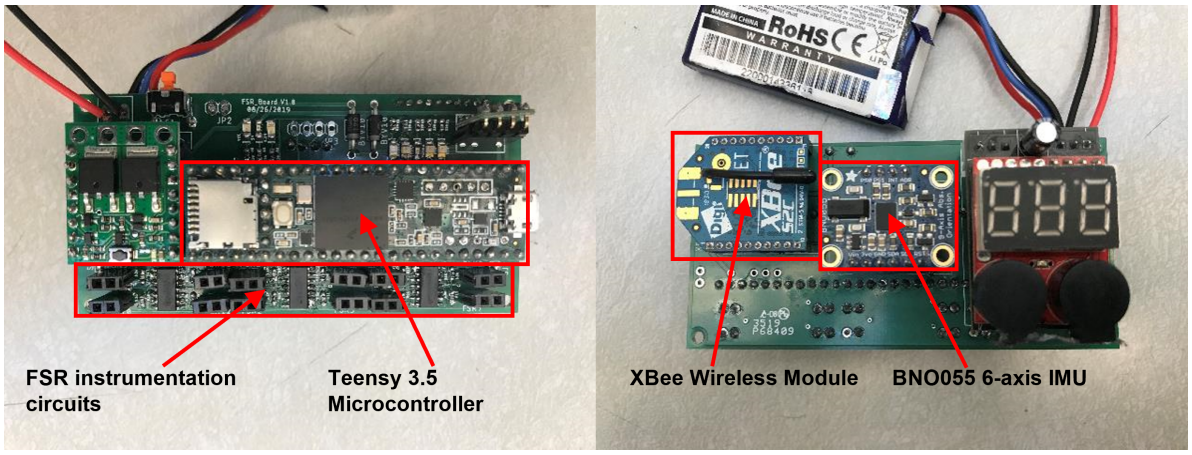

Figure 4.5: Images of the top and bottom sides of the fully assembled custom PCB for the embedded electronics in the first-iteration force-sensing tensegrity prototype.

payload casing to fit the custom embedded electronics and to accomodate FSR cable routing. More sophisticated attempts at central payload casing design will be covered in the second-iteration prototype. The fully assembled first-iteration prototype is shown in Figure 4.6.

To verify the performance of this system, we conducted a series of controlled physical interaction experiments with lab personnel to characterize the responses measured by the embedded force-sensor array. We will describe these preliminary physical interactions in more detail in the next section when we discuss inference strategies. For each experiment involving a single physical interaction type between human and robot, force readings are acquired from the twelve sensors at a frequency of $100Hz$ and stored in an onboard microSD card for subsequent processing. As an illustration of the performance of this system, force readings from a representative physical interaction in which the tensegrity is compressed (or "squeezed") vertically between two rigid surfaces is shown in Figure 4.7.

When compared to the simulated response in the squeeze test scenario, the forces that appear in the controlled experiment with the first-iteration prototype are quite similar, which gives confidence both in our theoretical representation of the dynamics and the appropriate instrumentation of the tensegrity structure. Note that the configured parameters of the simulation do not align exactly with the physical characteristics of the first iteration prototype (e.g. the simulation does not account for the added compliance in the sensor packaging of the first-iteration prototype). With the first-iteration prototype completed and operational, we can embark on an assessment of its advantages and disadvantages to inform our discussion of planned improvements for the second-iteration prototype design.

The primary advantage of the first-iteration prototype is the sensitivity and configurability of the force-sensor packages. Through the novel force-divider assembly, the range of force sensitivity of the nodes can be configured both to the needs of the application and the needs

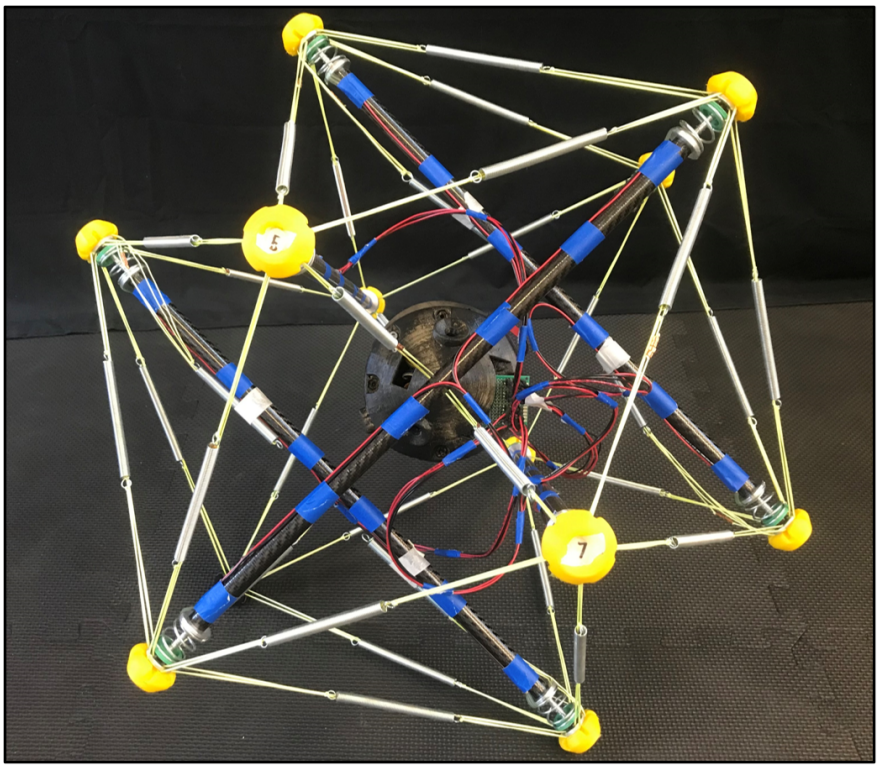

Figure 4.6: Image of fully assembled first-iteration force-sensing tensegrity. The full assembly includes 6 bars, 36 cables, and a central payload with embedded electronics enclosed inside. Each bar is instrumented with two force sensors—one at each node.

of the tensegrity structure itself. For example, the designer of the tensegrity robot might design a tensegrity structure with a higher overall stiffness by adjusting the elastic elements of the cables or their pretension through the initial lengths. Instead of needing to change the sensors or redesign the packaging, one can simply replace the compression springs in the force-divider assembly to result in a higher ratio of stiffnesses to support the increased loading without changing the force sensitivity range.

In terms of disadvantages, the added compliance of the rigid elements is perhaps the most glaring and open question in the design of the first-iteration prototype. While there are theoretical representations of tensegrity systems with compressible elements, we did not make any such assumptions in our preliminary analysis. Therefore, we leave ourselves open to the possibility that increased compressibility of bar elements may influence our ability to reconstruct physical interactions from force measurements. Furthermore, the extra linear degree of freedom has inherent friction that could have unintended effects on the force readings from the FSRs. We will also seek to improve on the embedded electronics implementation, including FSR instrumentation circuit, and its associated packaging in the

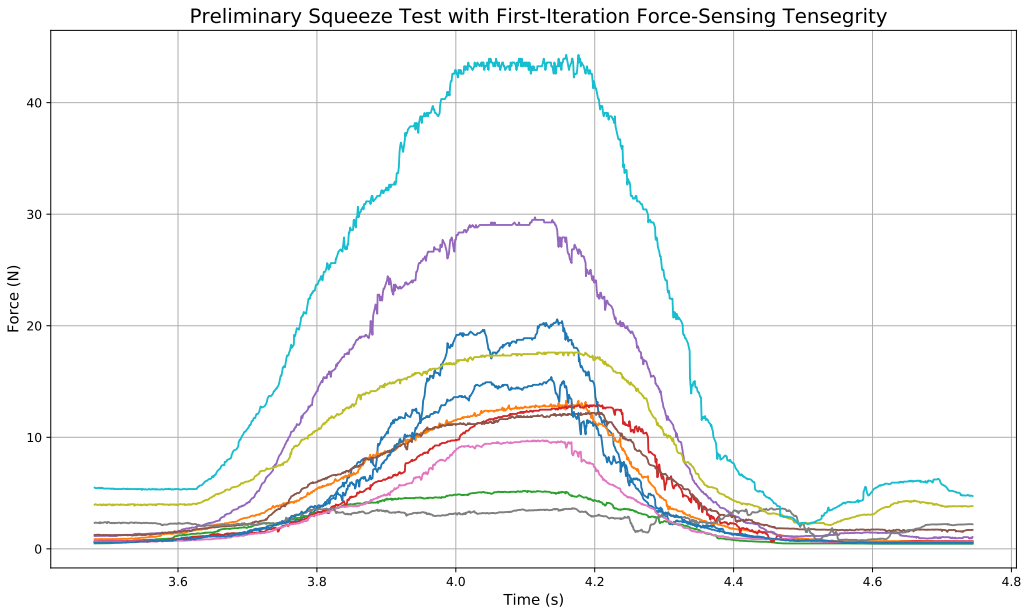

Figure 4.7: Force readings from preliminary squeeze test experiment with first-iteration force-sensing tensegrity prototype.

central payload of the device.

4.5 Second-Iteration Force-Sensing Tensegrity

In this section, we will describe the design and construction of the second iteration of the force-sensing tensegrity, taking into account the lessons learned in the creation of the first iteration design from the previous section. While we will use the same initial spherical six-bar tensegrity structure as a scaffolding like the first design, we will focus on creating a completely new node assembly to more readily accept an alternative FSR model and avoid the need for added compliance. Secondarily, we will discuss the design of a custom central payload and updated embedded electronics system with improved FSR instrumentation circuits.

The original node design strategy takes advantage of the tendency of the tensegrity structure to compress the rigid members in order to maintain the integrity of the node assembly without the need for fastening. We will adopt a similar approach here using a different geometry that eliminates the central bolt from the previous design. This will allow us to circumvent the need for a through-hole based FSR, which will open up possibilities for wider ranges of FSR models that have more suitable sensing characteristics. It will also

Flexiforce A201 Specs	
Minimum force	∼0N
Force sensitivity range	∼0 - 111N
Force repeatability	±2.5%
Hysteresis	±4.5%

Table 4.2: Performance specifications for *Tekscan Flexiforce* A201.

give us greater control over the design of the geometry of the interfacing components where the FSR will sit, which will create more consistent signals. The reason for this is that FSRs have specific requirements regarding where and how force should be applied on the face of the device in order to produce the most consistent signal. In the second-iteration prototype, we opted to use the *Flexiforce* A201 from *Tekscan*, which has a standard circular geometry. This model of FSR boasts improved force sensing characteristics over the FSR-404, which are shown in Table 4.2. In particular, note the improved force sensitivity range and hysterisis characteristics.

Using the previous node design as inspiration, we fashion a custom 3D-printed FSR enclosure out of PLA material. The custom enclosure consists of an upper node assembly and lower bar assembly similar to the original prototype, which are pictured in Figure 4.8. The upper node assembly includes a 3D-printed cylinder that is restrained by a cylindrical cavity in the 3D-printed enclosure of the lower bar assembly. The tension of the cables secure the upper node assembly in place via the cylindrical plug and its complementary cavity. Beneath the cylindrical plug of the upper node assembly is a 3D-printed component that serves several purposes in this design. This component is floating with respect to both the upper node assembly and the lower bar assembly, so it creates a separation to transfer exclusively compressive forces from the upper node assembly to the FSR beneath it. It has also been designed with the appropriate geometry on the bottom face of the component to only apply force in a prescribed circular area of the FSR surface to maintain consistent force signals. Special attention is also given to creating an aperture for easy cable routing of the FSR in the enclosure to avoid creasing and to protect the contact-sensitive regions of the device.

The second important design process we undertook for the next iteration of the force-sensing prototype relates to the design of the embedded electronics and their enclosure. Our goal was to create a central payload for the system that would be easier to use in future human subjects experiments. Specifically, we were hoping it would feature rapid assembly and disassembly, an outward facing interface board for selecting functions, and overall improvements in robustness to physical contact.

The original central payload was designed as an ellipsoidal enclosure consisting of two half ellipsoids each 3D-printed out of TPU material. The flexibility of the TPU material makes

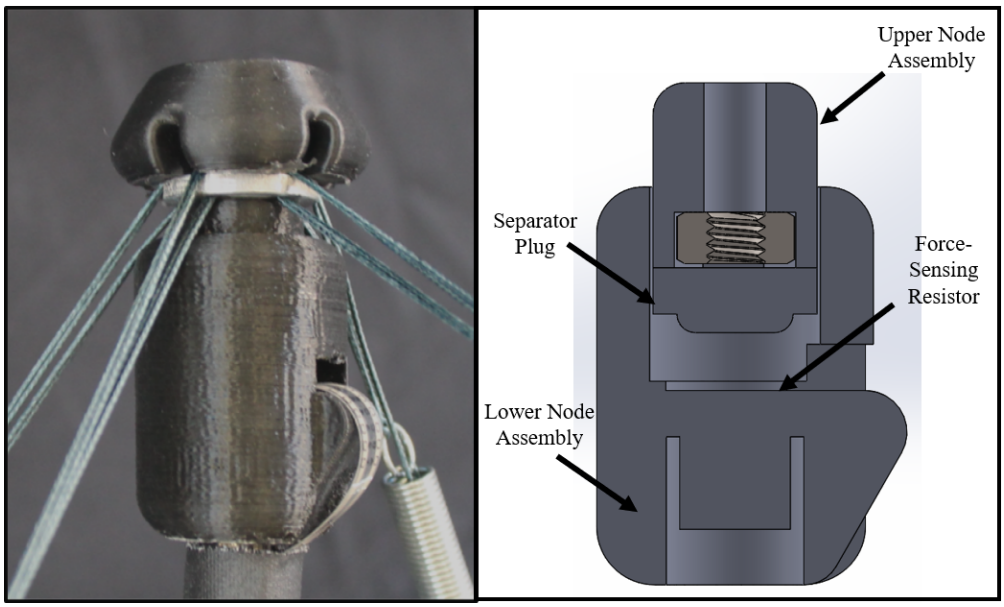

Figure 4.8: FSR integration in node of structure (second iteration). The left image shows the fully constructed node assembly with integrated FSR. On the right is a cross-section view of the node assembly CAD model showing new FSR enclosure.

it easy to enclose a fragile PCB without the need for rigid attachments and without worrying about impacts damaging the embedded system. However, our first iteration prototype involved a complex process of fastening the two halves of the central payload together with radially arranged bolts that served a dual purpose of securing the payload closed and also providing anchor points for attaching the cable elements of the outer structure, suspending the central payload in place. In other words, the central payload would need to be completely disassembled and removed from the structure in order to access any of the electronics in the system, including the battery and the onboard microSD card with experimental data.

We design a new central payload casing that features several distinct improvements over the original enclosure. The casing retains the original ellipsoidal form factor, but we introduce a "clam shell" type joining of the two halves of the casing to facilitate easy access to internal components. The two halves are joined via rotational joints at two points on each side of the payload that can be unlocked by removing a single pin at the axis of rotation. As a result, the payload can be opened from either side depending on the needs of the technician. The anchors for attaching the payload to the cable elements are embedded into independent sides of the payload instead of being used to fasten the two sides together. The second improvement involves designing an outward facing interface board for connecting sensors and providing additional control inputs for ease-of-use. Finally, we use a boolean modeling operation to create a custom internal cavity that directly conforms to the shape and volume

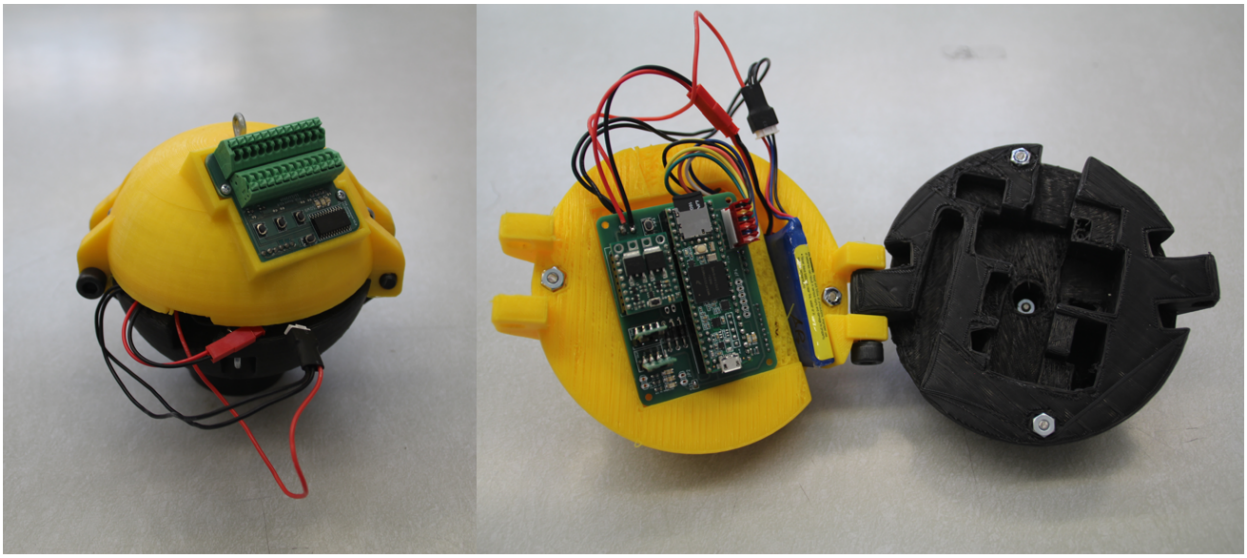

Figure 4.9: Custom central payload with "clam shell" design and external interface board. The payload is 3D-printed out of TPU material for flexibility and robustness to protect the internal embedded electronics.

of the internal embedded electronics. Figure 4.9 shows the newly designed central payload of the second-iteration prototype.

With the new payload design addressed, we can take this opportunity to describe the changes to the embedded electronics. The functionality of the previous iteration is maintained by including all of the original peripherals such as Bluetooth wireless communication, inertial measurement unit, and microcontroller with onboard microSD card. However, we opt to use a different FSR instrumentation circuit to improve on linearization processing on the raw sensor signal. Instead of a voltage divider configuration, we use a non-inverting amplifier to condition the signal to provide better linearity across the force sensitivity range and enable more direct force calculation in post-processing without the need for extensive empirical modeling. We take advantage of the extra real estate on the external interface board to add these extra circuits. The custom embedded system designed for second-iteration prototype is shown in Figure 4.10.

The independent outward facing interface board is a deliberate design choice to separate the sensors from the rest of the embedded electronics because it encapsulates all of the FSR measurement instrumentation including amplifier circuits, analog-to-digital converter, and mounting terminals. The mounting terminals consist of two linear rails of spring-cage locked terminal connectors that facilitate quick and secure attachment of the paired FSR wires. This eliminates the need for attaching custom connectors to FSR signal wires and allows for easy replacement in the case of faulty sensors. Data is transmitted over I2C protocol to the internal board for further processing and storage. By having a dedicated

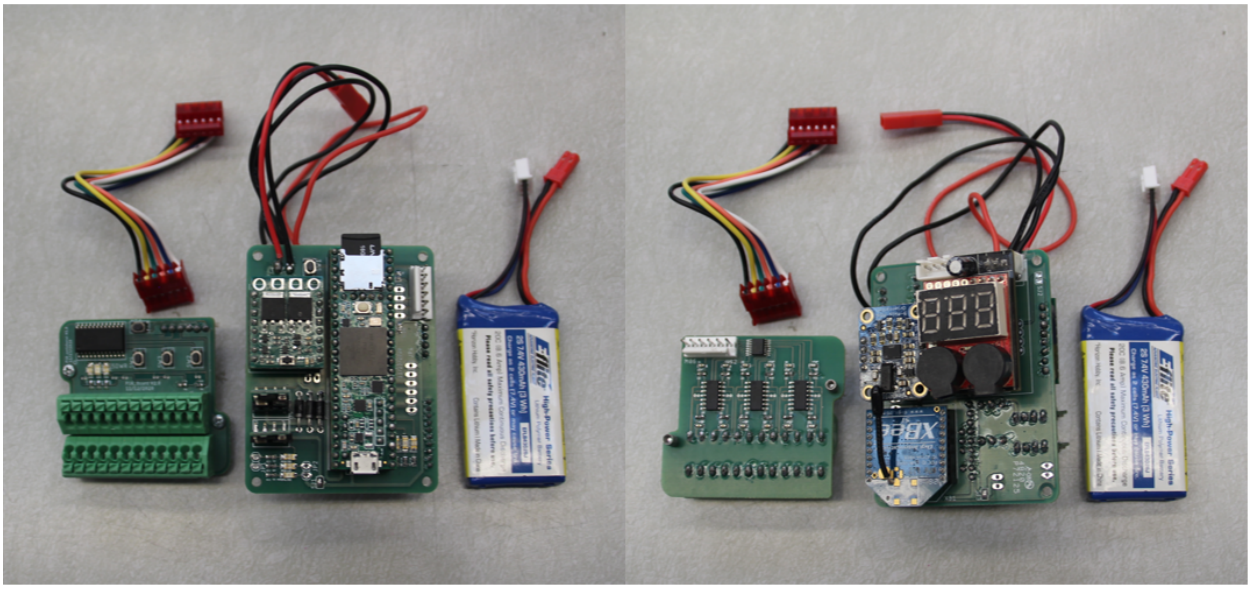

Figure 4.10: Embedded electronics system for the second-iteration force-sensing tensegrity, highlighting the separate outward facing instrumentation board.

FSR instrumentation board, we are able to make adjustments as necessary to any circuitry related to the sensors without having to redesign the entire embedded electronics system. Not only that, but we can now easily extend the use of this FSR-based force sensor array (including sensor packaging and instrumentation) to other tensegrity robot implementations. All that is required to do so is a single connection with power and two-wires dedicated to an I2C communication protocol, which are common to most tensegrity robot models developed by our lab and also to *Squishy Robotics Inc.* products.

Having an external board also gives us the ability to include a few manual switches to make it easier for operators to cycle through different functionalities if necessary without having to crack open the payload. Some indicator LEDs are included to provide system state and diagnostic information to the operator in the case of hardware malfunction. The disadvantage of having this external board, however, is that some sensitive electronics are exposed and unprotected by the TPU casing, which leaves them prone to damage via impact with either the environment or the structure of the tensegrity itself. To minimize this potential failure mode, we orient the board on a specific part of the central payload's surface that reduces the chances of impact with the rigid bar elements of the structure. The complete embedded electronics system is shown in Figure 4.10.

Similar to the previous iteration, we recalculate parameters for the cable elements in terms of initial length and resulting pretension based on the updated lengths of the bar elements with the added sensor packages at the nodes of the structure. FSRs are connected via cable pairs that travel down the length of the bars toward the center where the payload is

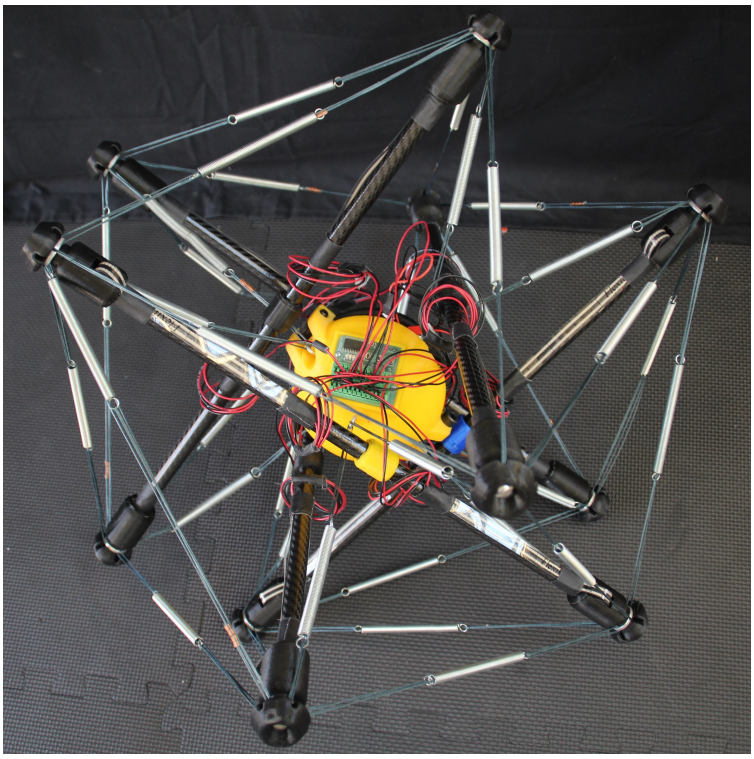

Figure 4.11: Image of fully assembled second-iteration force-sensing tensegrity. The full assembly includes 6 bars, 36 cables, and a central payload with embedded electronics enclosed inside. Each bar is instrumented with two force sensors—one at each node.

suspended. The fully assembled second-iteration force-sensing tensegrity is shown in Figure 4.11. As in the case of the first iteration, we conduct a series of preliminary tests with lab personnel to characterize the response of the force sensor array in the second-iteration prototype. The resulting force trajectories measured from a nominal squeeze test interaction are shown in Figure 4.12. We can see from the measurements displayed that the propagation of forces from the impact of the tensegrity closely resemble that of the simulation and the previous test with the first-iteration prototype.

Having converged on a design that demonstrates the required functionality from a purely technical standpoint, we can spend some time to review human-centered aspects of the design. Since this device will eventually be employed in experiments that bring it into contact with human operators, it is imperative that we perform an adequate assessment of potential safety risk factors. Fortunately, our current system is completely unactuated, which precludes risks associated with the independent movement of the robotic device as driven by either human input or autonomous functionalities. In other words, all potential risk factors are passive in nature. As a result, we focus on safety considerations that center around both anticipated and unanticipated physical interactions with the tensegrity device

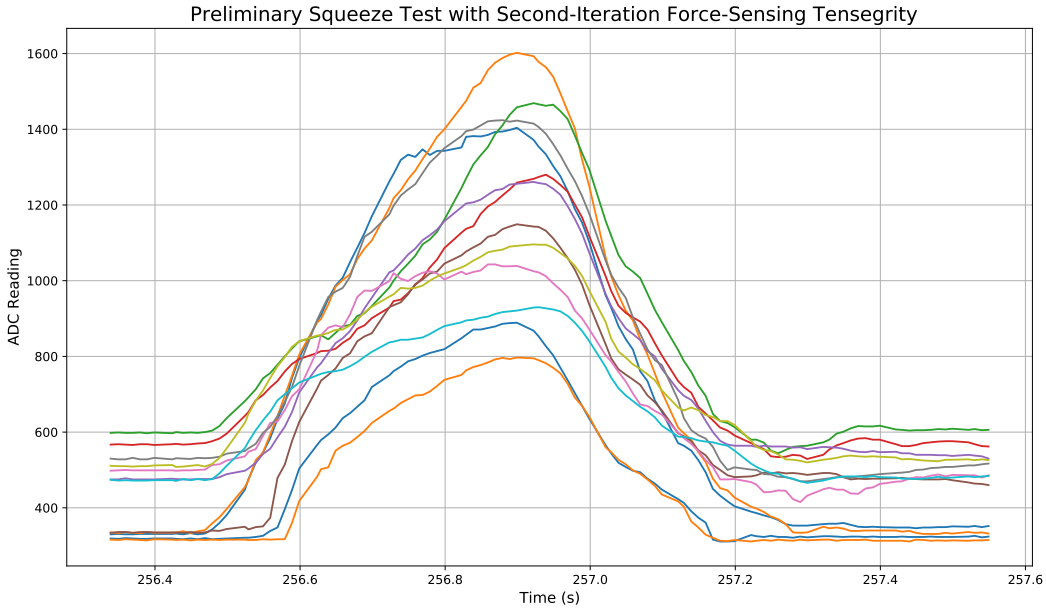

Figure 4.12: Force readings from preliminary squeeze test experiment with second-iteration force-sensing tensegrity prototype.

as initiated by the human operator.

To address unanticipated interactions, we designed all mechanical aspects of the system to be inherently safe for human handling in terms of material choice and overall inertia. We use flexible, light materials like TPU and carbon fiber in addition to opting for rounded geometry that is largely devoid of sharp edges. In the case of tangling in cables, the system is easily disassembled via separation of nodes from rigid elements. If disassembly is unhelpful, cables are made from nylon fibers and can be easily cut using standard cutting tools. It's also important to take into account anticipated handling of the device and potential edge cases for how a human might conceivably interact with it. One such consideration was identified in the first iteration prototype's FSR packaging that involved two exposed compression springs at the nodes of the structure. The risk of getting fingers or skin pinched in these openings contributed toward our updated packaging design in the second-iteration prototype. We expect that humans will also be tempted to interact with the central payload, which poses risks in terms of electrical shock. While the risk is low due to the low power of the system and the enclosed nature of the payload, we explicitly outline to subjects that interactions should be restricted to all areas excluding the central payload to protect their safety. Finally, we recognize that certain safety considerations are largely dependent on human conditioning.

For example, the system is certainly capable of being tossed by a human operator as part of a physical interaction. While a collision with a human might be admissable in certain scenarios, it is still possible to cause harm if coming in contact with a sensitive part of the body such as the head. Therfore, we restrict our initial studies to single human participants and explicitly instruct subjects to not lift the device above eye level.

At this point, we have arrived at a prototype device that is capable of reliably sensing external forces that are imparted on its structure. These force-sensing tensegrity prototypes will serve as excellent platforms for furthering our investigation of physical interaction with compliant robotic systems. In the next chapter, we will begin to strategize different approaches to reconstructing physical interactions from measured forces in an attempt to reason how physical human-robot interaction methodologies might be designed for this unique class of robots.

Chapter 5

Classifying Physical Interactions

5.1 Introduction

The intent of this chapter is to take the first steps into developing methodologies for communication, cooperation, and collaboration between human operators and compliant robotic systems through physical interactions. We discussed at length the implications of this exciting new avenue and modality of pHRI in previous sections, but we have yet to theorize what these interaction mechanisms might actually look like. Furthermore, we must hypothesize and test algorithms for processing the raw force signals measured by the force-sensing tensegrity platform and for inferring aspects of the physical interactions taking place. The latter is a particularly challenging problem due to the inherent difficulties of modeling tensegrity systems, which were covered in our discussion of theoretical representations. To support this effort, we will be leveraging modern machine learning approaches to reveal underlying relations between types of physical interactions and the resulting dynamic behavior of the tensegrity structure as measured by the integrated force sensing. Specifically, we present supervised learning frameworks that treat the mapping of force readings to physical interactions as a classification problem. In this process, we will attempt to generalize the results by investigating the feasibility of this methodology in a deployed system.

For the more familiar case of traditional serially-actuated robotic platforms, studies directed toward pHRI typically involve inferring either the intent of the human operator or the desired goal that the robotic agent should achieve. In the context of an anthropomorphic robotic arm, the desired goal takes the form of a certain trajectory or set of trajectories that accomplishes a task. The methodologies featured in these studies exploit the fact that humans are instructive in their gestures, so there is a great deal of rich information to be extracted from the physical interactions that take place as a result of this natural tendency to teach. If a human wants a robot to do a specific function, the human will attempt to draw from features that are characteristic to this function as much as possible in their interactions. We will demonstrate in our work that we can make use of natural human intuition in the case of physical interaction with compliant and mobile robotic systems like our force-sensing

tensegrity.

5.2 Prior Work

The synthesis, comprehension, and analysis of underlying models of operator intent in HRI contexts is a diverse field due to the breadth of both robotic architectures and potential interaction scenarios. Depending on the sophistication of the robotic system and the complexity of the desired function or task, the needs of the inference model can change dramatically. Generally, we are interested in strategies that attempt to address some aspect of intent detection from the robot's perspective. In pHRI with anthropomorphic robotic manipulators, high-level tasks can be projected into a human context, and inferences can be made about the likelihood that features from a given interaction align with an idealized human model with the help of Markov decision processes (MDPs) [48]. Even in cases where an ideal model is not present, generalizable convergence on intended goals and objectives can be achieved through iterative suggestion from an expert human operator [4, 47]. These examples involving robotic manipulators represent relatively high-level functionality that is grounded in specific and practical goal-oriented tasks such as pick-and-place and other point-to-point motion objectives. Other studies have been directed toward more subtle and abstract notions of intent inference surrounding social phenomena like human expression of emotion [68]. The question remains, however, which aspects of these interaction mechanisms and algorithms will translate into scenarios involving compliant robotic systems like tensegrities and what new avenues will become apparent.

In contrast to rigid robotic architectures that are the subject of many of the studies described above, HRI studies involving soft and compliant robots cannot generally rely on well-understood rigid-body dynamics and anthropomorphic action spaces. As a result, the approaches used to model these systems must be similarly flexible and varying in form. Recently, machine learning has been leveraged to great effect in the modeling, sensing, and control of novel soft robotic systems [15, 35]. Studies have shown that machine learning frameworks can create highly accurate models of physical deformation in soft robotic systems even with unstructured sensor networks [63]. We can also see examples of machine learning being used in concert with novel soft skins for human-robot interaction applications [57]. Sufficiently instrumented soft systems can become excellent platforms for classification of physical interactions through the use of contemporary machine learning algorithms like convolutional neural networks (CNNs) [39]. More generally speaking, the application of classification frameworks has created opportunities in the modeling of more abstract interactions with humans [38]. We will implement similar machine learning techniques to distinguish between different physical interactions that take place with our force-sensing tensegrity.

5.3 Contributions of this Chapter

In this chapter, we will present our strategy for inferring physical interactions from raw sensor data acquired from the FSR array in our force-sensing tensegrity prototypes. First, we examine the problem space by discussing the challenges specific to pHRI with tensegrity systems and then outline our proposed strategy for inferring physical interaction that leverages machine learning classification algorithms. Before testing out machine learning frameworks, we perform data exploration and feature engineering to reason about the effectiveness of classification-based strategies for inference. Multiple strategies for data processing and a range of contemporary classification algorithms, including deep neural network implementations, are presented and applied to real data from the force-sensing tensegrity in physical interaction scenarios. We discuss the implications of featurization and sample size on the performance and robustness of classifiers as well as practicality for embedded systems.

5.4 Physical Interaction Mechanisms

Interactions that take place with robots that have human-like characteristics are easy to understand for the simple reason that they often resemble interactions that are already encompassed by innate or learned human behavior. Whether intentional or incidental, the choice to model contemporary robotic manipulators and other similar systems based on human characteristics has the effect of enabling intuitive pHRI. In addition, the pervasiveness of these systems in automation in many industries have contributed to extremely well-established modeling and control approaches. The familiarity combined with the standardization of these platforms resulted in the tremendous acceleration of HRI research with anthropomorphic robotic systems. Conversely, emergent architectures like those in the field of compliant robotic systems are less familiar and less anthropomorphic than their rigid robotic counterparts. If we are to attempt to integrate these newer systems into human-centered applications, then we must begin to explore ways to leverage their characteristics for intuitive and useful interactions.

Having covered the properties and capabilities of tensegrity robots in previous chapters, it should be readily apparent that tensegrity systems like our six-bar spherical tensegrity are radically different than conventional robots both in form and function and do not inherit many human-like qualities. Even so, there are numerous applications for tensegrity robots that will place them directly in the hands of human operators and within human environments. In Chapter 2, we discussed an example application of tensegrity robots in the acquisition of mission critical data in disaster response scenarios. In this illustrative use case, we hypothesized a rich human-robot interaction involving physical contact that resulted in more efficient execution of a human-robot paired task. We can use this example application of disaster response as fuel for a more rigorous discussion of physical interaction mechanisms with compliant robotic systems like our force-sensing tensegrity.

Figure 5.1 illustrates a first responder in protective equipment interacting with a tenseg-

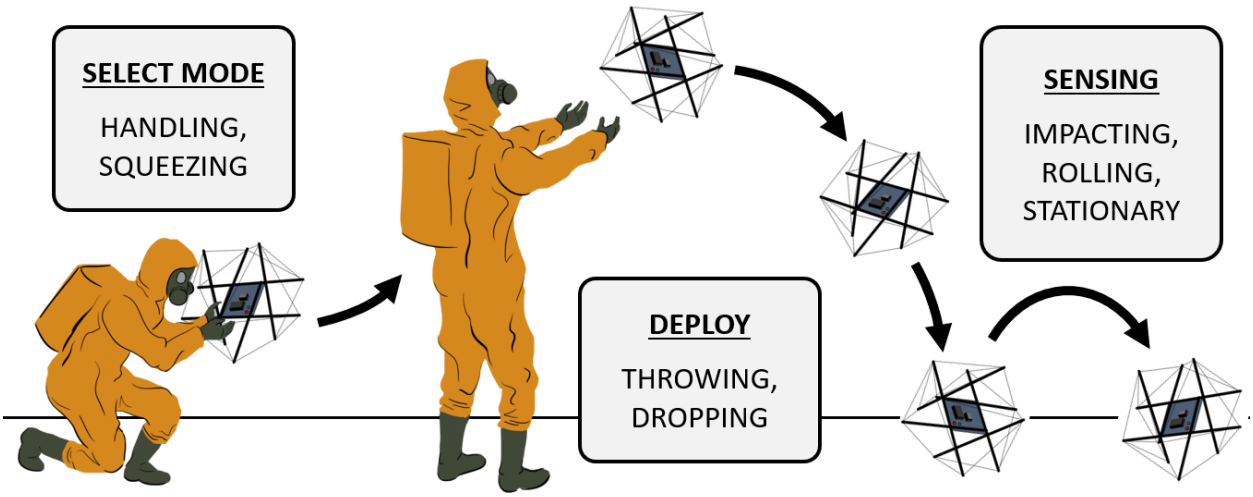

Figure 5.1: Illustration of a representative physical interaction between a first responder and a tensegrity highlighting and categorizing salient features based on context.

rity robot by configuring it and then subsequently deploying it to perform its sensing tasks. Throughout the process outlined in the figure, one can identify features of the physical interactions taking place that are semantically distinct and can be classified into a functional context. For example, a human operator handling and manipulating the device might be related to configuring the device in preparation for deployment. Throwing or dropping the tensegrity might communicate a deployment. The resulting impact or settling into a stationary state might result in the tensegrity activating sensing procedures and transmitting data. Importantly, each of these discrete interactions arguably might arise naturally in the execution of the task independent of the operator's understanding that the device can interpret these actions. We will further discuss the human-centered considerations for the design of intuitive physical interaction mechanisms in a later chapter. For the purpose of developing an initial attempt at a language of physical interaction with tensegrity robots, we will select a set of discrete interactions—like the aforementioned—as inputs to be distinguished from the perspective of the robot.

Now that we have a sense of what kinds of interactions might occur and what features might be relevant to identify, we can consider possible methodologies for classifying them based on raw force data. Ideally, we would like to be able to reconstruct the full state of both the tensegrity and the human in order to gain as much information as possible on the conditions of the interactions. Unfortunately, state estimation involving unanchored tensegrities is still an open problem due to the inherent complexities of modeling nonlinear tensegrity dynamics, which even in the best case of an anchored tensegrity system requires extensive instrumentation to accurately track system states. From our analysis in Chapter 3, we know that it is possible to distinguish between different static external loadings via

measurement of the internal forces in the bars of the structure. Therefore, there is a strong case to be made for the application of classification algorithms in order to identify specific types of physical interactions.

Using our understanding of the applications of these tensegrity devices, their mechanical properties, and the ways in which human operators are likely to interact physically, we can hypothesize a set of representative physical interactions that we will seek to disambiguate from the perspective of the robot using classification-based approaches. We first consider the salient physical characteristics of the force-sensing tensegrity and attempt to reason about how these characteristics inform the way a human interacts with it physically. Since the tensegrity structure's shape resembles an icosahedron, it is intuitive to imagine the entire system as approximating a spherical object—such as a ball. From this perspective, humans can project many previously learned behaviors from their experiences interacting with ball-like objects to their interactions with the force-sensing tensegrity. This is just one reason why we have speculated that the force-sensing tensegrity is a platform that lends itself to intuitive physical interactions. With an object like a ball—especially one that is known to be lightweight and compliant (e.g., a basketball versus a bowling ball)—a human might want to pick it up in one or more hands and attempt to compress it. In this context, the human is gathering tactile information about the properties of the ball to better control their handling of it. We can therefore consider the actions of squeezing and handling the tensegrity robot as valid classes of interactions to be used in an input framework that leverages physical contact. If we also consider the fact that the force-sensing tensegrity features an open structure, then it can be assumed that humans can grasp various points on structural elements instead of exclusively open-handed manipulation on the surface. As a result of this ability to grasp the components of the structure, we also consider interaction cases that involve using grasps to create tension on the structure through pulling. The interactions we have discussed so far span a broad range of potential interaction conditions involving continued contact between human and robot. However, the intended applications of this robotic hardware will eventually require for the robot to be deployed so that it can perform its autonomous tasks. In the specific case of disaster response applications, the robot is designed to be dropped or tossed toward it's objective. This dropping case constitutes yet another class of interactions that we can distinguish as relevant to the design of an input framework.

Later on in this work, we will assess the suitability of our choice of interactions in a structured and systematic approach with human subjects. This will give us the opportunity to reconsider our assumptions about the most intuitive and useful categorization of interactions by taking into account the subjective impressions of unbiased human operators. For now, we choose to consider the following physical interaction types as our target classes based on our discussion of relevant factors:

- **Null** : The tensegrity is has settled into a static equilibrium and is not being handled by a human operator.
- **Drop** : The tensegrity experiences an impact (or sequence of impacts) with a surface.

- **Squeeze** : The tensegrity experience compression from the outside, resulting in a deformation of the structure.
- **Pull** : The tensegrity experiences tension from the outside, resulting in a deformation of the structure.
- **Handle** : The tensegrity is being held by a human operator with intent to operate.

Throughout the following sections, our goal will be to construct frameworks for classifying the above interactions (or a subset of them). We will cast a wide net by comparing several data processing pipelines and also considering a multitude of classification algorithms including deep neural network implementations to accomplish this task.

5.5 Data Exploration and Feature Engineering

Before applying machine learning algorithms to this problem, it is important to spend some time exploring the data that will be used as inputs to these models. In particular, we must come up with a strategy for processing the transient raw sensor data into observations for training a classifier that ensures that the input observations retain useful information and are practical for real applications with deployed machine learning models. Given the fact that we are collecting data from as many as twelve distinct force sensors at a high frequency without any model correlation, it could be detrimental to the performance of our classifier to assume that the models will be able to recover critical interaction-specific features from raw data alone. We must therefore examine ways to help distill the raw data for use by the classification algorithms through feature engineering.

From our preliminary comparison of the raw data acquired from a drop test and squeeze test interaction earlier in this work, we can immediately recognize some features that might distinguish different types of physical interactions. While it may be qualitatively apparent that the force responses are associated with distinct interactions, we still need to translate that information into more digestible quantitative features. We propose a set of features derived from the dynamics of the force responses that more directly confer information to a classifier. The features are outlined below along with a brief description. The equations used to calculate these quantities are provided, where $F(t) : \mathbb{Z} \to \mathbb{R}$ is the force measured by a single FSR at sample time t.

- *total impulse* (J) : Discrete time integral of force over a given time window.

$$J = \sum_t \frac{\Delta t}{2}(F(t_{i-1}) + F(t_i)) \tag{5.1}$$

- *maximum yank* ($Y_{\max}$) : Maximum discrete time derivative of force with respect to time over a give window.

$$Y_{\max} = \max_t \frac{(F(t_{i+1}) - F(t_i))}{\Delta t} \tag{5.2}$$

- *maximum force* ($F_{\max}$) : Maximum force over a given time window.

$$F_{\max} = \max_t F(t) \tag{5.3}$$

Starting with the first feature, *total impulse* is intended to capture the total amount of energy being imparted to the tensegrity through an interaction. For example, a squeeze interaction involving force being applied steadily over a longer period will result in a higher total impulse than a more punctuated interaction like a drop. *Maximum yank*, on the other hand, will identify the maximum rate at which force is changing. By the same comparison as before, we can expect that squeeze interactions and drop interactions will have distinct values across the array of FSRs for maximum yank. The *maximum force* for a given FSR is self explanatory. We can calculate this set of features for each of the twelve FSR signals over the time span of a given interaction, resulting in a total of thirty-six features used as inputs to a classifier. Because these features are derived from either extremums or accumulations of the signals, we are abstracting away the temporal variations to some degree. Depending on the way these features are used toward inference, this could be seen as either an advantage or a disadvantage (i.e. an advantage in the case of removing unnecessary noise and a disadvantage for algorithms that leverage input temporality). We will attempt to investigate the effects of using abstract featurization and its relation to time dependence and scale of sample.

In the previous section, we proposed a set of discrete interactions to classify, but in reality, the term "discrete" is used loosely in this context because the interactions themselves are continuous and comprised of finer features that are temporally and spatially varying. We hypothesize that there is a tradeoff to be made with respect to the scale of sample being extracted from the continuous time-dependent force trajectories and the ambiguity of the overarching interaction, which we intend to explore. This has important implications for the deployment of these frameworks in embedded systems because there is an inherent need to process these continuous inputs efficiently for a classifier to be useful in that context. In order to assess the effects of time-dependence on the performance of our classifiers, we will segment the interactions into smaller sample sizes, or *windows*, based on time. As the window size is made smaller, we run the risk of separating useful features of an interaction but improve the potential practicality of the framework by reducing the need for in situ segmentation and subsequent discretization. A smaller window size also makes it possible to infer inputs at a faster and more consistent rate.

At this point, we have a range of possible processing pipelines for the raw data acquired by the force-sensing tensegrity. Next, we will discuss the different classification algorithms used in our proposed framework.

5.6 Classification Algorithms

We will begin the discussion of chosen classification algorithms by first describing the classification problem more explicitly. Let $(\mathcal{X}_1, y_1), (\mathcal{X}_2, y_2), ...(\mathcal{X}_n, y_n)$ be a set of n physical

interaction observations where each instance is comprised of a set of input features $\mathcal{X}_i \in \mathcal{D}$, where $\mathcal{D}$ is the space of features, and corresponding class label y_i. The goal of a classification framework is to learn a function $y_i = f(\mathcal{X}_i)$ that maps a set of input features $\mathcal{X}_i$ to its correct label y_i. Our specific case falls under the category of supervised learning in that we use observations that are correctly labeled to train our models. There is a broad range of possible approaches to learning the aforementioned mapping using contemporary multi-class classification algorithms, and we will review a few them here for clarity. For each algorithm presented, we will discuss their relevance to assessing the performance of physical interaction inference via classification. We present two contemporary classification algorithms to provide solid benchmarks from which to assess the feasibility of our proposed machine learning framework.

- **k-Nearest Neighbors (kNN)** : The kNN algorithm is a non-parametric method for classification that finds the k nearest samples in a given data set and assigns a label according to the labels in those nearest samples [21]. We can leverage the hyper-parameter k to control the degree to which the algorithm isolates a given clustering of samples based on label. As we increase k, we improve noise rejection but create more ambiguity between labels. The kNN algorithm is often a good choice for initial classification analysis due to its generalizability to different problems and its simplicity.

- **Random Forest (RF)** : The RF algorithm is an ensemble learning method that bases classification on a collection of constructed decision trees [44]. Decision trees are constructed on a random set of input features, and classifier outputs are reached by majority vote. Hyper-parameters for this algorithm include the number of trees and the height of each individual decision tree. RF is an extremely efficient algorithm for classification due to its low computational load for testing. It also has excellent resistance to overfitting due to the inherent randomization across the set of input features.

The above algorithms will be used in conjunction with the previously described processing methods in different combinations of processing steps and choice of algorithm to investigate their effect on classification performance. Now that we have covered some of the more traditional classification algorithms, we can describe our neural network implementations.

Recently, an array of neural network approaches to classification—in particular, deep learning implementations—have demonstrated impressive results toward the modeling of compliant systems, as discussed earlier in this chapter. It can be intuitive to think of deep learning models as simply your standard feed-forward network that combines multiple hidden layers, which makes them capable of learning more complex and nonlinear relations [25]. We present several deep learning models that will be used to classify physical interaction types in addition to the previous classificaton algorithms. The architectures of the proposed models are shown in Figure 5.2.

All of our deep learning methods are implemented using standard Tensorflow and Keras API methods. For our first deep neural network (DNN), we assemble multiple fully-connected

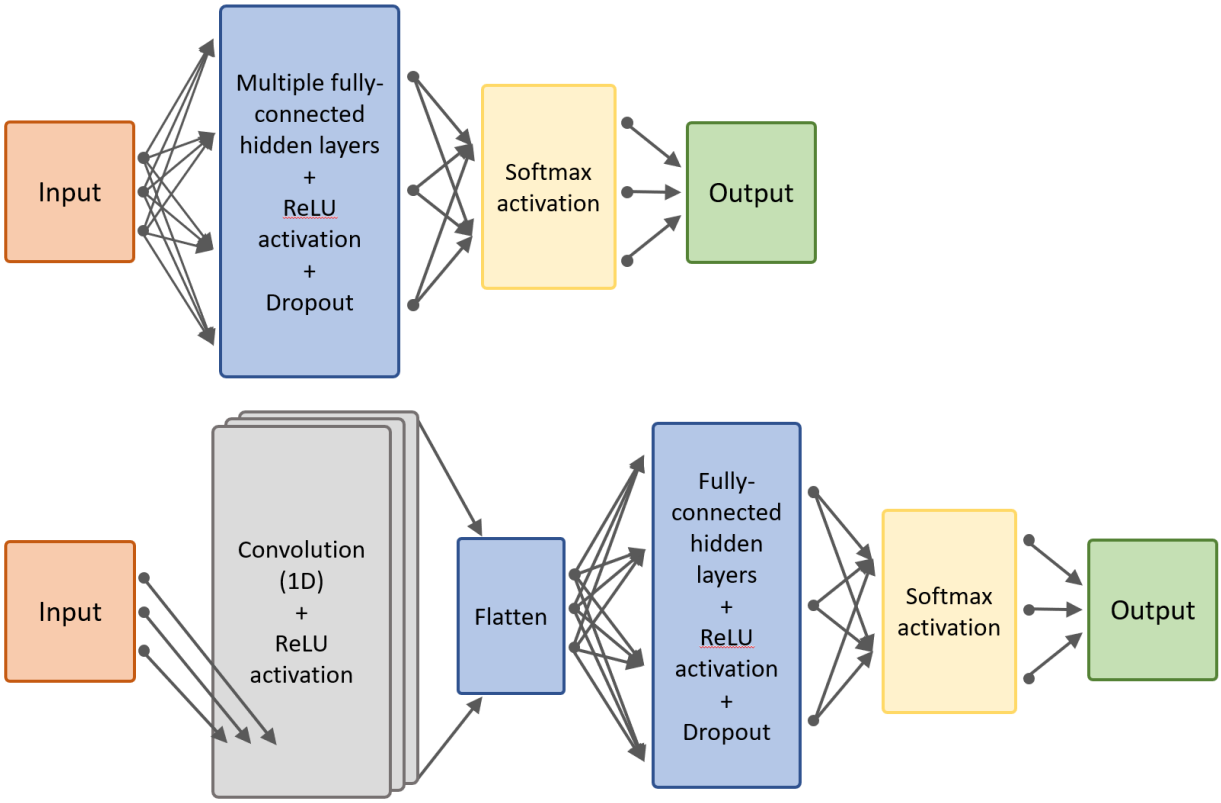

Figure 5.2: Architectures for our deep learning networks. Top is a standard deep neural network implementation featuring multiple fully-connected hidden layers. Bottom features a one-dimensional convolutional layer.

hidden layers using the rectified linear unit (ReLU) as our activation function. Between each hidden layer, we enforce a dropout layer to reduce overfitting of the models and to encourage flexibility in the assignment of weighting between layers. Since this is a classification problem (and not regression), we construct the output layer with a softmax activation function to produce our class weights. This is a fairly well-established architecture for DNN implementations, and we will show that it performs quite well for our application. Even so, we attempt to improve on this architecture by leveraging a convolutional neural network (CNN) approach. CNNs are a type of neural network that involve performing a convolution operation on inputs in order to reduce high dimensional data into a smaller internal feature map. Most commonly applied to image classification, CNNs are useful in applications involving large and spatially distributed data sets. Inputs are fed to a one-dimensional convolution layer from weights and then flattened for use in a series of conventional fully-connected hidden layers. As before, we use ReLU activation and softmax activation in our hidden layers and output layer respectively with dropout routines interspersed.

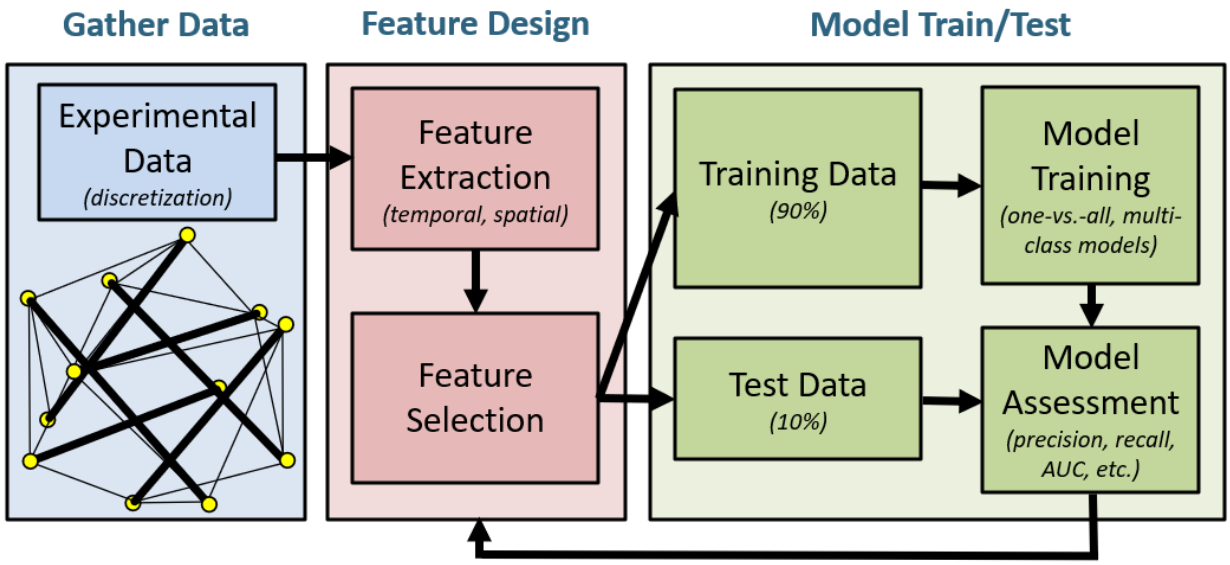

Figure 5.3: Diagram outlining our proposed classification framework including data acquisition, feature engineering, and model training and testing.

The process for configuring, training, and testing our models as a full pipeline is shown in Figure 5.3. Input observations in the form of force sensor data from physical interactions is acquired with human subjects in a controlled experimental setting. As a result of the heterogeneity in characteristics of the physical interactions being tested, the resulting data sets have a tendency to be heavily imbalanced. This can have detrimental effects on the training and subsequent performance of our classification algorithms. To address this, we apply the synthetic minority over-sampling technique (SMOTE) with multiple passes ($n-1$ passes where n is the number of interactions) [14]. The data is segmented manually based on experimental timings and then processed into a series of data sets that each contain discrete observations for a given window size of interest. Depending on the configuration being used, we compute the previously described feature sets over the individual observations.

For the conventional classification algorithms (kNN and RF), we use repeated stratified k-fold cross-validation to train our models and report validation scores as assessments. Preliminary experiments are conducted on exclusively the first-iteration prototype to demonstrate the feasibility of the framework and to report initial findings on the effect of window size on the performance of these models. The deep learning models are trained and assessed with validation metrics throughout the training process (i.e. after each epoch). We use only data from the second-iteration prototype and human-subjects experiments for training and testing the deep learning models (DNN and CNN).

5.7 Preliminary Experiments

In order to begin testing our these approaches to inference of physical interactions, we need to accumulate some preliminary data that can be used to train and test our models. In this section, we will present our experimental approach to gathering force sensor data for a set of physical interactions in a controlled fashion. Then, we will use this data to test with the benchmark classifiers (kNN and RF). For this preliminary set of experiments, we use the first-iteration prototype and are only considering four out of the five physical interactions discussed previously—**Null**, **Drop**, **Squeeze**, **Handle**.

The drop interaction consists of holding the tensegrity at a height of approximately 1 meter and then dropping it to the ground. The squeeze interaction consists of compressing the device between the surface on which it sits and a separate rigid surface that is held by a human assistant. The handle interaction consists of a human holding the tensegrity in a particular orientation and then turning it over one full rotation in their hands. Null interaction involves collecting data from the device as it sits stationary in a given orientation. For each of these interactions, we vary the initial orientation of the device. For example, the initial orientation for the drop interaction will directly control the point at which the tensegrity impacts the ground. Depending on the orientation, the tensegrity my experience initial impact on a set of one, two, or three of its nodes. In the squeeze interaction, initial orientation will have a similar effect in determining which nodes are experiencing compression. The amount of force used by the human operator to compress the structure in squeeze interactions is intentionally modulated at random to encourage generalization of input data for the classifier. Figure 5.4 shows two captured frames from a squeeze interaction test in which the device is compressed between two nodes on opposite sides of the structure.

As covered previously, we process the data by manually inspecting it, truncating based on experimental timings, labelled according to interaction type, and sectioned into individual observations based on a set window size. We vary the window size between 10 and 100 samples in intervals of 10 samples. For reference, this will translate to window sizes of $0.1sec$ to $1sec$ of length in time based on a 100Hz sampling frequency. One unfortunate drawback to this approach when accumulating a data set is that it will result in a discrepancy in total number of observations across the different window sizes, which may influence the performance of the associated classifiers due to limited training data. As an illustration, consider the total number of observations in our data set for a given window size shown in Table 5.1.

Table 5.1: Observation counts by class of interaction for window size of 60 samples.

Class	**Null**	**Drop**	**Squeeze**	**Handle**
Counts	3930	2643	4648	539

Note also the imbalance across the different classes, which is what necessitates our use of SMOTE to augment samples in under-represented classes. We compare performance

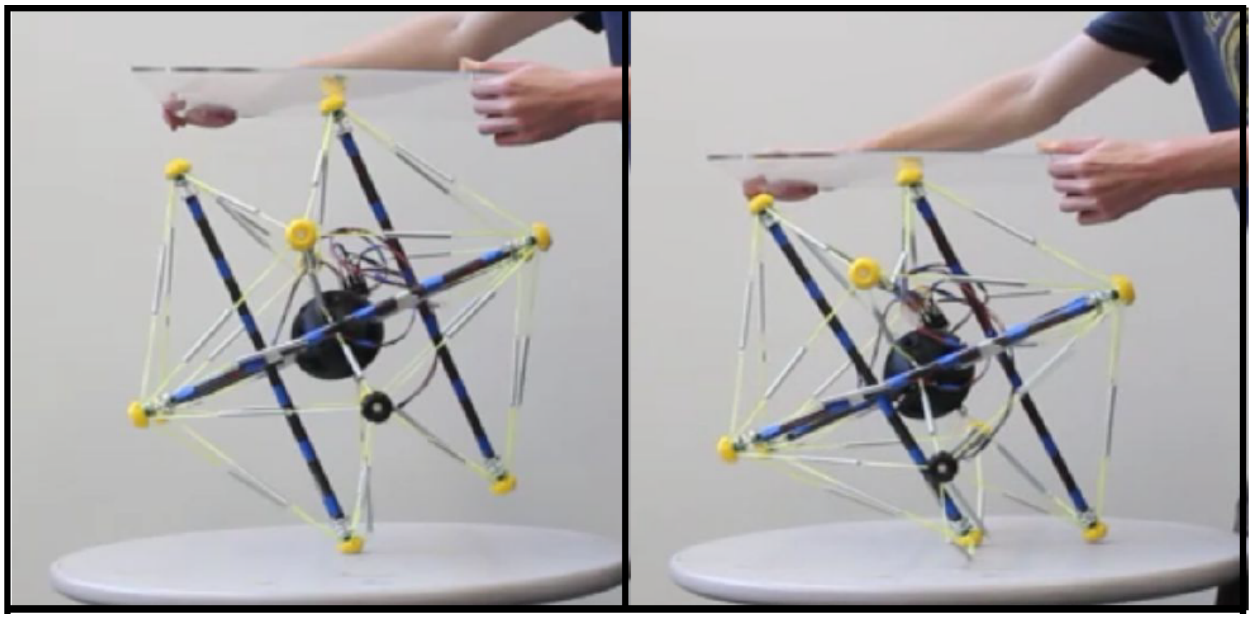

Figure 5.4: Two frames from a squeeze interaction test with the first-iteration force-sensing tensegrity intended to gather preliminary data for model training/testing.

between the use of raw force signals (specified as "Raw") and abstract featurization based on the statistical features presented earlier (specified as "Abst."), which are calculated for over the entirety of each observation. In order to assess the performance of the classifiers (and to not further reduce our training set), we compute metrics based on the validation data from our cross-validation and average over folds for k-folds. We calculate performance metrics using the following equations, which are useful for assessing multiclass classification results.

- *precision* : Number of true positives over number of total positives for a given class.

$$\text{precision} = \frac{TP}{TP + FP} \tag{5.4}$$

- *recall* : Number of true positives over number of relevant instances for a given class.

$$\text{recall} = \frac{TP}{TP + FN} \tag{5.5}$$

- *F1 score* : The harmonic mean of precision and recall.

$$\text{F1 score} = \frac{TP}{TP + \frac{1}{2}(FP + FN)} \tag{5.6}$$

where TP is the number true positives, FP is the number of false positives, and FN is the number of false negatives. In addition to these metrics, we calculate the area under the receiver operating curve (AUC or AUROC) across the different classes. We calculate the AUC score in a one-vs.-one approach based on class and then average over the classes to result in a single AUC score representing the classifier. This calculation distinct from a one-vs.-rest approach to obtaining the AUC score, which is also useful but communicates less about the differentiation between each class and the remaining classes. The AUC score is a measure of separability of the classes and will assess how well the classifier can distinguish between the available classes [27]. This is an important measure because it is an excellent demonstration of the underlying separability of the force data being generated by the different physical interactions through our chosen benchmark classifier algorithms. Finally, we include the overall categorical accuracy across all classes, the relevance of which to assessing the performance of the classifiers is self explanatory.

Table 5.2: Classification performance metrics within classes for best-performing window size for k-Nearest Neighbors algorithm.

Raw⁄Abst.	**k-Nearest Neighbors (KNN), Window = 100 Samples**			
	Null	**Drop**	**Squeeze**	**Handle**
Prec.	$^{0.61}\!/_{0.78}$	$^{0.74}\!/_{0.65}$	$^{0.95}\!/_{0.90}$	$^{0.98}\!/_{0.68}$
Recall	$^{0.83}\!/_{0.88}$	$^{0.61}\!/_{0.79}$	$^{0.78}\!/_{0.66}$	$^{0.89}\!/_{0.89}$
F1	$^{0.70}\!/_{0.82}$	$^{0.67}\!/_{0.71}$	$^{0.86}\!/_{0.76}$	$^{0.93}\!/_{0.77}$

From our training process, we found that the best-performing configuration for kNN was with a window size of 100 samples with $k = 5$. Overall, the kNN classifier performance left some to be desired in terms of classifier accuracy as evidenced by the low precision and recall scores for the various classes. Also, there was no clear effect from the use of raw signal inputs versus abstract featurization on the kNN performance. In contrast, our RF algorithm with nominal hyperparameter tuning performs quite well across raw and abstract feature inputs for a window size of 10 samples. It performs noticeably better when using abstract features as inputs as demonstrated by the high F1 scores across the board in Table 5.3.

Taking a look at Figure 5.5, we can see the categorical accuracy and AUC scores plotted as a function of window size for the various classifier configurations. The AUC score for the different classifiers shows strong stability as window size varies, with the exception of kNN with abstract features. In terms of overall accuracy, the use of abstract features clearly improves on the robustness of the classifiers in the presence of varying window sizes, which

Table 5.3: Classification performance metrics within classes for best-performing window size for Random Forest algorithm.

Raw/Abst.	**Random Forest (RF), Window = 10 Samples**			
	Null	**Drop**	**Squeeze**	**Handle**
Prec.	$^{0.95}/_{0.97}$	$^{0.78}/_{0.97}$	$^{0.97}/_{0.99}$	$^{0.96}/_{0.96}$
Recall	$^{0.78}/_{0.98}$	$^{0.96}/_{0.97}$	$^{0.98}/_{0.99}$	$^{0.99}/_{0.99}$
F1	$^{0.86}/_{0.97}$	$^{0.87}/_{0.97}$	$^{0.98}/_{0.99}$	$^{0.98}/_{0.98}$

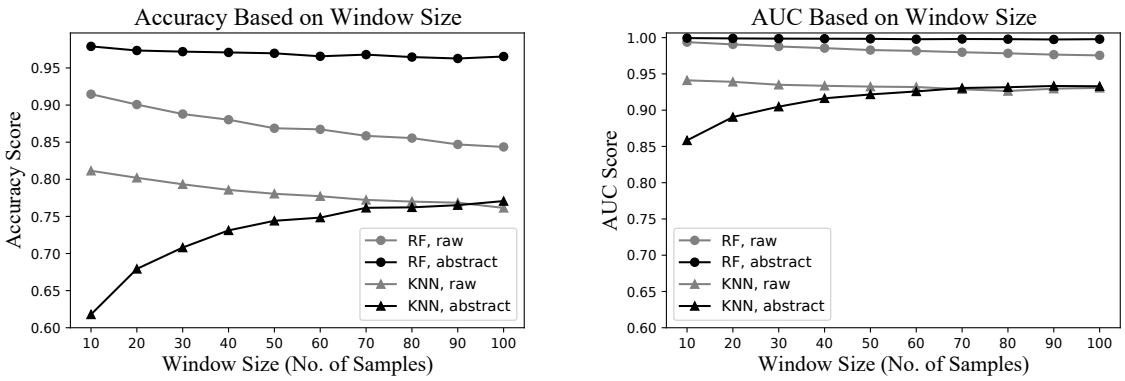

Figure 5.5: Accuracies and AUC scores plotted as a function of window size for kNN and RF algorithms with both raw and abstract features inputs.

indicates that this approach to processing inputs could be useful for creating classification frameworks that require flexibility in data sampling. For our preliminary experiments with the first-iteration tensegrity and these benchmark classifiers, the validation metrics show that RF with abstract features at a window size of 10 samples is the best-performing configuration of the framework.

Here, we have shown that with conventional classification algorithms and a range of data processing approaches, it is feasible to construct a classification framework that will be able to infer differences between a set of distinct physical interactions that take place with the force-sensing tensegrity. In the next chapter, we will present our first formal human subject experiment along with results from our deep neural network implementations.

Chapter 6

Physical Human-Robot Interaction Experiments

6.1 Introduction

The premise of our work on physical human-robot interaction with spherical tensegrities is that physical interactions with compliant robotic systems can be leveraged toward useful human-robot communication, collaboration, and cooperation. More specifically, pHRI with compliant systems can offer advantages in certain scenarios that make it a useful alternative or redundancy to more conventional modalities of interactions depending on the application. Finally, it has been suggested that pHRI with mobile, flexible, and robust tensegrity robots can be intuitive. Until now, we have only gone so far as to demonstrate the feasibility of identifying inputs in the form of physical interactions using a force-sensing tensegrity platform. We have yet to explore the human elements of this proposed physical interaction schema to assess its intuitiveness and suitability for real use. If we can show that physical interactions with a tensegrity system aimed at accomplishing tasks are easy to learn and execute, then we can make a strong argument for an effective modality for HRI.

To understand the human-centered advantages and disadvantages more concretely, we must design an experiment to target the intuitiveness of these interactions and how well they can be translated into practice for different applications. While there is no widely-accepted standard for assessing the intuitiveness of a human-robot interaction, we present a series of human subject experiments that target the qualitative responses of the participants as they interact physically with the force-sensing tensegrity toward the completion of application-inspired outcomes. Conducting this study will also provide additional data for investigating the efficacy of our classification approaches—in particular, our untested deep learning implementations. Ultimately, we hope to demonstrate that our approaches to inferring physical interaction can be generalizable and robust if trained properly.

6.2 Contributions of this Chapter

The primary contribution of this chapter is the design and execution of a set of human subject experiments that investigate the intuitiveness of physical interactions with the force-sensing tensegrity in practice. Using the second-iteration prototype force-sensing tensegrity, we demonstrate that our proposed set of physical interaction inputs and a mapping to a hypothesized set of functions is subjectively valid and useful from the perspective of unbiased and non-expert human operators. Secondarily, we discuss other qualitative findings about new directions for physical interaction types and frameworks based on the impressions and responses from experiment participants.

Also featured in this chapter will be a thorough assessment of the performance of our deep learning frameworks. Previously, we covered some preliminary experiments that sought to determine if classification were feasible given some benchmark classifier algorithms. We will use expert training data in concert with non-expert observations from our human subject experiments to reason about how well our deep learning frameworks perform in different configurations of parameter tunings (in particular, different window sizes) and training/testing data sets. The results of our tests show that although the deep learning frameworks are adept at learning accurate classification models for specific data sets, there is an express need for variability in training data to ensure generalizability and robustness to unseen inputs.

6.3 Prior Work

The process of extracting useful information from physical interactions is largely context driven in the sense that methodologies are tailored to both the robot and the set of functionalities that it is capable of performing. In most studies focusing on pHRI with traditional robotic manipulators, the scenarios are posed in such a way that the robot and human have similar action spaces as well as objectives. This makes intuitive sense because the robots are fashioned to be able to replicate human activities or tasks that were intended to be performed by humans. We can also see examples of the alternative in which humans interact with robots that are either non-anthropomorphic or do not inherit the same human functionalities. A recent study on safe-to-touch drones demonstrated that enabling physical contact with drones can reduce mental demands in the performance of tasks [2].

6.4 Assessing Human-Robot Interfaces

In order to explore the human elements of physical interaction with a tensegrity and to test our hypothesized framework, we developed a set of experiments with non-expert human subjects that attempts to determine whether the proposed interaction modality is intuitive from the unbiased human operator's perspective. The data we collect from the interactions will also be critical in testing the generalizability of the classifiers. In this section, we cover the experimental protocol used to conduct these tests in an unbiased and scientifically rigorous

way so as to maintain the integrity of the subjective results as well as the quantitative measures. It should also be noted that this set of experiments features human subjects and has been approved by the CPHS department[1] at the University of California, Berkeley under an IRB protocol with ID 2020-01-12906.

As we proposed earlier, the experiments will focus on assessing the qualitative aspects of how humans will interact physically with a force-sensing tensegrity. Specifically, the aspects that are of highest interest are those relating to the intuitiveness of the interface. Intuitiveness, by our own definition in this context, refers to the degree to which an activity is easily learned, understood, or assumed compared to the amount of effort or instruction required to facilitate the execution of said activity. While there is obviously no direct quantitative measure of this outcome, we can infer the intuitiveness of an interaction through other means. We start by recruiting a pool of human subjects that has no experience with tensegrities or other compliant robotic systems. We then construct a set of scenarios for the human subject to physically interact with the tensegrity that targets or leverages specific types of physical interaction (e.g. our previously discussed physical interaction classes) to accomplish a particular task outcome or objective without providing any explicit instructions to the subject on how to perform the intended physical interaction. We will measure the intuitiveness of the physical interaction by how often the human subject performs an action that resembles the intended action. Figure 6.1 shows two of our recruited subjects physically interacting the force-sensing tensegrity in part of our experiments.

For each of our proposed physical interaction types, we will provide the subject with a verbal prompt describing a desired task, objective, functionality, or context that should be communicated to the tensegrity and that could potentially be benefitted or accomplished through use of the associated physical interaction. The prompts will be crafted in such a way as to not give any indication to the subject what kind of physical interaction they should use to accomplish the goal. For example, a pull interaction might be useful in a scenario requiring the human operator to expand the tensegrity from a flattened storage state to be deployed for operation, and then a squeeze interaction could be used for the inverse. We hypothesize that these contexts will elicit specific and intuitive responses from human subjects that align with our expected or intended set of interactions.

Because the integrity of this experiment relies on the subjective impressions of the human subjects, it is of paramount importance that verbal interactions between experiment personnel and human subjects be controlled and free of confounding factors that may bias the reaction of the human subject. For this reason, we develop a script to be read aloud in order to facilitate controlled exposure to only the aspects of the experiment deemed necessary for safe execution of the tasks from the perspective of the human. The script begins with an exposition to the first experiment explaining the process so that the subject knows what to expect:

> "In this first experiment, you will be physically handling the tensegrity as a way to talk to it. The tensegrity can sense how you handle it through contact. The

[1] Website: https://cphs.berkeley.edu/

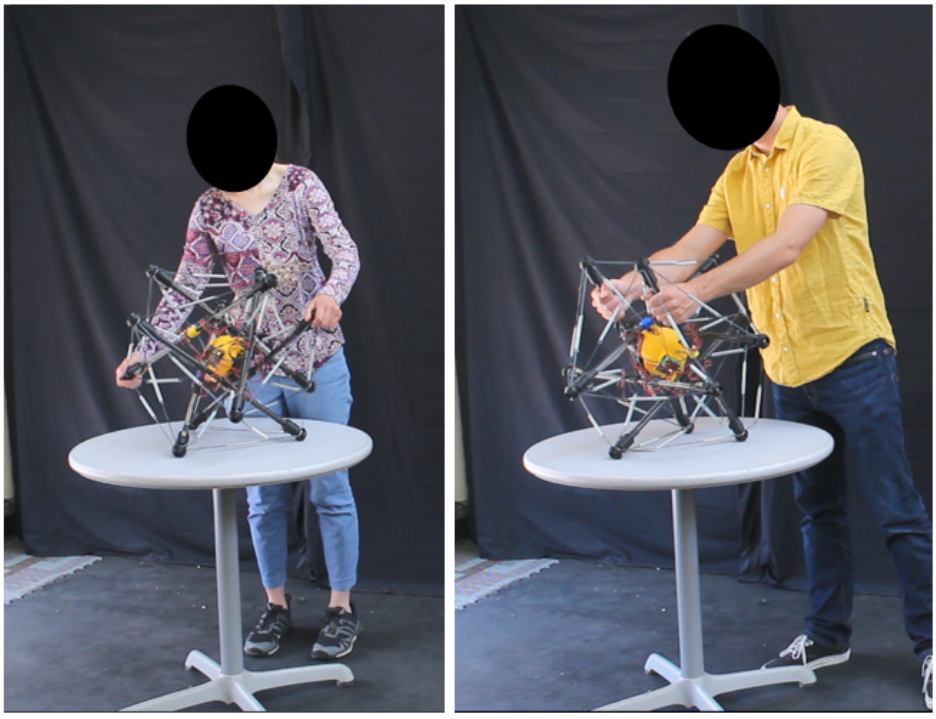

Figure 6.1: Still shots of two unbiased and inexperienced human operators physically interacting with the force-sensing tensegrity in response to verbal prompts. The left subject is attempting to pull on the structure of the tensegrity while the right subject is squeezing the structure.

> tensegrity is flexible, strong, and can withstand impacts, so you can manipulate it in any way that makes sense to you. I will be reading to you a series of prompts that describe things that you want the tensegrity to do. Your task will be to physically handle the tensegrity in a way that you think will communicate what you want the tensegrity to do. You can handle any part of the tensegrity, excluding the ball in the center. You don't have to do something new for each prompt. The tensegrity won't actually do anything in response, but you can imagine that it responds if you'd like. Do you have any questions before we begin?"

After reading the experiment exposition to the subject, the lab personnel will commence the experiment and begin reading out the first prompt. There are a series of eight prompts that span the four distinct physical interactions types being tested (two distinct scenarios for each type of interaction). The prompts are randomized for each subject to reduce potential ordering effects on the subject's response and each prompt is self-contained and not intended to be part of a sequence. The prompt scripts for the four interaction types are listed below:

1. **Squeeze**:
    a) "The tensegrity can shrink in size. Using physical interaction, tell the tensegrity to shrink itself to a smaller size."
    b) "The tensegrity can change its shape to suit different applications such as becoming flat for storage. Using physical interaction, tell the tensegrity to become flat so that it can be stored."
2. **Pull**:
    a) "The tensegrity can grow in size. Using physical interaction, tell the tensegrity to grow itself to a larger size."
    b) "The tensegrity can change its shape to suit different application such as becoming flat for storage. Imagine that the tensegrity is flat from being in storage. Using physical interaction, tell the tensegrity to expand from its flattened state."
3. **Handle**:
    a) "The tensegrity can sense when it's being used and wake itself up. Using physical interaction, tell the tensegrity to wake up."
    b) "The tensegrity can sense when it's being inspected. Using physical interaction, communicate to the tensegrity that you are inspecting it."
4. **Drop**:
    a) "The tensegrity can sense when it has been deployed by its human operator and begin doing its tasks autonomously. Using physical interaction, deploy the tensegrity so that it can begin its tasks."
    b) "The tensegrity can locomote across the ground. Using physical interaction, tell the tensegrity to begin moving on the ground."

The entire experiment is recorded on video in order to allow us to return to the recordings later and determine whether a particular interaction met the requirements to be considered a correct interaction based on predetermined criteria. The criteria for determining a correct interaction based on the type of interaction is shown below:

- **Squeeze** : The subject compresses the tensegrity's outer structure in two places using both hands or a combinations of their hands and another rigid surface.
- **Pull** : The subject increases tension by pulling on the tensegrity's outer structure in two places using both hands.
- **Handle** : The subject picks up the tensegrity and rotates it to some degree in their hands, resulting in new placement of one or more of their hands.

- **Drop** : The subject picks up the tensegrity and drops it onto a surface from some height (distinct from placing the tensegrity onto a surface).

Using this set of outcomes, we can accumulate measures of accuracy from the video recordings of the physical interactions in the first experiment. As part of this set of human subject experiments, we also would like to gather useable data for testing our classifier on samples that are generated by non-expert operators. Since the subjects are not guaranteed to reproduce the correct type of physical interaction to warrant a correct classification from our algorithms, we must conduct a separate experiment that gives more specific instructions to the subject. However, we will still not explicitly instruct them on how to accomplish the interaction so as to encourage variability in the samples. The exposition script for this second experiment is given below:

> "In this second experiment, you will once again be physically handling the tensegrity as a way to talk it. Instead of nonspecific prompts, I will give you specific instructions on how to physically interact with the tensegrity correctly. Please do your best to recreate the physical interaction based on the instructions given. You can handle any part of the tensegrity, excluding the ball in the center. You don't have to do something new for each prompt, and you don't have to do something distinct from the previous experiment. The tensegrity won't actually do anything in response, but you can imagine that it responds if you'd like. Do you have any questions before we begin?"

The associated prompts for this second experiment are shown next. Note that each instruction is still posed in the context of a specific task or function to be accomplished with the tensegrity. This will become relevant for our post-experiment questionnaire that we will have each of the subjects complete upon finishing the first and second experiments.

1. "Squeeze the tensegrity in order to flatten it for storage."
2. "Pull on the tensegrity in order to increase its size."
3. "Turn the tensegrity over several times in your hands to turn it on."
4. "While holding the tensegrity out in front of you, drop it to the ground to deploy it for its tasks."

While we were slightly limited in procurement of human subjects to the conditions surrounding the the COVID-19 pandemic, we were able to accumulate a pool of 20 subjects ($n = 20$) for our experiments. The subjects consisted of individuals above the age of 18 who self report as having no experience with or exposure to concepts relating to tensegrity systems. The experiments were held in the BEST Lab on University of California, Berkeley campus.

6.5 Human Subject Experiment Results

In this section, we present the statistical results from the first experiment on the intuitiveness of the physical interaction schema as well as a discussion of our qualitative interpretations of the responses from the subjects. Video data from the 20 human subjects was reviewed by lab personnel and overall accuracy scores for each class were calculated based on the number of successfully executed physical interactions over the total number of interactions for each type. The resulting accuracies for the non-expert human subjects are tabulated based on type of physical interaction below.

Table 6.1: Accuracy scores representing the frequency that non-expert human subjects were able to correctly execute the intended physical interaction from associated verbal prompts without explicit instruction.

Class	**Squeeze**	**Pull**	**Handle**	**Drop**
Accuracy (%)	97.5	87.5	57.5	30
Prompt	**S1/S2**	**P1/P2**	**H1/H2**	**D1/D2**
Accuracy (%)	95/100	95/80	30/85	40/20

We can see from the resulting accuracies in Table 6.1 that there was some striking disparity in accuracy between the different types of physical interactions. While certain types of interactions like squeeze and pull interactions were immediately inferred and executed by unbiased operators with consistency, others were less obvious or intuitive to our test subjects. This would indicate that there are certain goal/action pairs with the tensegrity robot—leveraging our proposed physical interaction types—that exhibit intuitive qualities to the average human operator. Our interpretation of these results for the best-performing types of physical interactions (squeeze and pull) is that they are inherently intuitive actions to perform with a compliant robotic system.

While the results illustrating the intuitivness of squeeze and pull interactions are compelling, there are certainly many potential factors that could be influencing a human operator's response to an open-ended prompt like the ones given in our first experiment. For example, we acknowledge the possibility that personal experience has a large effect on our independent interpretation of ambiguous instructions in unstructured contexts. Furthermore, our proposed selection of interaction types and their mapping to outcomes or functions is only one possible set of choices. This is evidenced by observations that were made during the experiment with respect to the handle interaction—specifically the first handle prompt—which were not frequently executed by subjects as intended. Instead of the intended physical interaction, subjects invariably chose to perform a different interaction that involved quickly tapping the outer structure with one hand. Upon observing these responses, it became obvious in our retrospection that an intuitive action to wake up a sentient device would be the same action that one would take to wake up a human.

As part of our assessment of the responses of our test subjects, we had our participants fill out a post-experiment questionnaire to collect information on their impressions of the experience of physically interacting with the force-sensing tensegrity. The short questionnaire consisted of four statements with Likert scale response options and then a fifth open-ended written free response question in case subjects were interested in expressing anything specific about their experience. Here are the exact wordings of the questions included in the post-experiment questionnaire:

1. I did not feel hesitant to physically interact with the robot. (1-7 Likert response)
2. I was not afraid of damaging the robot while physically interacting with it. (1-7 Likert response)
3. I was confident in how to communicate with the robot through physical interaction. (1-7 Likert response)
4. It made sense how to communicate with the robot through physical interaction (after learning the correct ways). (1-7 Likert response)
5. What was your impression of the robot? (Written free response)

We collected the responses for the $n = 20$ subjects and calculated the statistics (mean and standard deviation) for the Likert response questions. The results are plotted in Figure 6.2.

The resulting statistics indicated a marginally favorable impression of the physical interface across all measures from our questionnaire. With few exceptions, the subjects reported that they at least somewhat agreed with the statement that they did not feel hesistant to physically interact with the tensegrity. This would indicate that the subjects felt comfortable putting their hands on the tensegrity without explicit handling instructions. The degree to which the subjects were afraid of damaging the robot did vary a large amount, however. Perhaps expectedly, the subjects reported that they felt just above neutral with regard to their confidence level in physically interacting with the tensegrity. Even so, it is encouraging to see that without having the prior understanding of how to physically interact correctly, subjects still reported confidence in their actions to some level. Once subjects were given more explicit instructions (as in second part of the experiment), the average subject agreed that the interaction schema made sense.

We reviewed the free responses from the participants and made special note of any responses that concerned their perception of either the device itself or the experience of interacting with it. There were several recurring sentiments that stood out to us in the responses from test subjects. First, subjects were intriguied by the unconventional shape and mechanical behavior of the device. These responses seemed to reflect a general fascination with how the tensegrity system might be used toward a given application and often involved hypothesizing their imagined use cases. This result highlights another interesting property

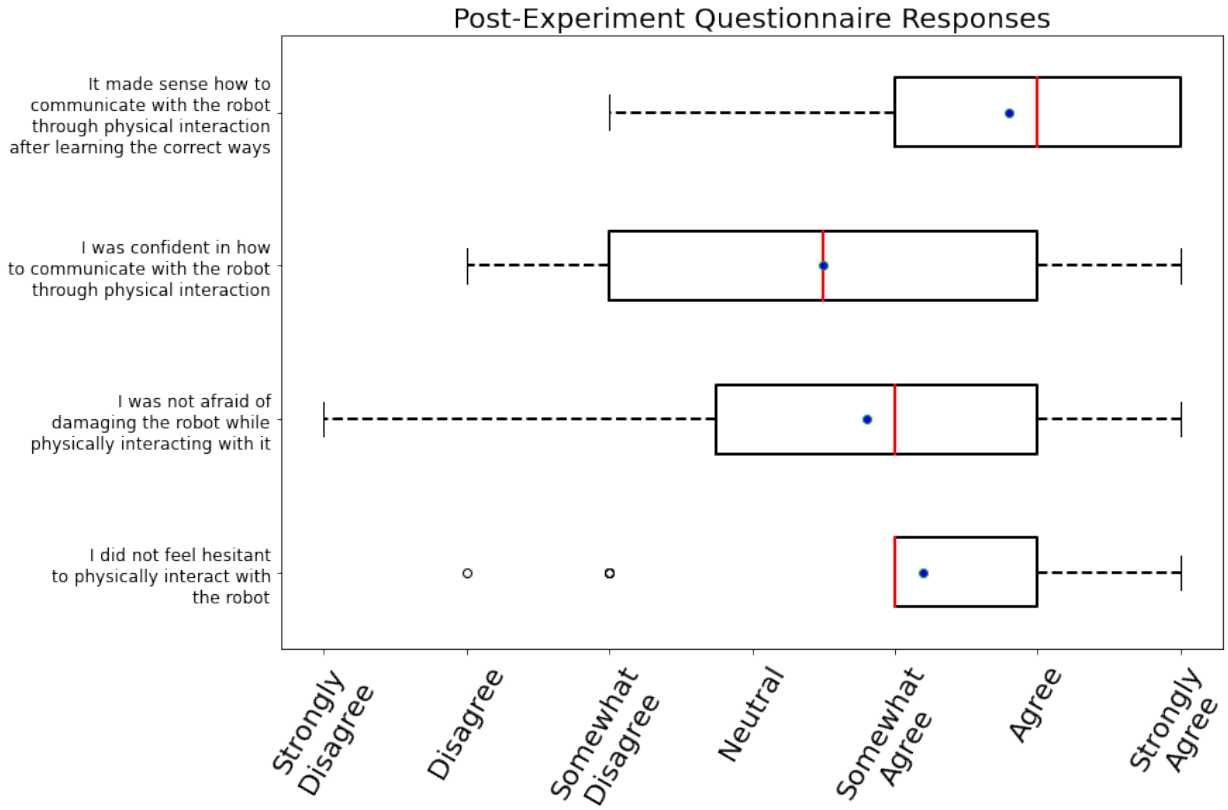

Figure 6.2: Resulting Likert question statistics from post-experiment questionnaire on participant impressions of pHRI with the force-sensing tensegrity.

of tensegrity robots in that they tend to capture the imaginations of individuals who have never been exposed to similar systems. Other responses from participants communicated a transition from initial hesitance in interaction to more confidence as they began to understand and recognize the physical resilience of the tensegrity through their handling of it. It was encouraging to see that inexperienced human operators were quickly gaining comfort in manipulating the device as they learned more about it by way of tactile feedback. Again, we interpret this as a point toward justifying the physical modality as an inherently natural form of interaction between human and compliant robot that can be learned quickly and independent of explicit instruction.

At the same time, there were also free responses that we classified as generally negative in their assessment of the robot and the interface. In these instances, subjects were particularly concerned with trying to project their previous understanding of robotic systems and robotic interfaces onto that of the tensegrity robot. When it was unclear how to do this, it became a source of frustration and confusion especially when tasked with trying to accomplish a goal

with limited instruction. Another source of negative feedback stemmed from their imagination of the intended use case as described by the prompts in our study. Since the device itself is passive (unactuated) and won't actually perform the operation described by the prompts, our human subjects would occasionally report that it was difficult to visualize how the robot would function toward accomplishing its tasks. This was an important data point because it illustrates the importance of having a demonstration of functionality to condition how an operator attempts to communicate concerning said functionality. In interacting physically with a system that has some physical output, we can leverage commonalities in operation and interaction to yield an intuitive communication such as in the case of physically guiding an anthropomorphic manipulator through a task. As an equivalent example, we might have the tensegrity robot compress itself or expand itself as intended in response to being squeezed or pulled by an operator. In the future, we consider it an essential goal to be able to augment actuated tensegrity systems with our force-sensing system to enable such studies, which we believe will result in more representative human-robot interaction scenarios.

6.6 Classification Results

As part of our human subject experiments, we collected data on all of the physical interaction scenarios in both the first and second parts of the experiment to utilize in our classification framework testing. In particular, we will focus on data from the second part of the experiment that involves prompting the subjects with specific, albeit limited, instructions on how to physically interact correctly based on our hypothesized mappings. Since there is no guarantee that the subjects would produce the correct interaction from this prompt, we refer back to the video recordings to qualify or disclude the data associated to each interaction based on whether or not the subject executed the interaction based on our previously established criteria. We then process the data into observations for training and testing using the same processing pipeline as before. We combine this data with data accumulated from controlled testing as described in the preliminary results section of last chapter. It should be noted that all of the results being presented in this section are related to the second-iteration force-sensing tensegrity.

We start by considering the DNN implementation, and we train it using exclusively data from controlled testing with lab personnel (referred to in subsequent figures as "V2" data). As with the RF and kNN tests previously, we compare raw signal inputs and abstract feature inputs on the performance of the classification. Figures 6.3 and 6.4 show the resulting confusion matrices illustrating the performance of the DNN classifier.

The DNN classifier has excellent accuracy for both types of input processing with abstract featurization performing slightly better overall. We can see that as the window size increases, there is some dropoff in performance for both types of inputs, which indicates that the framework is more suited toward classifying smaller sample sizes. This is particularly encouraging to embedded implementations of this type of intent inference methodology because of the need for real-time decision making in operation. In order to further test the

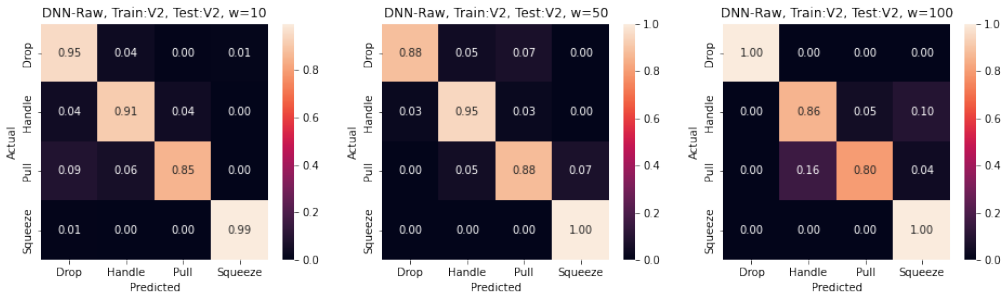

Figure 6.3: Confusion matrices for DNN with raw signal inputs trained and tested on control data (V2) over various window sizes.

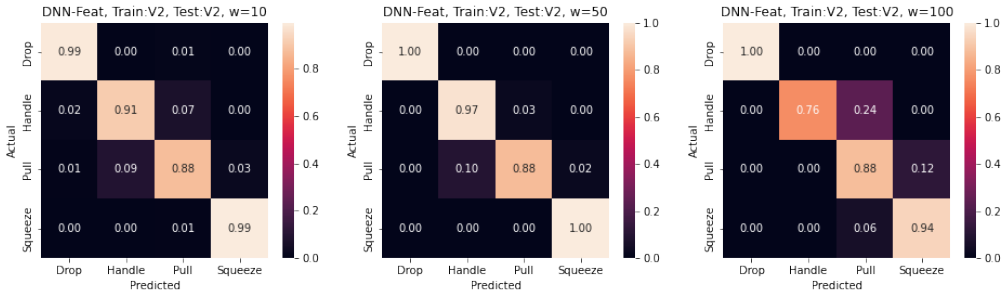

Figure 6.4: Confusion matrices for DNN with abstract feature inputs trained and tested on control data (V2) over various window sizes.

robustness of this framework, we broaded our training data set to include observations from our non-expert human subject trials (referred to in subsequent figures as "HSE"). In this way, we can explore the generalizability of the framework to less controlled data sets that may be more representative of actual end-users. Figures 6.5 and 6.6 show confusion matrix results for our DNN classifier with raw signal inputs and abstract feature inputs respectively after being trained on V2/HSE data and tested on combinations of V2 and HSE data over different window sizes.

In general, the DNN classifier does a serviceable job of retaining accuracy even in the presence of observations with greater variance than the original data set. However, there is a significant decrease in accuracy in comparison to the DNN model trained and tested on exclusively V2 data, which indicates that it is not as generalizable as we would like it to be. Instead of attempting a different network structure or heavily adjusting our parameterization, we introduce a CNN-based approach to try to take advantage of the temporal dependence of the physical interactions in our classification algorithm. To enable this approach, we use exclusively raw signal inputs instead of the abstract featurization, as processing the

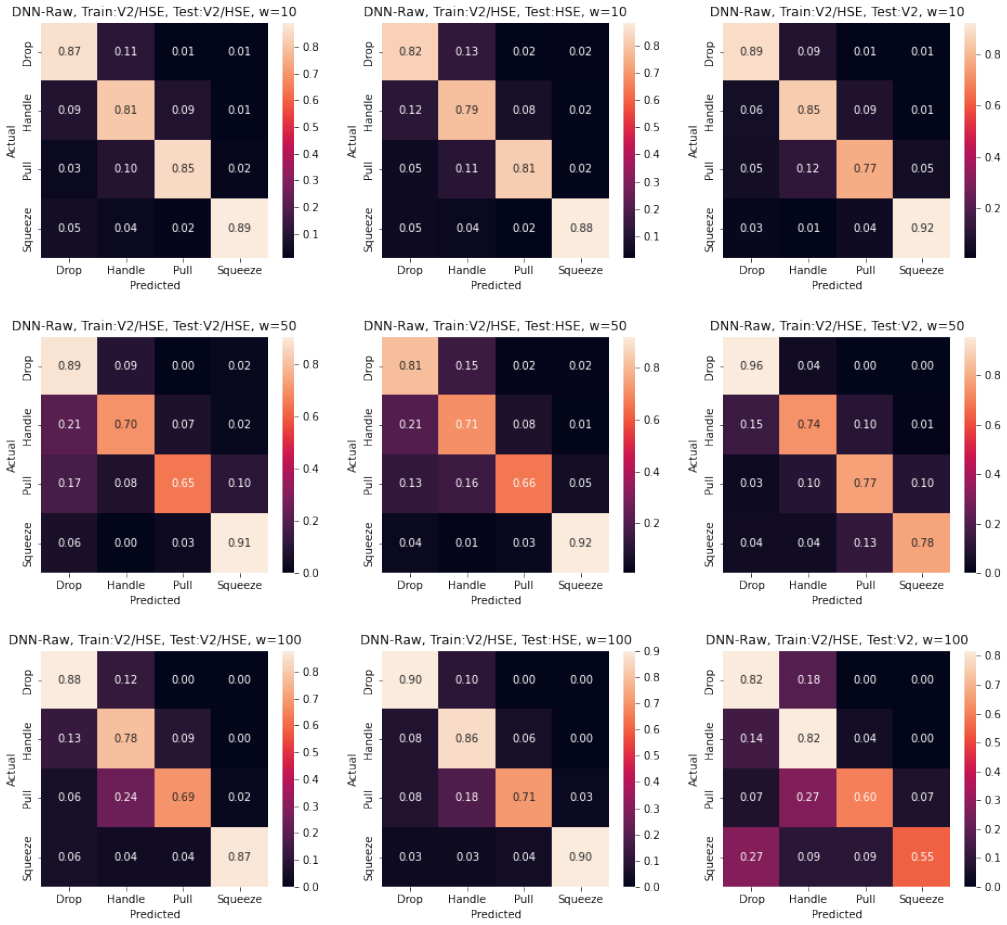

Figure 6.5: Confusion matrices for DNN with raw signal inputs trained on a combination of control data (V2) and human subject data (HSE) and tested on V2/HSE data, HSE data, and V2 (left to right) over various window sizes (increasing from top to bottom).

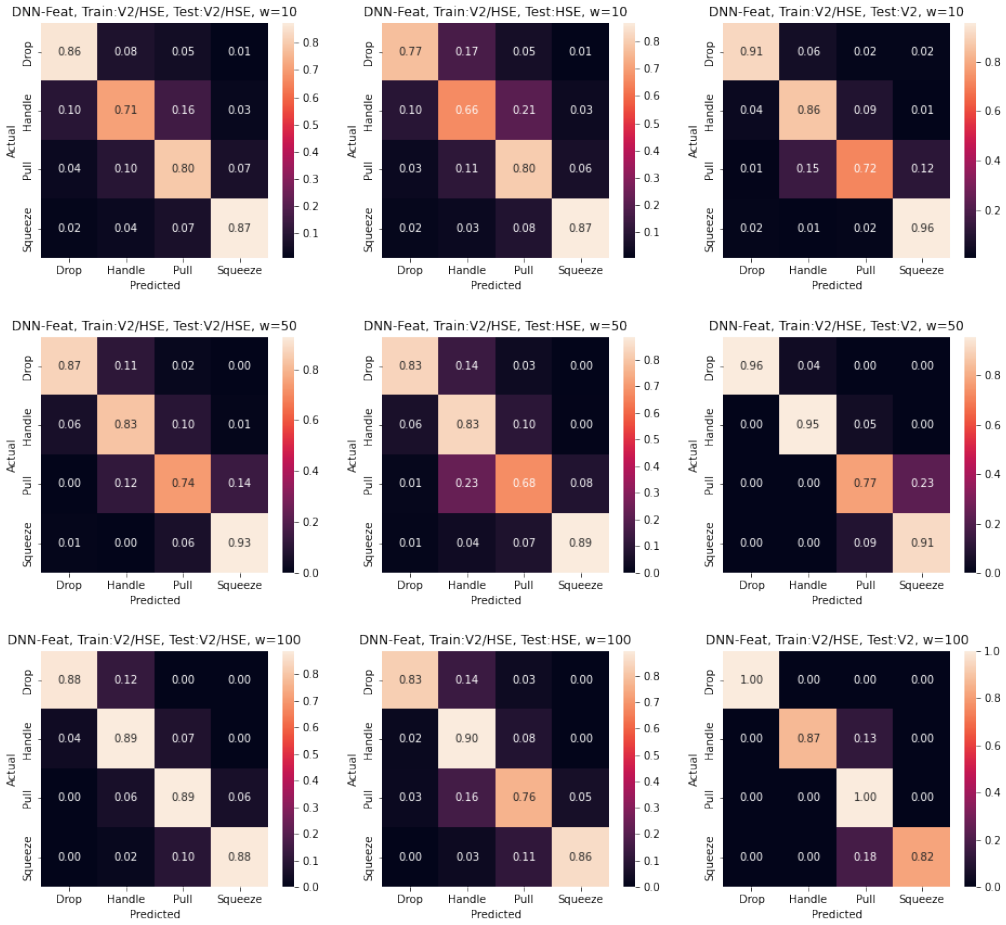

Figure 6.6: Confusion matrices for DNN with abstract feature inputs trained on a combination of control data (V2) and human subject data (HSE) and tested on V2/HSE data, HSE data, and V2 (left to right) over various window sizes (increasing from top to bottom).

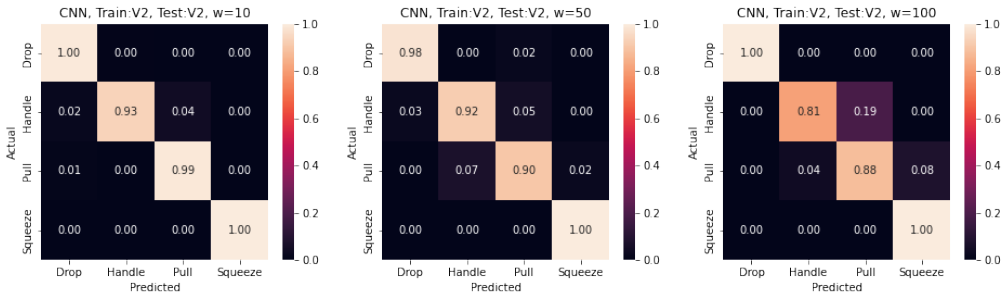

Figure 6.7: Confusion matrices for CNN with raw signal inputs trained and tested on control data (V2) over various window sizes.

signals into temporally-abstracted statistics would defeat the purpose of the CNN layer's convolution operation. First, we show the CNN implementation's performance after being trained and tested on V2 data in order to compare a baseline to our DNN models. The confusion matrices for the CNN model with V2 data is shown in Figure 6.7.

As shown in Figure 6.7, the CNN model performs better than either of the DNN models in terms of categorical accuracy (both raw signal and abstract feature inputs) across all window sizes. We can also examine how well it performs in the presence of additional observations from our human subject testing during training and testing. The resulting confusion matrices can be found in Figure 6.8

The CNN model greatly improves on generalizability from the DNN models we tested. At a window size of 10 samples (shown on the top row of Figure 6.8) tested over both V2 and HSE data, we achieve a categorical accuracy of 91%. While the CNN model is still better overall at an impressive accuracy of 98%, we should consider the context of the data being used and the implications for the deployment of a similar system for use in real applications. The data contained in the HSE data set is exctracted from completely untrained and novice human operators whose only instruction was a single sentence prompt. With minimal instruction and training of the human operator, the classifier was still able to correctly classify across a set of distinct physical interactions with considerable accuracy. Somewhat counterintuitively, the CNN model performance has difficulty with larger sample size, and the accuracy declines as window size increases. We can gain more insight into this phenomenon by examining the loss and accuracy curves during the training phase of the CNN model in both cases of training data sets. This data is displayed in training/validation loss curves and training/validation accuracy curves in Figure 6.9.

In particular, we highlight the loss curves for both the V2 and V2/HSE data sets on the left two plots of Figure 6.9. For a window size of 100 samples, we begin to see strong instability in the validation loss as we progress through the training epochs. Typically, this is an indication that the data itself either has too much variability within class or that the model is not effectively capturing underlying features as a result of complexity or tuning issues. In

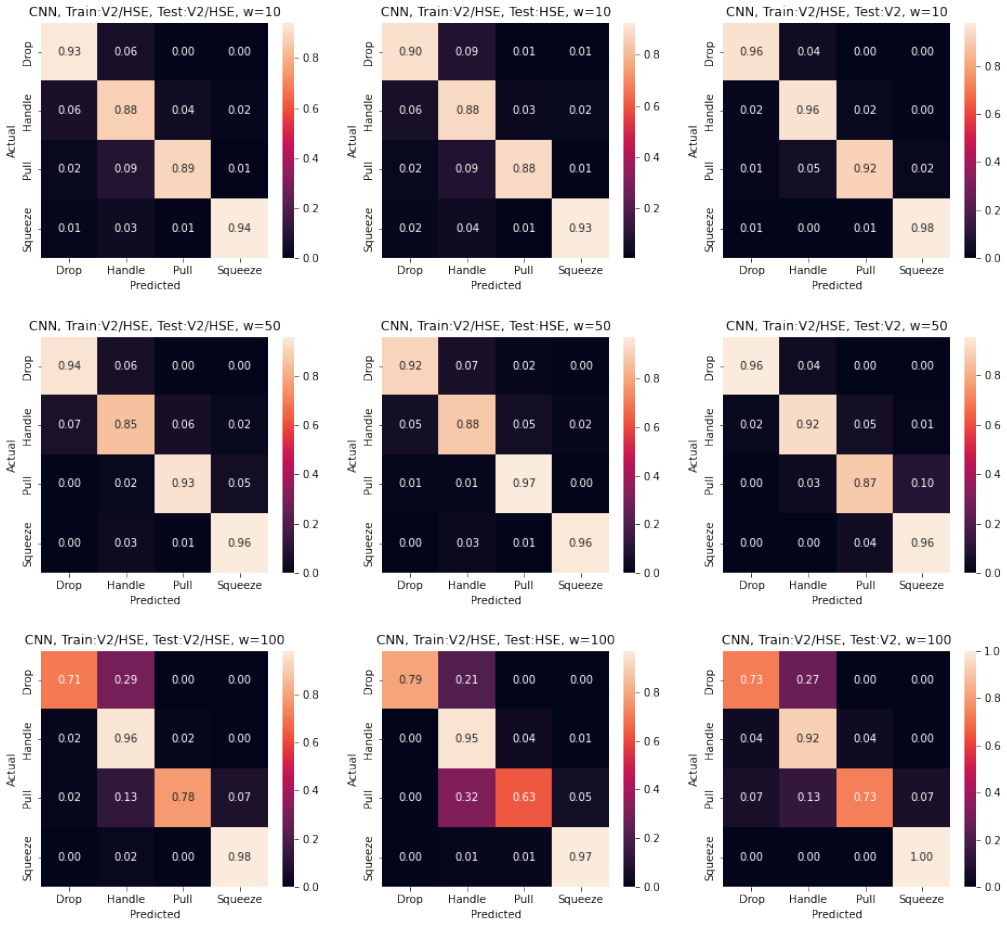

Figure 6.8: Confusion matrices for CNN with raw signal inputs trained on a combination of control data (V2) and human subject data (HSE) and tested on V2/HSE data, HSE data, and V2 (left to right) over various window sizes (increasing from top to bottom).

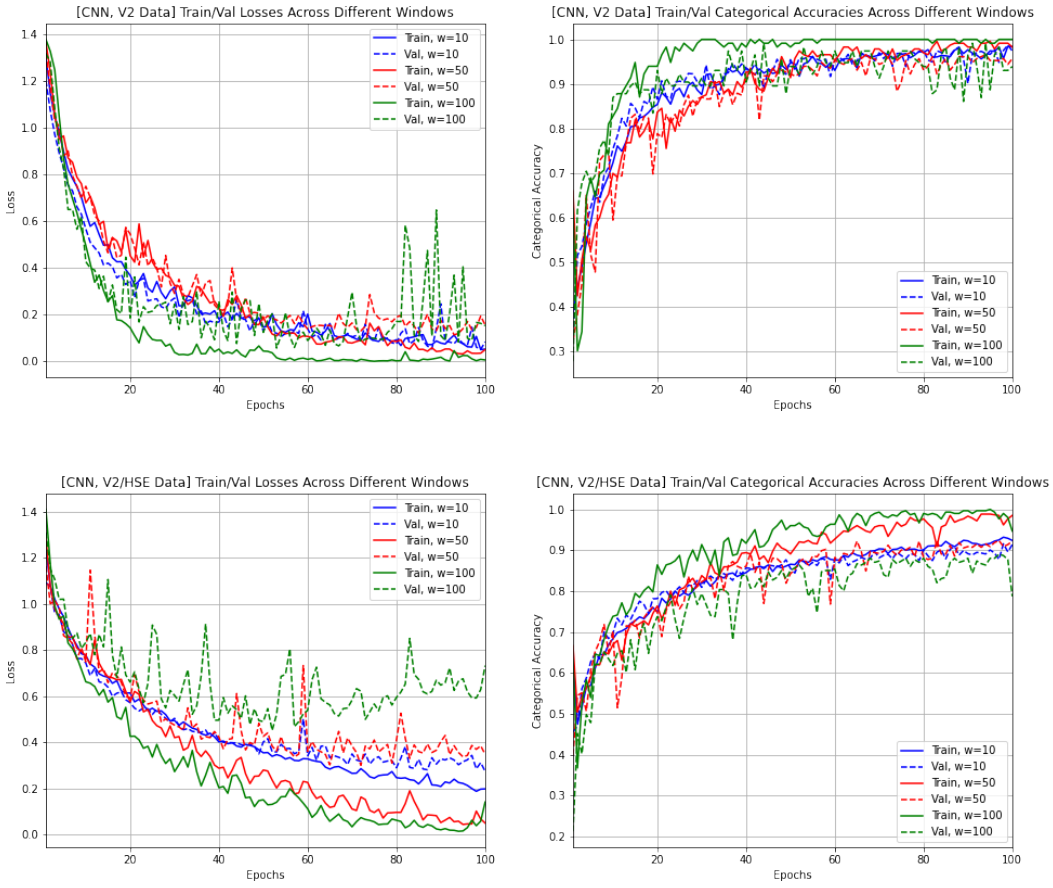

Figure 6.9: Training and validation loss curves (left) and categorical accuracy curves (right) for V2 data and V2/HSE data for CNN model training.

the case of the V2 data (top left), the model converges very quickly, so our initial attempts at improving accuracy were focused on adjusting learning rates; however, this resulted in only slight improvements to accuracy. The V2/HSE data set, on the other hand, reveals more clearly the cause of this phenomenon through the stark deviation in training/validation loss curves over the training process. This separation between training and validation loss increases as a function of window size even under the optimal tuning conditions for each case—as determined by iterative parameter tuning. As we initially suspected, the length of the input (in terms of window size) results in too much variability in the signal characteristics to yield a robust classifier, which will always tend to overfit.

Another way we can examine the overall feasibility of this classification-based methodology for inferring physical interactions is by taking a look at the AUC scores across window size for the CNN model. As mentioned in our analysis of the benchmark classifiers in our

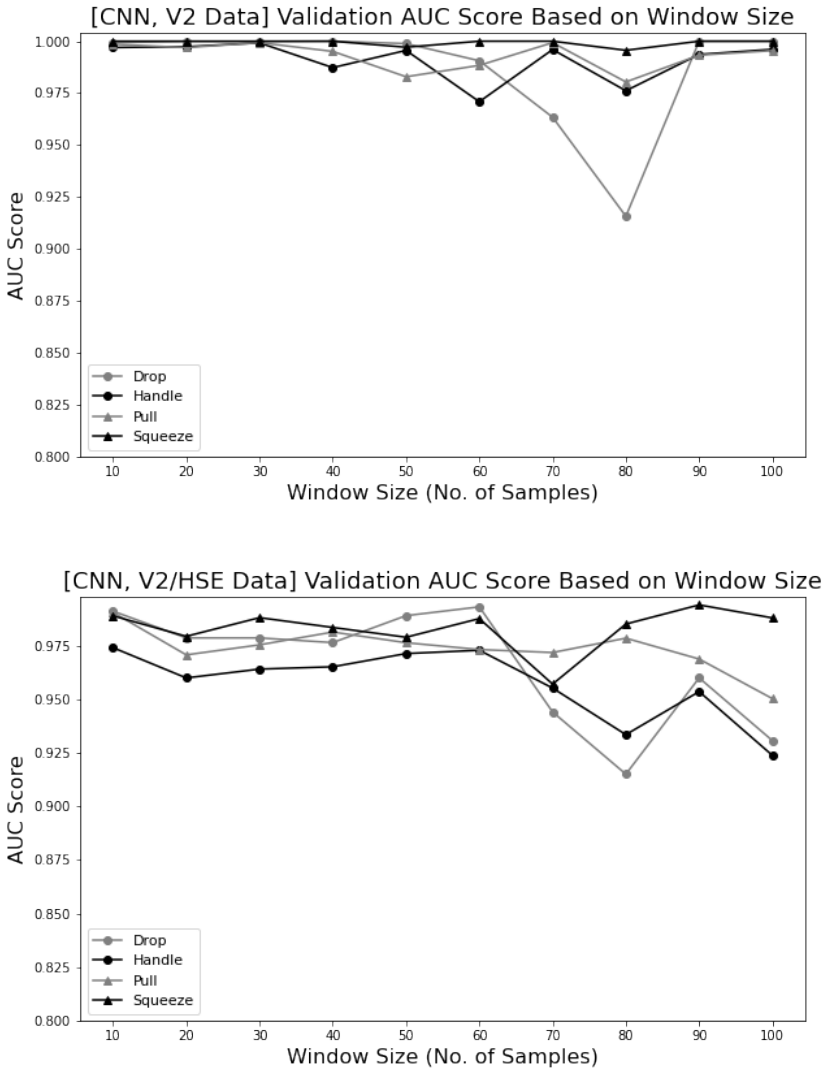

Figure 6.10: AUC scores during validation testing for our CNN model with V2 data (top) and V2 and HSE data (bottom) across different window sizes.

preliminary experiments, AUC is an effective indicator of the separability of classes based on the receiver operating curve of a classifier. The AUC scores are shown in Figure 6.10.

In both cases, the AUC scores demonstrate consistently high separability with some slight decreases at larger window sizes. This gives us confidence that the underlying data extracted from both controlled (V2) and inexperienced (HSE) use cases are readily distinguishable using our CNN framework. It also further solidifies smaller window sizes as more generalizable and consistent for classification of our chosen set of physical interactions.

6.7 Sequential Classification Using HMM

Now that we have a framework for classifying independent samples of physical interactions accurately, we examine how well the framework performs in a more representative scenario where samples are extracted sequentially from a whole physical interaction from start to finish. This is intended to simulate an operational situation in which the deployed classifier is being used to infer the physical interaction over time, which is then stored as an internal state to be used toward some desired function. We consider four different whole interactions (squeeze, pull, drop, handle) and perform classification at each time step over the course of the interaction. It should be noted that in a real scenario, there would be limitations imposed by hardware and model complexity on the rate that we can perform this classification in real-time. Our work here is completed entirely offline on controlled interactions from our V2 data set. The results of the classification with physical interaction type indicated by color are projected over the raw data used in the classifier in Figure 6.11.

Assessing the performance of the classifier in each type of interaction, we can observe that the overwhelming mass of the interaction is classified accurately with the occasional section of noise interspersed. This is an inherent drawback of the chosen methodology in sequential classification scenarios because each individual sample is classified independent of the previous sample and without regard to any underlying belief of the current classification. If we seek to extend this approach to create a practical interface, we require more consistency over contiguous interaction events.

Conveniently, we have some useful tools for determining state evolutions based on observational data. A Hidden Markov Model (HMM) is a representation of a Markov process that seeks to recover the underlying (or hidden) state of said process by considering only an observation of the state. They are commonly applied in the context of estimating discrete states from noisy measurements on stochastic processes. In the case of our problem, we start by assuming that the type of physical interaction being performed by the human operator is the state in a Markov process in which the likelihood of the human performing a certain type of interaction in the current state is only dependent on the previous state. Our measurement process is represented by the classification of physical interactions from the force sensor data, which has some inherent noise as a result of model inaccuracies. We constuct an HMM with some assumed transition and emission probabilities that are weighted toward creating contiguous state sequences. We then apply the forward algorithm to filter the sequence of hidden states in a given sequential classification effort such as the previous cases shown.

To demonstrate this approach in practice, we present a scenario in which a human operator is required to input a sequence of physical interactions using a predefined input scheme for leveraging physical interaction toward controlling the locomotion of an arbitrary device. In other words, we hypothesize a mapping from physical interactions with a force-sensing tensegrity (acting as a controller in this context) to two-dimensional motion of an agent in space. The hypothetical input scheme can be described as follows:

- Picking up the tensegrity (*handle interaction*):

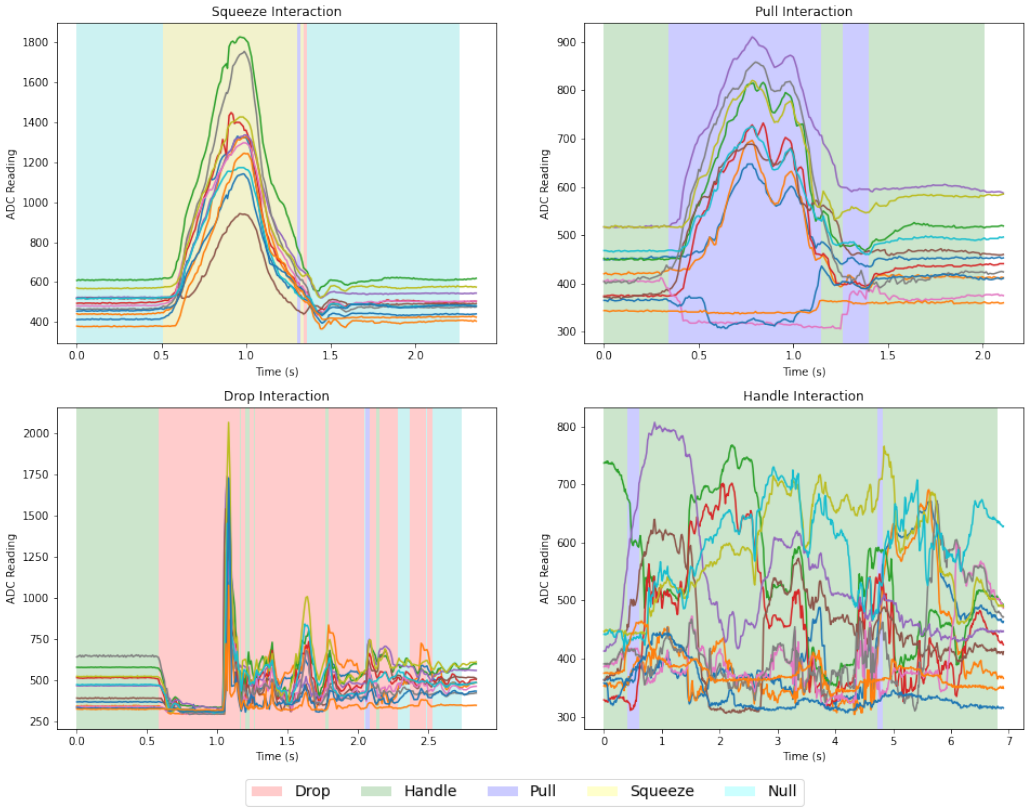

Figure 6.11: Sequential classification results on whole interactions by type of interaction. Classification results are illustrated by color and projected over the raw data.

  - If uninitialized, detect accelerations for determining an initial reference frame.
  - If initialized, continue last motion direction and wait for new input.

- Squeezing the tensegrity (*squeeze interaction*):
  - Detect accelerations for new motion direction.
- Pulling on the tensegrity (*pull interaction*):
  - Stop all motion and wait for new motion direction.
- Moving tensegrity in 2D direction (no assigned physical interaction):
  - Extract direction of acceleration and apply motion in detected direction.

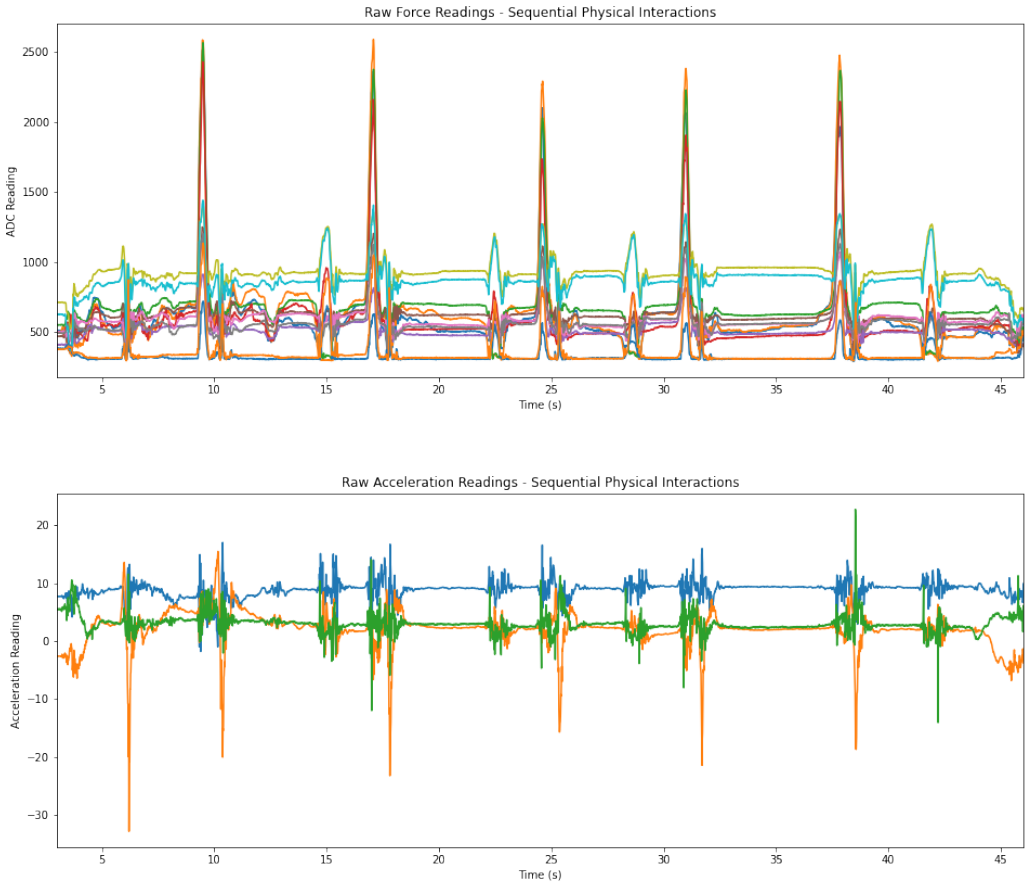

Figure 6.12: Raw force data (top) and raw acceleration data (bottom) from sequence of physical interactions in hypothesized scenario.

Using this input scheme, we can simulate a scenario in which a human operator is controlling an agent to execute a two-dimensional trajectory by using a sequence of physical interactions. To test how well we can extract a sequence of inputs using our classification framework, we perform a sequence of physical interactions that would produce an arbitrary trajectory based on the previously described input scheme. We then process the raw data offline to illustrate the accuracy of our classification framework in a sequential classification task. Figure 6.12 shows the raw force and acceleration signals from an example sequence of physical interactions. For clarity, we will describe the expected sequence of inputs that yielded this raw data (handle interactions are interspersed throughout the sequence but are omitted for brevity):

- Direction (initialization) →Squeeze →Direction →Pull →Squeeze →Direction →Pull

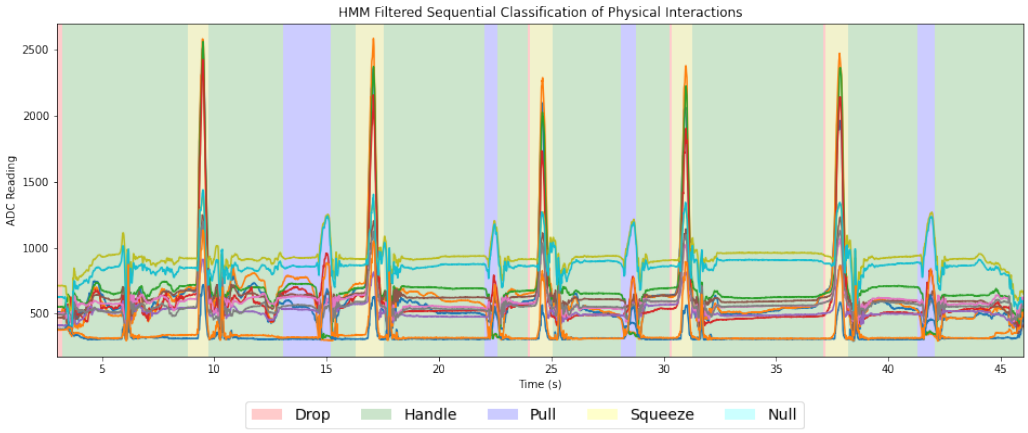

Figure 6.13: Sequential classification results on simulated interaction sequence. Classification results are illustrated by color and projected over the raw data.

→Squeeze →Direction →Pull →Squeeze →Direction →Squeeze →Direction →Pull.

The first step in processing this sequence is to perform initial classification on overlapping samples of raw force sensor data using our CNN-based model with a window size of 50 samples. This results in an inital noisy sequence of classifications spanning the entire interaction sequence. These observations then pass through our HMM filter to reveal the underlying physical interaction states. We use the equivalent of a state machine implementation to process the filtered inputs into functions based on our input scheme and correlate with raw acceleration data for directional inputs. Directions are inferred by projecting all accelerations onto the two-dimensional plane established by the gravity vector and then referencing them to an initial direction provided at the start of the interaction sequence. The final sequential classification is shown in Figure 6.13. Inferred directions for each post-squeeze directional input are shown in Figure 6.14.

We simulate the input sequence scenario by using it to control a tensegrity in a grid world simulation. As described in our outline of the input framework, the input sequence will control the tensegrity's locomotion through a 2D path. The paths are generated by first constructing waypoints from the inferred sequence of interactions (i.e., mapping directions and timings of physical interactions to propagate the tensegrity's state). We then use an A* path planning approach to plan paths between the various waypoints. The resulting simulated path is shown in Figure 6.15. The tensegrity begins at the "start" position waypoint and receives a command from our input framework to move forward for a certain amount of time resulting in its transition from the "start" waypoint to waypoint 1. The remainder of the path is executed accordingly.

As shown in Figure 6.13, the HMM filtering contributes tremendously to the consistency

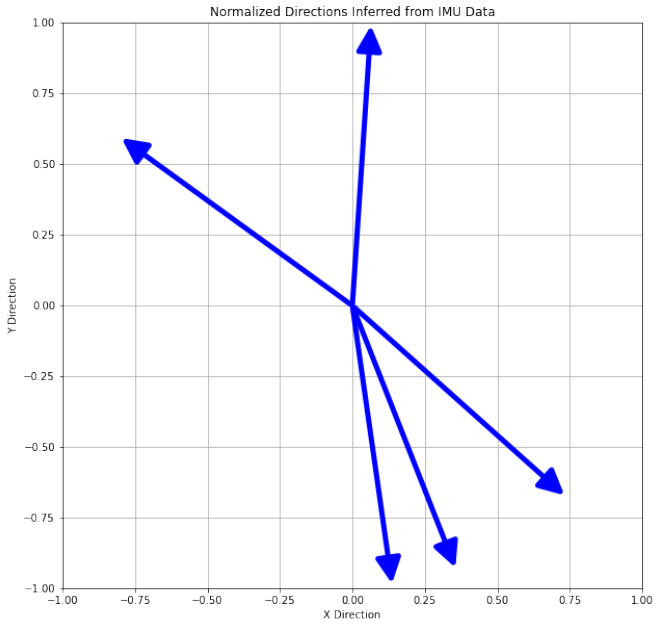

Figure 6.14: Normalized direction vectors extracted from IMU data after being correlated with classified inputs in sequence. Directions are given in a world frame. Refer to Figure 6.15 for an illustration of the resulting path.

of classification accuracy. While there are still several brief segments of incorrect classifications within the sequence, these instances can be filtered out using simple thresholding on length of state segment. Using this final inferred sequence, it would be straight forward to program an agent to use these inputs toward motion control in two-dimensional space. This is just one example that makes due with the fact that the force-sensing tensegrity is currently limited to sensing only. Other input schemes could be leveraged to provide inputs to a device that is also capable of actuating or performing other useful functions with some creative interface design, as suggested in the beginning of our discussion on applications for this technology.

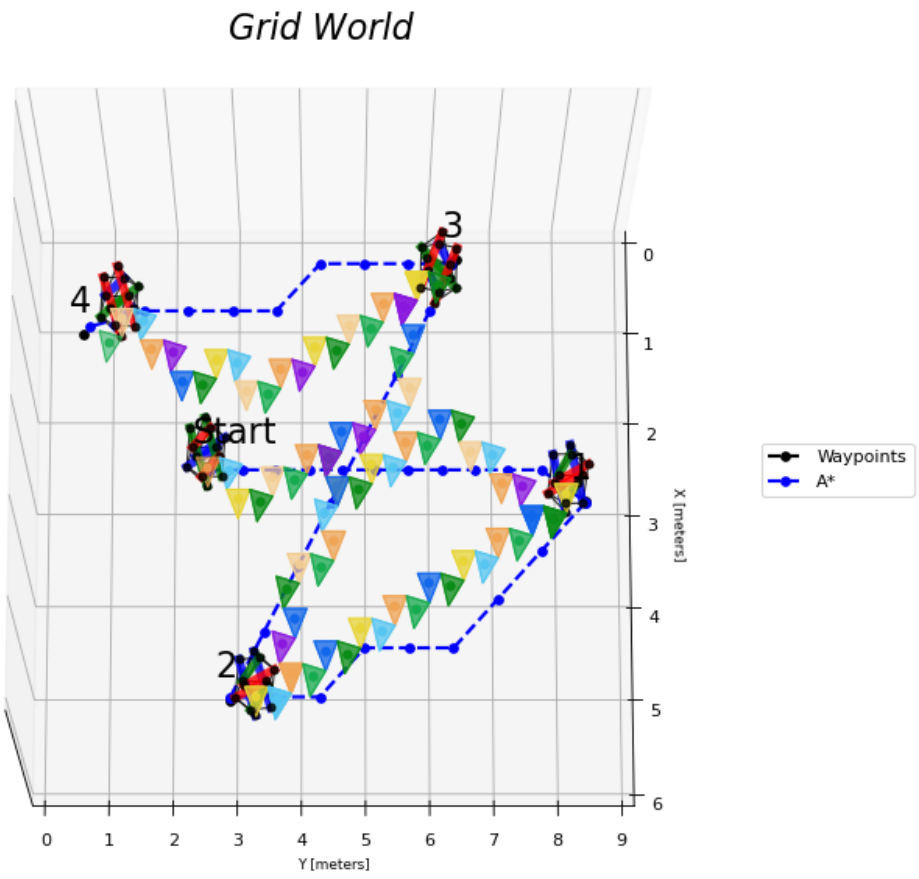

Figure 6.15: Simulated path of six-bar spherical tensegrity in response to input sequence from physical interaction input framework. The paths are generated by connecting waypoints inferred from directional commands and connected by an A* path planning routine. The triangles represent faces of the tensegrity that are resting between steps in the locomotion of the device.

Chapter 7

Conclusions and Future Work

7.1 Conclusions

The world we live in is large, unstructured, and constantly changing. As we continue to develop intelligent robotic systems that are intended to operate in human contexts, roboticists must recognize the importance and inevitability of physical contact and leverage it in order to achieve robust and efficient operation in dynamic environments. Toward this goal, we have presented our work on the development of new hardware platforms and practical methodologies that look toward the future of physical human-robot interaction with compliant robotic systems like our spherical tensegrities. We hope that this project will inspire future efforts focusing on the development of hardware and software frameworks for realizing emergent mechanisms of physical human-robot interaction that break the mold of relying on conventional anthropomorphic and rigid robotic systems.

We began this dissertation by highlighting some of the most important factors in the design of contemporary robotic architectures to outline challenges that researchers face in making these systems more physically tolerant. Our discussion of pHRI in its many forms in current literature helped us understand how traditional approaches to pHRI are limited by the mechanical characteristics of the platforms used to research them. In response, we introduced tensegrity robotics as an exciting new direction for robotic architectures that offers dramatically improved robustness to physical contact. With compliant robotic systems like tensegrities, we could explore novel mechanisms for pHRI that challenge our previous assumptions about how humans and robots should interact physically. This fuels our conversation of the future of resilient tensegrity robots that welcome physical contact as a way to improve the intuitiveness and efficiency of human-robot collaborative tasks such as those seen in disaster response scenarios.

As a first step toward developing an investigative platform using tensegrity design concepts, we introduced a standard representation and specific topology of tensegrity that would be useful for our study. Using our assumed tensegrity model, we conducted a series of analyses on theoretical tensegrity statics and simulated dynamics. We presented a strategy for

the selection of a subset of internal members that, when instrumented with force sensors, will allow for the distinction of unique physical interactions in a static case. A simulation of simplified tensegrity dynamics gave us key data points from which to design sensor instrumentation in a prototype system.

One of the most important contributions of our research toward physical human-robot interaction with tensegrity systems is the iterative prototyping of a force-sensing tensegrity platform. Our first iteration featured novel sensor packaging in order to demonstrate the feasibility of our force sensor array design. Initial results with this system were critical in confirming that by instrumenting the chosen subset of structural members, we could reliably distinguish categories of physical interactions. The second iteration prototype refined our sensor packaging approach, improved the embedded infrastructure, and resulted in a more robust platform for conducting human subject experiments.

Investigating the hypothesized framework for classifying different physical interactions relied on a varied search into contemporary supervised learning algorithms and methodologies with an emphasis on deep learning architectures. In particular, we focused on using this approach to understand the effects of choosing different featurization and modeling techniques on the performance and practicality of the classification framework for real use cases. We settled on a CNN-based model and concluded that smaller sample sizes of raw force signals resulted in greater overall accuracy and generalizability of classification. To support this conclusion, we performed tests from data gathered in both controlled experiments with lab personnel and with unbiased non-expert human operators.

In order to understand how well this physical interaction framework translates into intuitive interactions from a human's perspective, we created a set of experiments that were designed to assess intuitiveness of interactions in the context of hypothesized use cases. These experiments placed unbiased and non-expert human subjects into specific scenarios that required them to use intuition and creativity in order to infer what interaction would result in the correct function for a given scenario without explicit instruction. The results of these experiments demonstrated that our hypothesized framework and the prototype itself facilitated an intuitive understanding of the appropriate way to interact with compliant robotic systems like our force-sensing tensegrity. We are encouraged by the positive impressions reported by participants in our study and consider it an indication of the suitability of this interface for adoption in real applications.

Upon the conclusion of these research efforts, we reflect upon some of our main takeaways and some critical implications for the field of physical human-robot interaction with compliant robotic systems. We began our research with the goal to investigate how the emergence of compliant robotic systems like tensegrity robots could expand possibilities for physical human-robot interaction. We demonstrated in this work that—in addition to their well-established mechanical advantages and characteristics—tensegrity structures can facilitate the detection of physical interactions through novel sensor instrumentation design methodologies. While we focused on one particular topology of tensegrity robot in the spherical six-bar tensegrity, these techniques can be extended to all similar tensegrity realizations and applications given the appropriate assumptions. We imagine other implementations of

tensegrity robots with arbitrary shape and function that can leverage the same approaches toward force-sensing in a number of physically demanding applications. The hardware design choices we presented are also of particular relevance to future extensions of this technology. By focusing our sensor packaging design on the connection points of the tensegrity structure instead of the elastic elements or rigid elements, we enable the design of similar sensor arrays for any tensegrity implementation agnostic to the characteristics of constiuent structural elements.

The nature of this research study is inherently forward looking toward the continued appearance of compliant robotic systems in real-world applications within human contexts and the potential for the design of innovative mechanisms for pHRI. The ultimate goal is to take advantage of the compliance and physical resilience of robots like tensegrities to explore physical interactions in new ways that were previously impossible with traditional rigid robotic systems. To that end, this work resulted in some clear indications that the proposed space of new physical interactions offers possibilities for pHRI that are uniquely intuitive and expressive in the context of the robot's intended use cases.

7.2 Future Work

As we reflect on the work presented in this dissertation, we envision future work that will benefit greatly from the foundation provided by our investigation into pHRI with the force-sensing tensegrity. Of increased interest to us is an exploration into how different force-sensing tensegrity topologies that are distinct from the spherical six-bar tensegrity featured in this work could offer avenues for creating new classes of physical interactions that are unique to those specific shapes. One of the great advantages of tensegrity robot platforms is their configurability, which allows them to be adjusted in shape and function depending on the needs of the application. We already descrined numerous previous works that feature tensegrity topologies that are vastly different from our proposed platform in terms of structure and application. We are interested in investigating whether enabling these types of tensegrity systems with force-sensing capabilities will unlock unseen potential for useful pHRI outcomes while also demonstrating the extensibility of the methodologies demonstrated in this dissertation.

Another future research direction that we alluded to earlier during the assessment of our human subjects experiments was the development of a fully cable-actuated force-sensing tensegrity. While having a platform dedicated to exclusively sensing greatly simplifies the process of prototyping and testing this interface, it does not allow us to investigate full realizations of the intended functionality where a physical interaction input directly maps to and results in the intended action, such as locomotion, tensioning and untensioning, or reshaping of the tensegrity structure. In order to accomplish this, we propose leveraging actuated versions of the spherical tensegrity—notably *Squishy Robotics Inc.*'s mobile spherical tensegrity—along with an added force-sensor array, taking into consideration the design principles established in this dissertation. We could then apply similar experimental pro-

tocols with the added benefit of having tangible functionality demonstrated in real-time as opposed to relying on the description of functions by lab personnel or the imagination of the human subjects.

In addition to the ability to detect and distinguish physical interactions as inputs, we might also be interested in using the force-sensing capacity of the spherical tensegrity to provide critical state information beyond human-robot physical contact. For example, we might use force sensing as a way to understand static environmental factors such as surface conditions. This information could be essential to modulating a control policy for locomotion that is capable of operating robustly over different surface materials or slopes. It is also possible that the addition of internal force data could be constructive for model-based state estimation to supplement current filtering approaches that previously relied on only IMU data and encoder feedback from actuated cable elements.

At this point, we have limited our discussion of the implications of this research on future work to be within the domain of tensegrity systems; however, we see the methodologies presented in this dissertation as being instructive for other similar manifestations of physical interaction with compliant robotic systems. Our intent in exploring pHRI with compliant robotic systems is to better understand how their favorable mechanical characteristics might reveal more useful pHRI mechanisms and frameworks that would be otherwise impossible with rigid architectures. In demonstrating the functionality of our tensegrity platform as well as investigating the usefulness of our proposed input framework, we now have a better understanding of how to design similar frameworks for other compliant robotic systems.

Finally, there are many human-centered aspects of the design of these interaction frameworks that have yet to be considered. Toward the design of physical interactions that are intuitive and expressive, we anticipate an iterative process of experimentation with human subjects that will expose the advantages and disadvantages of certain kinds of physical interactions depending on a range of different human factors. Especially important to this process will be the development of interaction experiments that resemble or simulate relevant applications such as the illustrative example of disaster response. We hope to eventually test a refined version of our input framework and prototype force-sensing tensegrity with actual first responders so that we can better understand the specific needs of these end users.

We are tremendously excited about the future prospects of developing more sophisticated tensegrity devices that leverage this new modality of pHRI and look forward to the continued use of tensegrity concepts toward the development and adoption of compliant robotic systems in human contexts. Beyond tensegrities, our greatest hope is that this work will inspire a broad range of interesting new investigations into how compliant systems in general can offer roboticists an alternative perspective on the design of physical interfaces for human-robot interaction.

Bibliography

[1] Haider Abidi and Matteo Cianchetti. "On intrinsic safety of soft robots". In: *Frontiers in Robotics and AI* 4 (2017), p. 5.

[2] Parastoo Abtahi et al. "Drone near me: Exploring touch-based human-drone interaction". In: *Proceedings of the ACM on Interactive, Mobile, Wearable and Ubiquitous Technologies* 1.3 (2017), pp. 1–8.

[3] Don Joven Agravante et al. "Collaborative human-humanoid carrying using vision and haptic sensing". In: *2014 IEEE international conference on robotics and automation (ICRA)*. IEEE. 2014, pp. 607–612.

[4] Baris Akgun et al. "Trajectories and keyframes for kinesthetic teaching: A human-robot interaction perspective". In: *Proceedings of the seventh annual ACM/IEEE international conference on Human-Robot Interaction*. 2012, pp. 391–398.

[5] Farzad Alamdar, Mohsen Kalantari, and Abbas Rajabifard. "Towards multi-agency sensor information integration for disaster management". In: *Computers, Environment and Urban Systems* 56 (2016), pp. 68–85.

[6] Omar Aloui, Jan Lin, and Landolf Rhode-Barbarigos. "A theoretical framework for sensor placement, structural identification and damage detection in tensegrity structures". In: *Smart Materials and Structures* 28.12 (2019), p. 125004.

[7] Brenna D Argall and Aude G Billard. "A survey of tactile human–robot interactions". In: *Robotics and autonomous systems* 58.10 (2010), pp. 1159–1176.

[8] Jerzy K Baksalary and Oskar Maria Baksalary. "Particular formulae for the Moore–Penrose inverse of a columnwise partitioned matrix". In: *Linear algebra and its applications* 421.1 (2007), pp. 16–23.

[9] R Adam Bilodeau and Rebecca K Kramer. "Self-healing and damage resilience for soft robotics: a review". In: *Frontiers in Robotics and AI* 4 (2017), p. 48.

[10] Joran W Booth et al. "Surface actuation and sensing of a tensegrity structure using robotic skins". In: *Soft Robotics* (2020).

[11] Andrea Calanca, Luca Capisani, and Paolo Fiorini. "Robust force control of series elastic actuators". In: *Actuators*. Vol. 3. 3. Multidisciplinary Digital Publishing Institute. 2014, pp. 182–204.

[12] Angelo Brian Micubo Cera. *Design, Control, and Motion Planning of Cable-Driven Flexible Tensegrity Robots*. University of California, Berkeley, 2020.

[13] Brian Cera and Alice M Agogino. "Multi-cable rolling locomotion with spherical tensegrities using model predictive control and deep learning". In: *2018 IEEE/RSJ International Conference on Intelligent Robots and Systems (IROS)*. IEEE. 2018, pp. 1–9.

[14] Nitesh V Chawla et al. "SMOTE: synthetic minority over-sampling technique". In: *Journal of artificial intelligence research* 16 (2002), pp. 321–357.

[15] Keene Chin, Tess Hellebrekers, and Carmel Majidi. "Machine learning for soft robotic sensing and control". In: *Advanced Intelligent Systems* 2.6 (2020), p. 1900171.

[16] Andrea Cirillo et al. "A conformable force/tactile skin for physical human–robot interaction". In: *IEEE Robotics and Automation Letters* 1.1 (2015), pp. 41–48.

[17] Agostino De Santis et al. "An atlas of physical human–robot interaction". In: *Mechanism and Machine Theory* 43.3 (2008), pp. 253–270.

[18] Jeffrey Delmerico et al. "The current state and future outlook of rescue robotics". In: *Journal of Field Robotics* 36.7 (2019), pp. 1171–1191.

[19] Julia Fink. "Anthropomorphism and human likeness in the design of robots and human-robot interaction". In: *International Conference on Social Robotics*. Springer. 2012, pp. 199–208.

[20] Fernando Fraternali and A Amendola. "Novel Actuators and Sensors with Tensegrity Architecture". In: *Key Engineering Materials*. Vol. 826. Trans Tech Publ. 2019, pp. 105–110.

[21] Jerome H Friedman. *The elements of statistical learning: Data mining, inference, and prediction*. springer open, 2017.

[22] Jeffrey Friesen et al. "DuCTT: A tensegrity robot for exploring duct systems". In: *2014 IEEE International Conference on Robotics and Automation (ICRA)*. IEEE. 2014, pp. 4222–4228.

[23] Abel Gawel et al. "3d registration of aerial and ground robots for disaster response: An evaluation of features, descriptors, and transformation estimation". In: *2017 IEEE international symposium on safety, security and rescue robotics (SSRR)*. IEEE. 2017, pp. 27–34.

[24] Wojciech Gilewski, Joanna Kłosowska, and Paulina Obara. "Applications of tensegrity structures in civil engineering". In: *Procedia Engineering* 111 (2015), pp. 242–248.

[25] Ian Goodfellow, Yoshua Bengio, and Aaron Courville. *Deep learning*. MIT press, 2016.

[26] Sami Haddadin and Elizabeth Croft. "Physical human–robot interaction". In: *Springer handbook of robotics*. Springer, 2016, pp. 1835–1874.

[27] James A Hanley and Barbara J McNeil. "The meaning and use of the area under a receiver operating characteristic (ROC) curve." In: *Radiology* 143.1 (1982), pp. 29–36.

[28] Sylvia L Herbert et al. "FaSTrack: A modular framework for fast and guaranteed safe motion planning". In: *2017 IEEE 56th Annual Conference on Decision and Control (CDC)*. IEEE. 2017, pp. 1517–1522.

[29] Shao-Chen Hsu, Vaishnav Tadiparthi, and Raktim Bhattacharya. "A Lagrangian method for constrained dynamics in tensegrity systems with compressible bars". In: *Computational Mechanics* 67.1 (2021), pp. 139–165.

[30] Isabella Huang and Ruzena Bajcsy. "High Resolution Soft Tactile Interface for Physical Human-Robot Interaction". In: *2020 IEEE International Conference on Robotics and Automation (ICRA)*. 2020, pp. 1705–1711. DOI: 10.1109/ICRA40945.2020.9197365.

[31] Donald E Ingber. "Tensegrity: the architectural basis of cellular mechanotransduction". In: *Annual review of physiology* 59.1 (1997), pp. 575–599.

[32] Donald E Ingber. "The architecture of life". In: *Scientific American* 278.1 (1998), pp. 48–57.

[33] Jonas Jørgensen, Kirsten Borup Bojesen, and Elizabeth Jochum. "Is a Soft Robot More "Natural"? Exploring the Perception of Soft Robotics in Human–Robot Interaction". In: *International Journal of Social Robotics* (2021), pp. 1–19.

[34] Navvab Kashiri et al. "CENTAURO: A hybrid locomotion and high power resilient manipulation platform". In: *IEEE Robotics and Automation Letters* 4.2 (2019), pp. 1595–1602.

[35] Daekyum Kim et al. "Review of machine learning methods in soft robotics". In: *Plos one* 16.2 (2021), e0246102.

[36] Sangbae Kim, Cecilia Laschi, and Barry Trimmer. "Soft robotics: a bioinspired evolution in robotics". In: *Trends in biotechnology* 31.5 (2013), pp. 287–294.

[37] Friedrich Lange, Wieland Bertleff, and Michael Suppa. "Force and trajectory control of industrial robots in stiff contact". In: *2013 IEEE International Conference on Robotics and Automation*. IEEE. 2013, pp. 2927–2934.

[38] Jessica Lanini et al. "Human intention detection as a multiclass classification problem: Application in physical human–robot interaction while walking". In: *IEEE Robotics and Automation Letters* 3.4 (2018), pp. 4171–4178.

[39] Chris Larson et al. "A deformable interface for human touch recognition using stretchable carbon nanotube dielectric elastomer sensors and deep neural networks". In: *Soft robotics* 6.5 (2019), pp. 611–620.

[40] Steven Lessard et al. "A bio-inspired tensegrity manipulator with multi-DOF, structurally compliant joints". In: *2016 IEEE/RSJ International Conference on Intelligent Robots and Systems (IROS)*. IEEE. 2016, pp. 5515–5520.

[41] Steven R Lessard. *The Design, Consturction, and Evaluation of Crux: A Tensegrity-Inspired Compliant Robotic Upper-Extremity Exosuit*. University of California, Santa Cruz, 2018.

[42] Faming Li and Robert E Skelton. "Sensor/actuator selection for tensegrity structures". In: *Proceedings of the 45th IEEE Conference on Decision and Control*. IEEE. 2006, pp. 2332–2337.

[43] Lengxue Li et al. "Robotic Tensegrity Structure With a Mechanism Mimicking Human Shoulder Motion". In: *Journal of Mechanisms and Robotics* 14.2 (2021), p. 025001.

[44] Andy Liaw, Matthew Wiener, et al. "Classification and regression by randomForest". In: *R news* 2.3 (2002), pp. 18–22.

[45] Zhichao Liu and Konstantinos Karydis. "Toward impact-resilient quadrotor design, collision characterization and recovery control to sustain flight after collisions". In: *2021 IEEE International Conference on Robotics and Automation (ICRA)*. IEEE. 2021, pp. 183–189.

[46] Dylan P Losey et al. "A review of intent detection, arbitration, and communication aspects of shared control for physical human–robot interaction". In: *Applied Mechanics Reviews* 70.1 (2018).

[47] Dylan P Losey et al. "Physical Interaction as Communication: Learning Robot Objectives Online from Human Corrections". In: *arXiv preprint arXiv:2107.02349* (2021).

[48] Catharine LR McGhan, Ali Nasir, and Ella M Atkins. "Human intent prediction using markov decision processes". In: *Journal of Aerospace Information Systems* 12.5 (2015), pp. 393–397.

[49] Erich Mielke et al. "Human-robot co-manipulation of extended objects: Data-driven models and control from analysis of human-human dyads". In: *arXiv preprint arXiv: 2001.00991* (2020).

[50] Akhil Padmanabha et al. "Omnitact: A multi-directional high-resolution touch sensor". In: *2020 IEEE International Conference on Robotics and Automation (ICRA)*. IEEE. 2020, pp. 618–624.

[51] Michael A Peshkin et al. "Cobot architecture". In: *IEEE Transactions on Robotics and Automation* 17.4 (2001), pp. 377–390.

[52] Panagiotis Polygerinos et al. "Soft robotics: Review of fluid-driven intrinsically soft devices; manufacturing, sensing, control, and applications in human-robot interaction". In: *Advanced Engineering Materials* 19.12 (2017), p. 1700016.

[53] Andrew P Sabelhaus et al. "Design, simulation, and testing of a flexible actuated spine for quadruped robots". In: *arXiv preprint arXiv:1804.06527* (2018).

[54] Andrew P Sabelhaus et al. "Inverse statics optimization for compound tensegrity robots". In: *IEEE Robotics and Automation Letters* 5.3 (2020), pp. 3982–3989.

[55] Andrew P Sabelhaus et al. "System design and locomotion of SUPERball, an untethered tensegrity robot". In: *2015 IEEE international conference on robotics and automation (ICRA)*. IEEE. 2015, pp. 2867–2873.

[56] H-J Schek. "The force density method for form finding and computation of general networks". In: *Computer methods in applied mechanics and engineering* 3.1 (1974), pp. 115–134.

[57] Benjamin Shih et al. "Electronic skins and machine learning for intelligent soft robots". In: *Science Robotics* 5.41 (2020).

[58] Roland Siegwart et al. "Legged and flying robots for disaster response". In: *World Engineering Conference and Convention (WECC)*. ETH-Zürich. 2015.

[59] Robert E Skelton and Mauricio C De Oliveira. *Tensegrity systems*. Vol. 1. Springer, 2009.

[60] Robert E Skelton, Jean Paul Pinaud, and D Lewis Mingori. "Dynamics of the shell class of tensegrity structures". In: *Journal of the Franklin Institute* 338.2-3 (2001), pp. 255–320.

[61] Cornel Sultan, Martin Corless, and Robert E Skelton. "The prestressability problem of tensegrity structures: some analytical solutions". In: *International Journal of Solids and Structures* 38.30-31 (2001), pp. 5223–5252.

[62] Cornel Sultan and Robert Skelton. "A force and torque tensegrity sensor". In: *Sensors and Actuators A: Physical* 112.2-3 (2004), pp. 220–231.

[63] Thomas George Thuruthel et al. "Soft robot perception using embedded soft sensors and recurrent neural networks". In: *Science Robotics* 4.26 (2019).

[64] AG Tibert and Sergio Pellegrino. "Review of form-finding methods for tensegrity structures". In: *International Journal of Space Structures* 18.4 (2003), pp. 209–223.

[65] Hoang Chi Tran and Jaehong Lee. "Advanced form-finding of tensegrity structures". In: *Computers & structures* 88.3-4 (2010), pp. 237–246.

[66] James Walker et al. "Soft robotics: a review of recent developments of pneumatic soft actuators". In: *Actuators*. Vol. 9. 1. Multidisciplinary Digital Publishing Institute. 2020, p. 3.

[67] Satoshi Yagi et al. "Evaluation of shape-changing tensegrity structure robot for physical human-robot interaction". In: *2019 IEEE International Conference on Advanced Robotics and its Social Impacts (ARSO)*. IEEE. 2019, pp. 20–24.

[68] Steve Yohanan and Karon E MacLean. "The role of affective touch in human-robot interaction: Human intent and expectations in touching the haptic creature". In: *International Journal of Social Robotics* 4.2 (2012), pp. 163–180.

[69] Haoyong Yu et al. "Human–robot interaction control of rehabilitation robots with series elastic actuators". In: *IEEE Transactions on Robotics* 31.5 (2015), pp. 1089–1100.

[70] Yufeng Yue et al. "A multilevel fusion system for multirobot 3-d mapping using heterogeneous sensors". In: *IEEE Systems Journal* 14.1 (2019), pp. 1341–1352.

[71] Jiaming Zha et al. "A collision-resilient aerial vehicle with icosahedron tensegrity structure". In: *2020 IEEE/RSJ International Conference on Intelligent Robots and Systems (IROS)*. IEEE. 2020, pp. 1407–1412.

[72] JY Zhang and M Ohsaki. "Adaptive force density method for form-finding problem of tensegrity structures". In: *International Journal of Solids and Structures* 43.18-19 (2006), pp. 5658–5673.